Structural Engineering Report No. 95

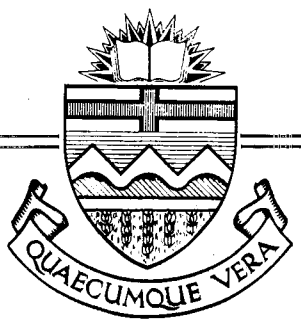

LOCAL BUCKLING OF W SHAPES USED AS COLUMNS, BEAMS, AND BEAM-COLUMNS

by
J. L. DAWE
and
G. L. KULAK

March 1981

LOCAL BUCKLING
OF W SHAPES USED AS
COLUMNS, BEAMS, AND BEAM-COLUMNS

by

J. L. DAWE

and

G. L. KULAK

DEPARTMENT OF CIVIL ENGINEERING

THE UNIVERSITY OF ALBERTA

EDMONTON, ALBERTA

MARCH, 1981

ABSTRACT

An analytical model, based on an extended Rayleigh-Ritz technique, has been developed for the purpose of predicting local buckling behaviour of columns, beams, or beam-columns composed of W shape sections. A tangent modulus buckling theory is used and a tri-linear stress - strain curve for an elastic - plastic - strain-hardening material is assumed. The effects of residual stresses as well as the interactive effects of web - flange restraints are included directly in the formulation. The flexibility of the analytical model allows for the possibility of separate flange or web buckling as well as simultaneous buckling of the web and flanges. An elaborate formulation of plate component stiffness matrices permits the use of varying material properties for longitudinal strips of a member as yielding and strain-hardening progress during loading.

A computer program based on the analytical model was verified by an extensive comparison of results with available classical results for elastic local buckling of plates. The validity of the local buckling analysis beyond the elastic range was well-established by comparison of computer results with the results of 57 tests conducted by various investigators using column, beam, and beam-column specimens.

Having thus been verified, the computer program was used to conduct an exhaustive study of the effect of various parameters

which were expected to have an important effect on local buckling behaviour. As a result of this study, various modifications to existing web and flange slenderness limitations for columns, beams and beam-columns are indicated. Further research in the form of full-size laboratory specimen tests is recommended and various suggestions are made with regard to future testing.

ACKNOWLEDGEMENTS

This study was carried out in the Department of Civil Engineering at the University of Alberta. It forms part of a continuing research investigation into the local buckling behaviour of W shape sections. The project is funded by the Canadian Steel Construction Council and the National Sciences and Engineering Research Council of Canada.

The authors wish to acknowledge the assistance of Dr. T.M. Hrudey and Dr. D.W. Murray for their helpful suggestions during the early stages of the theoretical development.

TABLE OF CONTENTS

LIST OF TABLES

LIST OF FIGURES

LIST OF SYMBOLS

The following is a list of the more commonly used symbols which are presented here for ease of reference. The meanings of all symbols used in the text are also defined where they first appear.

Dimensions and Displacements

α_t, α'_t	=	Locations of material boundaries (Compression flange)
α_b, α'_b	=	Locations of material boundaries (Tension flange)
β_1, β_2, β'_2, β_3, β'_3	=	Locations of material boundaries (Web)
b	=	Flange width
h	=	Web height
L	=	Length of a specimen
t_l	=	Tension flange thickness
t_u	=	Compression flange thickness
t_w	=	Web thickness
y_1	=	Distance to neutral axis from mid-height of web
u, v, w	=	x-, y-, and z- Components of displacement
u_i, u_j, u_k	=	Subscript notation for displacements

w_o = Displacement due to initial imperfection

w_1 = Displacement beyond w_o

Forces and Moments

M = Applied end moment

M_{cr} = Critical local buckling moment

M_p = Plastic moment

M_{pc} = Plastic moment reduced for compressive load

M_y = Yield moment

M_{yc} = Yield moment reduced for compressive load

M_x, M_{xy}, M_y = Plate bending moments per unit width

N_x, N_{xy}, N_y = In-plane plate forces per unit width

P = Compressive axial force

P_{cr} = Critical local buckling axial force

P_y = Column yield load

Geometric Properties

A_u = Area of compression flange

A_l = Area of tension flange

A_w = Area of web

$b\sqrt{F_y}/2t$ = Flange slenderness term

f = A general function

F_i = Buckling factors based on longitudinal shapes

$h\sqrt{F_y}/w$	=	Web slenderness term
I	=	Moment of inertia of a unit strip of plate
m	=	Number of longitudinal half sinewaves
π	=	Ratio of circumference to diameter of a circle
$S(\zeta)$	=	Flange shape function at a cross-section
x, y, z	=	Rectangular coordinates in three dimensions
η, ζ, ξ	=	Natural coordinates
$P_o(\zeta)$	=	Longitudinal shape envelope

Material Properties

D_x, D_y, D_{xy}, D_{yx}	=	Plate bending rigidity factors
E	=	Modulus of elasticity
E_o	=	Slope of yield plateau of stress - strain curve
E_{st}	=	Strain-hardening modulus
E_t	=	Tangent modulus
E_x, E_y, E_z	=	Material moduli of anisotropic materials
G	=	Shear modulus
G_t	=	Tangent shear modulus
ν	=	Poisson's ratio

Matrices and Vectors

$[C]$	=	Matrix of shape function coefficients
$\{F_o\}$	=	Equivalent lateral load vector

$\{H\}$ = Vector of polynomial terms

$[I]$ = Identity matrix

$[K]$ = Bending stiffness matrix

$[K_G]$ = Geometric stiffness matrix

$[K_{G_o}]$ = Intermediate geometric stiffness matrix

$[K_l]$ = Stiffness matrix of tension flange

$[K_u]$ = Stiffness matrix of compression flange

$[K_w]$ = Stiffness matrix of web

$[S]$ = Sweeping matrix

$[\Phi_i]$ = Component stiffness matrices

$\langle\phi\rangle$ = Transpose of shape function vector

$\{\phi\}_i$ = Eigenvectors

$\{\theta\}$ = Vector of coordinate displacements

$\{\theta\}_o$ = Vector of initial coordinate imperfections

Strains

ε_a = Applied axial strain

ε_b = Applied bending strain in compression

ε_b' = Applied bending strain in tension

ε_c = Strain at mid-height of web

ε_{rc} = Residual compressive strain

$\varepsilon_i (i = 1,2,3,4,5)$ = Residual strains on a W shape section

$\varepsilon_{b_{cr}}$ = Critical compressive bending strain

ε_y = Yield strain

$\bar{\varepsilon}^{(P)}$ = Effective plastic strain

ε_{st} = Strain at onset of strain-hardening

e_x, e_y, e_z = Strains in the x-, y-, and z - coordinate directions

γ_{xy}, γ_{yz}, γ_{zx} = Shear Strains

Stresses

F_y = Specified minimum yield stress

$s_i (i = 1,2,3,4,5,6)$ = Piecewise linear stress components

$\sigma_i (i = 1,2,3,4,5)$ = Residual stresses on a W shape section

σ_y = Yield stress

σ_{rc} = Residual compressive stress

σ_x, σ_y, σ_Z = Stress in the x-, y-, and z-coordinate directions

τ_{xy}, τ_{yz}, τ_{zx} = Shear stresses

Tensors

C_{ijkl} = Fourth-order tensor of material constants

e_{ij} = Strain tensor

$e_{ij}^{(P)}$ = Plastic strain tensor

S_{ij} = Stress deviator tensor

δ_{ij} = Kronecker delta

σ_{ij} = Stress tensor

Miscellaneous

d = Differential operator (eg. dS)

δ = Variational operator (eg. δw)

H'	=	Slope of effective stress - strain curve
k^2	=	Constant defining a von Mise's yield surface
J_2	=	Loading function used in von Mise's criterion
λ	=	An eigenvalue
λ_o	=	An intermediate eigenvalue
λ'	=	An eigenvalue strain
λ''	=	An eigenvalue difference (= $\lambda_o - \lambda'$)
μ	=	Eigenvalue shift
ω	=	Smallest eigenvalue of a system (= $1/\lambda$)
ω_s	=	Eigenvalue after shift applied

Chapter 1

INTRODUCTION

1.1 General

A large proportion of the members used in present-day steel structures are uniform throughout their lengths and have I-shaped cross-sections[1]. Such members are referred to as W shapes and are particularly efficient when used as beams for transferring bending moments within a structure. W shapes are also used as columns for transferring pure axial compression and as beam-columns for transferring combined axial compression and bending. Depending on the width-to-thickness ratios of their flanges, W shapes are classified as Class 1, Class 2, Class 3, and Class 4 sections[1]. Because of their thin-walled characteristics these members are particularly susceptible to local buckling[1,2,3] of their component plates and this local instability limits the load-carrying capacity of the members. Thus, in limit states design[1,4] local buckling of component plates of W shapes is one limit which must be met.

1.2 Local Buckling

In the present study the limit state of local buckling is isolated from other limit states such as those related to overall instability, material strength and excessive deflections[1]. This

procedure coincides with present design philosophies which require that local buckling be prevented prior to the attainment of the maximum strength of a member[1,3,5]. Since local buckling is isolated, a fundamental assumption is that all members are fully braced against overall instability. Local buckling of W shapes may be defined as a bifurcation phenomenon[5] whereby a component plate subjected to in-plane stresses may be in equilibrium in its original planar configuration or in a neighboring deflected configuration. This critical state can occur in the elastic or inelastic regions of material response depending on the level of yield stress, the plate width-to-thickness ratio, and plate boundary conditions[2,3,6,7]. Because of the nature of buckling, it is more precisely defined by a mathematical formulation. In the present study such a formulation is based on the principle of virtual work[8] and is presented in Appendix A.

1.3 Design Considerations

As already established by previous investigators[2,3,6,7], a significant parameter affecting the stability of a plate is its width-to-thickness ratio. Therefore, a designer must consider the width-to-thickness ratios of flanges and webs when determining the local buckling resistance of W shapes. Other factors which affect plate stability in W shapes are the type of plate edge supports at the ends of a member, the type of stress distribution on a member cross-section, and the material properties of the steel[2,7]. Because of the significant effect that the yield stress level has on plate buckling[7], the present design code[4] specifies limitations on the width-to-thickness ratios of webs and flanges multiplied by the square root of the yield stress.

1.3.1 Current Requirements for Flanges and Webs

The current Canadian design standard used for steel[4], specifies width-to-thickness terms for four classes of W shape beam-columns. It is required that Class 1 sections permit the attainment of the reduced plastic moment and also allow for sufficient rotation capacity for subsequent redistribution of load before local buckling occurs. A Class 2 section is required to permit the attainment of the reduced plastic moment capacity with no provision for the requirement of subsequent load redistribution. A Class 3 section must permit the attainment of the reduced yield moment and for a Class 4 section the limit state of structural capacity is local buckling of elements in compression. Class 4 sections are light-gauge cold-formed sections and their behaviour does not form a part of this study. The present design limitations for Class 1, 2, and 3 sections are presented in detail in Chapter 6. These limitations are such that for a given class of section, local buckling of the component plates must not occur until the section has satisfied the minimum requirements for its classification. Since columns are not designed according to a required bending moment capacity, they are not classified as above. However, it is usual to use the same limitation for column flanges as that specified for Class 3 sections, while column webs are limited by a maximum width-to-thickness term[4].

1.3.2 Previous Requirements for Flanges and Webs

Previous design codes[9] have presented width-to-thickness ratios for flanges and webs of W shapes subjected to axial compression, bending, and axial compression and bending combined. As will be examined further in Chapter 2, these values are based on the results of an investigation

by Haaijer and Thurlimann[7]. Recently, however, studies performed at the University of Alberta by Kulak et al[10,11,12,13] have shown that previously specified width-to-thickness limitations were overly conservative. As a result of these studies, the present code[4] uses values that supersede previously specified width-to-thickness limitations for component plates of columns, beams, and beam-columns.

1.4 Objectives

The investigations conducted at the University of Alberta have been largely experimental and empirical in nature. The work has resulted in new design equations and graphs which are presently in use[4]. The present study is a continuation of this work with emphasis on the theoretical nature of plate buckling as it relates to W shapes subjected to axial compression, bending, and axial compression and bending combined.

The objectives of the present study are as follows:

1. to establish an idealized mathematical model to study local buckling of W shapes subjected to axial compression, bending, or to axial compression and bending combined.
2. to establish the validity of the mathematical technique by comparing analytical results with test results.
3. to present design equations and graphs for a broad spectrum of practical cases for which test results are not available.
4. to suggest, where appropriate, additional revisions

to presently specified width-to-thickness limitations for component plates of W shapes.

1.5 Scope

The mathematical formulation presented herein permits an analysis for local buckling of W shapes of various cross-sectional dimensions and material properties. The analysis is performed for axial compression, bending, and combined axial compression and bending applied at the member ends. The effects of residual stresses are included and web, flange, or combined web and flange buckling is predicted in the elastic or inelastic ranges. The restraint interaction of flanges and web is also accounted for by the mathematical model.

In Chapter 2 a review of the available literature that relates to the present study is outlined. In Chapter 3 the general mathematical formulation technique is discussed in detail and the application of this technique to the general case of combined axial compression and bending is presented in Chapter 4. In Chapter 5 the analytical technique is applied to the investigation of local buckling of 57 specimens that have been tested by various investigators. Theoretical and test results are compared. Analytical results for a wide range of Class 1, 2, and 3 columns, beams, and beam-columns are presented in Chapter 6, and in addition these theoretical results are interpreted for application to design. Also presented in Chapter 6 is a study of the parameters considered important in the analysis. The conclusions of the present study and the resulting design recommendations are presented in Chapter 7.

The mathematical formulation of plate buckling based on the

principle of virtual work[8] is presented in Appendix A and the material properties are discussed in Appendix B. Because of the nature of the mathematical formulation which employs the use of matrix algebra as well as the use of iterative techniques for the inelastic cases, hand computation is highly impractical. Therefore, a computer program coded in Fortran IV and suitable for use with an Amdahl 470V/6 or an IBM 3032 computer was used for the computations. A listing of the program with explanations of the subroutines and typical input data is available in the Ph.D. thesis entitled "Local Buckling of W Shapes Used as Columns, Beams, and Beam-Columns" by John L. Dawe as submitted to the Faculty of Graduate Studies and Research at the University of Alberta, Edmonton, Canada (Fall, 1980).

Chapter 2

LITERATURE SURVEY

A review of the available literature indicates that the problem of elastic plate buckling has been thoroughly investigated since the publication in 1891 of the original work done in this area[14]. The theoretical investigations include the closed-form solutions of single plates having regular geometric shapes and various stress and displacement boundary conditions. These solutions have been well-documented and are readily available in the literature[2,3,6,15,16].

It was not until the 1920's that the problem of inelastic plate buckling first began to receive some attention. In much the same way as for columns, inelastic buckling of rectangular plates was first treated by replacing the elastic modulus by a reduced modulus or a tangent modulus above the proportional limit. Bleich[6], for example, assumed that above the proportional limit, the reduced modulus would be effective in the direction of uniaxial stress while the elastic modulus remained effective in the transverse direction. It was further assumed that an effective shear modulus equal to the geometric average of the elastic and reduced moduli would be applicable. Alternatively, Ros and Eichinger[17], assuming isotropy in the inelastic range, suggested using the reduced modulus in all directions. Of the two, it was found that Bleich's assumptions led to values in closer agreement with test results.

Other investigators have attempted to improve upon the

existing knowledge in this area by including the total elastic-plastic stress-strain relationships in the plate buckling analysis. Prominent among those investigators were Bijlaard[18], Ilyushin[19], and Stowell[20] who used the deformation theory of plasticity[8] while Onat and Drucker[21] and Handelman and Prager[22] promoted the use of the incremental theory[8] in the plastic analysis of plate buckling. While the former method showed much better agreement with test results, it has been recognized that the latter method is the mathematically correct one[7,21,23,24]. The main reason for this paradox appears to be the prediction by the incremental theory of a value of the shear modulus in the inelastic range equal to its value in the elastic range[7,21,23,25]. It has been shown that a reduction in this value leads to much better correlation between theory and test results[7,25].

Early investigations of web and flange stability for W shape members were based on several simplifying assumptions. For both elastic and inelastic buckling it was assumed that the plate components at web-to-flange junctions were either rigidly supported or simply supported and the effects of residual stresses were neglected. Using these assumptions as well as Bleich's assumption of anisotropy in the inelastic range it was possible to arrive at closed-form solutions for several types of in-plane loadings[2,6,26].

In the late 1950's Haaijer and Thurlimann published the results of an investigation of inelastic local buckling in steel[7]. The main purpose of this investigation was to determine maximum plate width-to-thickness ratios for W shapes suitable for plastic design. An incremental theory[22] was used in the analysis and the inelastic value of the shear modulus was reduced by 80 per cent. (The investigators

attributed this reduction to the effects of initial imperfections. However, in a more recent investigation[25], Lay discounted this effect of initial imperfections and arrived at a similar reduction in the shear modulus by applying slip-line field theory).

In their investigations, Haaijer and Thurlimann presented analytical solutions for single web or flange plates assuming either simple support or fully rigid support at the web-to-flange junctions. The effects of residual stresses were not included directly in the analysis. However, for the buckling strength of columns and plates in uniaxial compression, an empirical transition curve was suggested for use above the proportional limit. The experimental investigation of W shapes included six axial specimens and six flexural specimens. The present code limitations for flanges and webs of Class 1 W shapes are based on the results of these tests[4].

Although Haaijer and Thurlimann did not test any specimens subjected to axial and flexural loadings combined, they used the results of a semi-empirical method to suggest plate width-to-thickness values for such members. In this method it was assumed that values obtained for axial specimens failing by web buckling would be applicable to an average strain in the compression zone of the webs of beam-columns. The present code limitations for plate components of Class 1 W shape beam-columns are based on the results of this semi-empirical method[4].

In the years following the work of Haaijer and Thurlimann many investigators published results of research concerning the elastic and inelastic buckling strength of single plates. With the aid of discretization techniques and computer methods it has been possible to investigate many different cases[27,28,29,30,31,32]. However, although

useful, none of these works is concerned directly with the understanding of local buckling behaviour in W shape members. More to the point, other studies have been directed towards local buckling in W shape beams. The studies of Lay[33], Culver[34], and McDermott[35], for example, have all indicated a flange width-to-thickness limitation of $b\sqrt{F_y}/2t = 54$ for sections required to reach the strain-hardening strain. Results of tests performed by Lukey and Adams[36] have indicated that a flange width-to-thickness term of 64 can be used for sections required to develop the full plastic moment capacity. A study by Basler and Thurlimann[37] has indicated that webs of girders required to reach M_y can have a value of $h\sqrt{F_y}/w$ as high as 980. More recent research by Croce[38] has indicated that $h\sqrt{F_y}/w$ can have a value as high as 750 for beams used in plastic design.

In 1973 a study of coupled local buckling in beam-columns was presented by Rajasekaran and Murray[39]. The method of analysis was based on finite element techniques and could accommodate a large variety of boundary conditions. The method assumed linear elastic material response and did not include the effects of residual stresses. It was found that the analysis gave good results for flange local buckling but web buckling could not be accurately predicted.

In 1977, Akay, Johnson, and Will presented a study of lateral and local buckling of beams and frames[40]. A finite element technique using plate elements for webs and line elements for flanges was used. The buckling modes were restricted by the assumption that straight lines across the flanges and normal to the web remain straight during buckling. Although the method is quite general with regard to

plate geometry and boundary conditions it assumes linear elastic response and neglects the effects of residual stresses.

In 1978, a study of local, distortional, and lateral buckling of W shape beams was presented by Hancock[41]. A finite strip technique was used in the analysis and an elastic, linear material response was assumed. The effects of residual stresses were not included in the analysis. Other studies using finite strip techniques were presented in 1964 by Plank and Wittrick[42] and in 1974 by Goldberg, Bogdanoff, and Glauz[43], who extended the work of Przemieniecki[32]. Plank and Wittrick suggested a method for analysing thin-walled sections for lateral-torsional buckling. Presumably local buckling could be predicted by iterating on the length parameter. Plate thickness as well as geometry, material properties, and loading could be varied for a given member. However the effects of residual stresses were not included and apparently the method was not suitable for local buckling of W shapes since it was neither used, nor recommended, for this purpose.

As mentioned above, Goldberg, Bogdanoff, and Glauz[43] extended the work of Przemieniecki[32] to include lateral buckling modes as well as more complicated states of stress. An elastic material response was assumed and the effects of residual stresses were not included in the analysis. Again, the method was neither applied to, nor recommended for, the analysis of local buckling of W shapes.

None of the above-mentioned techniques has been applied to an in-depth study of local buckling of Class 1, Class 2, and Class 3 W shape sections. In 1973, Kulak initiated such a study on an experimental basis[10]. A total of ten beams (eight Class 2 and two

Class 1 sections) were tested under equal third-point loadings. Based on the results of these tests it was concluded that the existing web width-to-thickness limitations for Class 2 sections were conservative and a need for additional tests on beams and beam-columns was indicated. Other tests followed, and in 1975 two Class 3 beams were tested and an increase in the existing web limitations for Class 3 beams was indicated[11].

In 1974 Kulak and Perlynn published the results of a study in which nine Class 2 W shape beam-columns were tested under various amounts of axial load[12]. Again it was determined that the existing web limitations were too conservative for Class 2 beam-columns and a need for additional tests on Class 3 beam-columns were indicated. In 1976, the results of such a study were reported by Kulak and Nash[13]. It was indicated that web limitations for Class 3 beam-columns could also be somewhat relaxed. As a result of the work carried out by Kulak, et al. at the University of Alberta, significant changes in the web limitation requirements for W shapes have been implemented for Class 2 and Class 3 sections[4].

The investigations carried out by Kulak, et al, were largely experimental although two semi-empirical methods for determining critical web width-to-thickness ratios were presented[12]. Method I was based directly on test results and Method II combined test results with a variation of the method used by Haaijer and Thurlimann[7]. Because of the limited number of test results used, the methods were valid only for sections that were similar to those tested. Furthermore, the methods did not allow for variations in flange sizes, lengths of specimens, residual stresses, and material properties. For the types of

specimens tested, the methods were valid only between the limits of P/P_y equal to 0.15 and 0.80 since these were the lower and upper limits used in the tests. A purely analytical method was not developed.

Chapter 3

GENERAL ANALYTICAL METHOD

3.1 Introduction

The problem of plate buckling in the elastic range has been thoroughly investigated and solutions are available for many cases including various plate shapes and stress and displacement boundary conditions[2,3,16,44]. Solutions for the analysis of orthotropic plates and for buckling capacities of plates in the inelastic range have also been published[2,6,18,44]. The technique for obtaining a mathematical formulation for such problems is based on either an equilibrium method or an energy method[2].

In the equilibrium method[2,6], the equations of equilibrium are formulated on a deformed configuration of the plate. This configuration is compatible with the expected mode of buckling. Once the equations of equilibrium are solved simultaneously, the problem reduces to that of the solution of a biharmonic differential equation. This method makes use of the fact that, during buckling, a plate may be in equilibrium in its original planar configuration as well as in a neighboring buckled configuration; that is, the plate is at a point of bifurcation.

Two commonly used energy techniques for formulating plate buckling problems are the principle of minimum potential energy and the principle of virtual work[8]. Of these two methods, the principle of virtual work is a more general statement of the principle of the

conservation of energy. It does not require the assumption of the existence of a strain energy function and it can be applied to an elastic or an inelastic material[8,45]. In the present analysis the principle of virtual work is used for the formulation of a plate buckling condition. In applying this method, a buckled configuration is first assumed. Then, a virtual displacement[46] from a buckled configuration is postulated. By equating the internal work done by the equilibrium stress field existing in a plate during this virtual displacement to the work done by the external forces acting on the plate during the same displacement, an integral differential equation is obtained. Using a Rayleigh-Ritz technique[5,46,47] and a displacement field defined in terms of a set of nodal displacement coordinates, a matrix buckling condition is obtained and a standard eigenvalue problem results[48,49,50]. This technique is developed in detail in Appendix A.

3.2 Idealized Cross-section

The technique outlined above is applied to W shapes having idealized cross-sections such as that illustrated in Figure 3.1. All subsequent mathematical formulations are referred to the mid-planes of the component plates of a W shape. Thus, the assumed height of web extends into each flange by a distance equal to one-half the flange thickness. Consequently, the area corresponding to each projection is twice included in the calculations of axial loads and bending moments. The purpose of this is to recognize that fillets at web-to-flange junctions do exist and that these additional areas of projection do, to some extent, account for them.

The width-to-thickness ratio for a flange is obtained by dividing one half the flange width by the flange thickness. In determining the width-to-thickness ratio of a web it is assumed that web-to-flange fillets have leg lengths equal to one-half the flange thickness. Therefore, the length of the web is taken as the clear distance between flanges minus the fillet leg lengths. The purpose of this is to take into account, to some extent, the effects of the fillets in decreasing the effective buckling height of a web.

As shown in Figure 3.1, variations in flange dimensions are permitted by using different flange widths and thicknesses. In subsequent discussions, in addition to the notations shown in Figure 3.1, A_l represents the area of a lower flange, A_w represents the area of a web, and A_u represents the area of an upper flange. Furthermore, for clearness of discussion, it is assumed that an upper flange is one that will normally be in compression and a lower flange will normally be in tension under an applied bending moment. The subscripts, l and u, are used to refer to the lower and upper flanges respectively.

3.3. Material Properties

In applying any mathematical technique to the prediction of plate buckling capacities it is necessary to have an accurate evaluation of the material properties to be used. In the method presented herein, a uniaxially stressed longitudinal fibre of a W shape section is assumed to have an idealized tri-linear tensile stress - strain response such as that shown in Figure 3.2. It is further assumed that this stress - strain response also applies to a fibre in compression. At the point where yielding occurs in a fibre, the strain

is designated by ε_y and the corresponding yield stress is designated by σ_y. For values of strain less than the yield strain, the fibre has an elastic modulus (also called Young's modulus) designated by E. At the point where strain-hardening of a fibre begins, the strain is represented by ε_{st}. For strains larger than this, the fibre displays an increased resistance to further straining. This fibre stiffness is evaluated as the strain-hardening modulus, E_{st}.

In the intermediate range of strain between ε_y and ε_{st}, the fibre yields and a yield modulus, E_o, represents the slope of this portion of the curve. If the value of E_o is zero there exists no explicit and definable relationship between stress and strain. That is, at the yield stress level, a fibre can assume an arbitrary value of strain and, if the direction of loading is such that strains tend to increase, it is likely that the strain-hardening modulus will govern the behaviour of a fibre that has yielded. The assumption that strain-hardening material properties govern buckling behaviour for strains above the yield strain has been successfully used by several investigators[25,34,51,52,53,54] and this assumption is also made in the present investigation.

3.4 Analytical Technique

As explained in section 3.1 a plate buckling condition is derived using the principle of virtual work. This derivation is presented in detail in Appendix A and it results in an integral differential equation for the buckling condition. For a uniaxially stressed orthotropic plate, the buckling condition is as follows:

$$\int_x \int_y (D_x w,_{xx} \delta w,_{xx} + D_y w,_{yy} \delta w,_{yy} + D_{xy} w,_{yy} \delta w,_{xx} + D_{yx} w,_{xx} \delta w,_{yy}$$

$$+ 4G_t I w,_{xy} \delta w,_{xy}) dxdy - \int_x \int_y N_x w,_x \delta w,_x dxdy = 0 \qquad \text{(A-35)}$$

where D_x, D_y, D_{xy}, and D_{yx} are plate bending rigidities, G_t is the tangent shear modulus, and I is the moment of inertia per unit length of plate. These properties are further discussed in Appendix B. Also in Equation A-35, w represents the deflection of a point normal to the middle plane of the plate, δw represents a virtual deflection in this direction, x and y represent Cartesian coordinate directions, and differentiation is indicated using comma notation[47].

In Equation A-35 the first integral represents the virtual work resulting from the strain energy of plate bending while the second integral represents the virtual work done by the in-plane stresses which act during buckling.

Once a plate buckling condition has been formulated into a mathematical expression using an energy method, one may try to obtain an exact mathematical solution or an approximate solution. Because of the complexity of the present formulation, solutions are obtained using the Rayleigh-Ritz technique[48]. This method has also been applied quite successfully by other investigators[4,47,48,49,50].

A basic assumption of this technique is that the displacement field describing a buckled shape can be expressed in terms of a set of assumed shape functions and corresponding coordinate displacements[55].

Together these must form a set of kinematically admissible generalized coordinate displacements which requires that the assumed displacement function satisfy the boundary conditions of the physical problem. The development of appropriate shape functions is discussed in a later section. However, it is appropriate here to state that a displacement function can be defined as follows:

$$w = f\langle\phi\rangle\{\theta\} \tag{3.1}$$

where $\{\theta\}$ is a vector of displacement coordinates defined at distinct nodal points in a cross-section (Figure 3.4) and $\langle\phi\rangle$ is a set of shape functions which interpolate the coordinate displacements over a cross-section. The function, f, is a shape function which interpolates a set of cross-sectional displacements over the length of a member. By substituting this assumed displacement function into Equation A-35, the problem is reduced from a continuum problem, with an infinite number of degrees of freedom, to a problem with a finite number of degrees of freedom equal to the total number of coordinate displacements defined at the nodes. As a result, a system of algebraic equations, rather than a partial differential equation, must be solved. This procedure is carried out in detail in Appendix A where it is shown that the problem of local buckling reduces to the form:

$$\left[[K]-\lambda[K_G]\right]\{\theta\} = \{0\} \tag{A-51}$$

where $[K]$ is a bending stiffness matrix depending on material properties and plate dimensions, $[K_G]$ is a geometric stiffness matrix depending on the distribution and magnitude of applied in-plane stresses, and λ is a

multiple of the applied loading which causes buckling.

The expression in brackets represents the reduced stiffness of a plate which buckles when, depending upon the value of λ, the determinant of the reduced stiffness matrix beomes zero. The corresponding values of λ and $\{\theta\}$ are referred to as the eigenvalue and eigenvector, respectively. The eigenvalue in this case is the critical stress at which a plate buckles and the eigenvector defines the critical buckled shape.

The solution to the buckling problem as presented herein reduces to the problem of extracting the lowest eigenvalue from the system of equations expressed by Equation A-51. If, in this equation, $[K]$ and $[K_G]$ are each of dimension n x n, then the characteristic equation[50] of the reduced stiffness matrix will have n roots, each one corresponding to an eigenvalue of the system. However, in problems concerning statical stability only the lowest of these roots is of interest. A method that is commonly used to find the smallest eigenvalue of a system, and also one that is readily adaptable to electronic computation, is that of inverse matrix iteration[50].

Using this technique, Equation A-51 is first rewritten as:

$$[K]\{\theta\} = \lambda[k_G]\{\theta\} \tag{3.2}$$

Multiplying both sides of Equation 3.2 by the inverse of $[K]$ and dividing by λ result in:

$$[K]^{-1}[K_G]\{\theta\} = \frac{1}{\lambda}\{\theta\} \tag{3.3}$$

or:

$$[E]\{\theta\} = \omega\{\theta\} \tag{3.4}$$

where,

$$[E] = [K]^{-1}[K_G] \tag{3.5}$$

and,

$$\omega = \frac{1}{\lambda}. \tag{3.6}$$

In the solution of Equation 3.4, an initial shape vector, $\{\theta\}_o$, is assumed and this vector is multiplied by matrix [E]. The resulting vector, $\{\theta\}_1$, is then normalized by dividing by the highest-valued element of the vector. The process is then repeated with this new normalized vector. It has been shown[50] that, after several cycles of iteration, ω converges to the highest eigenvalue of the system. As a result, the lowest critical value of $\lambda = 1/\omega$ is obtained for the original system, Equation 3.2, and the corresponding eigenvector gives the critical buckled shape.

In certain eigensystems the smallest eigenvalue may appear as a positive value or a negative value. For example, the bending stress required to cause local buckling in a doubly-symmetric W shape may occur as a positive or negative eigenvalue of the associated eigensystem. This result is due solely to the symmetry of the system and the positivity or negativity of the eigenvalue has no physical significance. It does however result in considerable mathematical difficulty in achieving convergence during matrix iteration. This is because the rate of convergence is proportional to the ratio of the

lowest eigenvalue to the next higher value[50], and for values of this ratio approaching 1.0 the rate of convergence is very slow. For problems of the type described above, the first two eigenvalues of the system are equal but of opposite sign; that is, $\omega_1 = -\omega_2$. Therefore, the rate of convergence is $\omega_1/\omega_2 = -1.0$ and the technique will not converge.

To avoid this problem, a constant shift, μ, is applied to all of the eigenvalues of the system, in which case the rate of convergence is proportional to $(\omega_1-\mu)/(\omega_1+\mu) < 1.0$ and the method will converge. Applying a shift, μ, to the system, Equation 3.4 becomes:

$$[E]\{\theta\}-\mu\{\theta\} = \omega\{\theta\}-\mu\{\theta\} \tag{3.7}$$

or,

$$\Big[[E]-\mu[I]\Big]\{\theta\} = \omega_s\{\theta\} \tag{3.8}$$

where $\omega_s = \omega-\mu$ and [I] is an identity matrix of the same dimension as [E]. It has been shown[50] that the eigensystem defined by Equation 3.8 has the same eigenvectors as those defined by the original system described by Equation 3.4. The relationship between the eigenvalues of the two systems is given by:

$$\omega-\mu = \omega_s \tag{3.9}$$

or,

$$\omega = \frac{1}{\lambda} = \omega_s+\mu \tag{3.10}$$

In subsequent sections, the eigenvalue problem is formulated in such a way that only the smallest positive eigenvalue is

required. Although the eigenvalue shift technique increases the rate of convergence in most cases, it does not guarantee the convergence will be to the lowest positive root. In some cases it is found that the process converges to the lowest negative root. It is desirable therefore to have a method for eliminating certain eigenpairs from the system so that inverse iteration can be repeated to determine the lowest positive root. The method used to do this in the present analysis is referred to as a sweeping technique[48,50].

Since the eigenvectors, $\{\phi\}_i$, of an eigensystem are linearly independent[50], they provide a vector basis for the system, and any starting vector, $\{\theta\}$, may be expressed as a linear combination of these eigenvectors, that is:

$$\{\theta\} = \sum_{i=1}^{n} c_i \{\phi\}_i \tag{3.11}$$

If it is desired to remove the kth eigenmode from the system, a starting vector should be selected as follows:

$$\{\theta\}_o = \{\theta\} - c_k \{\phi\}_k \tag{3.12}$$

The value of c_k is found by pre-multiplying Equation 3.11 by $\langle\phi\rangle[K_G]$ and using the orthogonality properties[50] of eigenvectors. Doing so, results in:

$$c_k = \frac{\langle\phi\rangle_k [K_G]\{\theta\}}{\langle\phi\rangle_k [K_G]\{\phi\}_k} \tag{3.13}$$

Substituting this value into Equation 3.12 gives:

$$\{\theta\}_o = \left[[I] - \frac{\{\phi\}_k \langle\phi\rangle_k [K_G]}{\langle\phi\rangle_k [K_G] \{\phi\}_k}\right]\{\theta\}$$

$$= [S]_k \{\theta\} \qquad (3.14)$$

where $[S]_k$ is the desired sweeping matrix. Using this value of $\{\theta\}_o$ as a starting value, Equation 3.8 becomes:

$$\Big[[E] - \mu[I]\Big][S]_k\{\theta\} = \omega_s\{\theta\} \qquad (3.15)$$

which represents an eigensystem with the k^{th} mode removed. In the analytical technique presented herein this method is used to remove negative eigenvalues and corresponding eigenvectors from a system. It has been found that only one application of a sweeping matrix is required for the majority of cases where the first eigenvalue calculated is negative.

3.5 Effects of Initial Imperfections

As described previously, the present analysis uses a precise mathematical formulation to describe the local buckling condition. This implies that the maximum strength of a plate or system of plates is limited only by critical local buckling and this is the basis on which the formulation is made. The assessment of the effects of initial imperfections on the buckling strength of plates is also based on this type of formulation.

It is assumed for this purpose that $\{\theta_o\}$ is a set of initial

coordinate displacements defined at the nodes of a plate system. Using the same interpolation functions as those in Equation 3.1, initial deflections may be described by:

$$w_o = f<\phi>\{\theta_o\} \tag{3.16}$$

and additional deflections due to applied in-plane loads are given by:

$$w_1 = f<\phi>\{\theta\} \tag{3.17}$$

Therefore, the total out-of-plane deflection at any point is given by:

$$\begin{aligned} w &= w_o + w_1 \\ &= f<\phi>\{\theta_o\} + f<\phi>\{\theta\} \end{aligned} \tag{3.18}$$

To evaluate the effects of initial imperfections, the appropriate values of deflection are substituted into the buckling condition, Equation A-35. Since the first integral in Equation A-35 represents the work done by bending of a plate from its initially deflected position to its buckled shape, the net deflection, $w-w_o$, must be used to evaluate this integral[2]. The second integral in Equation A-35 represents the work done by the in-plane forces during buckling of a plate. It can be evaluated by calculating the work done by the in-plane forces acting through displacements caused by initial imperfections only. The net work is then obtained by subtracting this value from the work done by the in-plane forces acting through displacements caused by the total deflection of a plate. By proceeding in this manner, and using the concepts of bending and geometric stiffness matrices, as used in Section 3.4, Equation A-35 results in the following set of equations:

$$\left[[K]-\lambda[K_G]\right]\{\theta\} = \lambda[K_G]\{\theta_o\} \tag{3.19}$$

From this relationship it can be seen that the effect of initial imperfections is to simulate an equivalent lateral load of:

$$\{F_o\} = \lambda[K_G]\{\theta_o\} \tag{3.20}$$

The effect of this equivalent lateral load is to cause deflections to increase gradually as the in-plane loads are increased. However, the mathematical definition of buckling can be expressed by setting the determinant of the reduced stiffness matrix equal to zero. Since the reduced stiffness matrix formulated with initial imperfections included is identical to that for the case of a perfectly straight plate, initial imperfections do not affect the value of the critical buckling load as defined herein. As the in-plane loads increase, lateral deflections increase gradually and as the critical buckling load is approached the lateral deflections become asymtotic to the critical buckled shape.

3.6 Coordinate Systems

In the formulation of the theory for local buckling, the shape functions are referred to a system of natural coordinates[50,55]. Figure 3.3. illustrates the relationship between a natural coordinate system for a plate of length ℓ, and a Cartesian coordinate system. Points 1, 2, and 3 in this figure are referred to as nodes at which the coordinate displacements comprising the vector, $\{\theta\}$, are defined. At these nodes the elements of $\{\theta\}$ may represent translations,

rotations, curvatures, and higher order derivatives. Using these coordinates and an appropriate set of interpolating polynomials it is possible to define a set of shape functions at a cross-section for the flanges and web of a W shape section.

Local natural coordinate systems for the flanges and web of a W shape cross-section as well as the corresponding node numbering system are shown in Figure 3.4. Each coordinate displacement defined at a given node is interpolated by a polynomial function over the cross-sectional edge of a flange or a web. The order of each such interpolating polynomial is equal to the number of coordinate displacements that must be interpolated for a flange or web. Thus, for example, if a translation and a rotation are defined for each of three nodes of a flange, a quintic polynomial interpolating function is used for each nodal displacement.

3.7 Flange Shape Functions

Polynomial functions used to interpolate coordinate displacements along a plate edge at a cross-section may be obtained by a matrix technique[55] or by inspection. Since the latter method is used herein it is described in detail below. Quintic polynomials are used to interpolate the nodal displacements for flanges at a cross-section. At each of three nodes on a flange, a translation and a rotation are interpolated. These interpolation functions and their shapes are shown in Figure 3.5.

The method of inspection for obtaining shape functions is presented as an illustration for the particular case of interpolating a translation at node number one of Figure 3.4. Since a total of six

coordinate displacements are defined (a translation and a rotation at each of three nodes) a fifth order polynomial is first assumed as follows:

$$S(\zeta) = \zeta^2(\zeta-1)^2(a_o\zeta+b_o) \tag{3.21}$$

A shape function evaluated at the coordinate displacement being interpolated must have a value of 1.0 and must have a zero value when evaluated at all other coordinate displacements. The first factor of the above function ensures that the translation and rotation at $\zeta=0$ are both zero. The second factor ensures that the translation and rotation at $\zeta=1$ are zero. The third factor is chosen so that the function will be a fifth order polynomial. Also, the constants, a_o and b_o, can be determined so that at $\zeta=-1$, the rotation is zero and the translation is positive and unity. Evaluating a_o and b_o for these two conditions results in the function:

$$S(\zeta) = \frac{1}{4}\zeta^2(\zeta-1)^2(3\zeta+4) \tag{3.22}$$

The value of this expression is positive unity at the coordinate displacement being interpolated while at all other coordinate displacements its value is zero.

3.8 Web Shape Functions

Octic polynomials are used to interpolate nodal displacements for webs at a cross-section. For the purpose of studying local buckling of W shapes, it is assumed that the line of intersection of two plates at a flange-to-web junction does not translate during buckling. This line appears as a nodal point on a cross-section of a W shape and the

corresponding translations are not interpolated for the flange or web since they have zero value. Therefore, octic polynomials are used to interpolate rotations and curvatures of a web at its extremities and translation, rotation, and curvature at its center for a given cross-section. The interpolating polynomials for webs are obtained by the method of inspection as described previously for flanges. The polynomials and their corresponding shapes for coordinate displacements of a web at a cross-section are shown in Figure 3.6.

3.9 Longitudinal Shape Functions

A buckled shape which has been established at a cross-section of a W shape member must be interpolated over the length of the member. For plates simply supported at the loaded edges and subjected to uniaxial stresses, it has been determined[2,6] that the buckled shape in the direction of applied stress occurs in the form of a sine wave. This result is inherent in the nature of the solution to a partial differential equation which defines the plate buckling of a simply supported rectangular plate subjected to uniaxial stresses.

For this reason, and because the Rayleigh-Ritz solution is not very sensitive to the actual shapes used[4,47,48,50], a sine shape is included as a principle component of longitudinal shape functions used in this study. As shown in Figure 3.7, the effect of various boundary conditions can be accounted for by multiplying a sine function by a polynomial function which adequately describes the boundary conditions. Essentially, this technique applies an envelope to a sine function.

The general form of a longitudinal shape function is $P_o(\xi)\sin m\pi\xi$. In this form $P_o(\xi)$ represents a polynomial envelope of a

sine function where m is the number of half sinewaves that occurs along the length of a plate during buckling. The complete buckled shape of a plate component of a W shape is given by:

$$w = P_o(\xi)\text{Sin } m\pi\xi<\phi>\{\theta\} \tag{3.23}$$

As described previously, $<\phi>\{\theta\}$ describes the buckled shape of a flange or a web at a cross-section. Each polynomial of $<\phi>$ is a function of ζ when referring to a flange, and a function of η when referring to a web. ξ is the natural coordinate in the longitudinal direction of a member. The natural coordinates, ξ, ζ, and η and the corresponding natural coordinate systems are defined in Figure 3.8 for a W shape.

3.10 Integration of Cross-Sectional Shape Functions

As is evident from the formulation presented in Appendix A, extensive use of integration and differentiation of shape functions is required. Furthermore, shape functions expressed in terms of natural coordinates must be integrated and differentiated with respect to Cartesian coordinates. The function in Equation 3.22, for example, may be integrated as follows:

$$\int_0^{b/2} S(\zeta)dy = \frac{b}{2}\int_0^1 S(\zeta)d\zeta \tag{3.24}$$

In this operation, the limits of integration and the differential element dy in the Cartesian coordinate system were transformed to a natural coordinate system using the relationship,

$$\zeta = \frac{2y}{b} \tag{3.25}$$

as defined in Figure 3.5. Differentiation of the function in Equation 3.22 proceeds as follows:

$$\frac{\partial S(\zeta)}{\partial y} = \frac{\partial S}{\partial \zeta} \cdot \frac{\partial \zeta}{\partial y} = \frac{2}{b} \frac{\partial S}{\partial \zeta} \tag{3.26}$$

where the chain rule of differentiation[56] and the relationship of Equation 3.25 were used.

As indicated by Equations A-42 to A-51, it is necessary to integrate many different functions and products of functions in order to obtain a solution for a given problem. These operations are best performed by computer if they are first expressed in terms of matrices. As an illustration of the technique, the following integral from Equation A-48 will be considered:

$$[\Phi_2] = \int_y \{\phi,_{yy}\}\langle\phi,_{yy}\rangle \, dy \tag{A-48}$$

A set of shape functions, $\{\phi\}$, may be expressed by:

$$\{\phi\} = [C]\{H\} \tag{3-27}$$

where $[C]$ is a matrix of constant coefficients of shape functions and,

$$\{H\} = \begin{Bmatrix} 1 \\ \zeta \\ \zeta^2 \\ \zeta^3 \\ \zeta^4 \\ \zeta^5 \end{Bmatrix} \tag{3.28}$$

for a quintic polynomial. Differentiating Equation 3.27 twice with

respect to y gives:

$$\{\phi_{,yy}\} = [C]\{H_{,yy}\}$$

$$= \frac{4}{b^2}\,[C]\begin{Bmatrix} 0 \\ 0 \\ 2 \\ 6\zeta \\ 12\zeta^2 \\ 20\zeta^3 \end{Bmatrix} \tag{3.29}$$

where the relationship given by Equation 3.25 was used.

Using the relationships of Equation 3.29, the integrand of Equation A-48 may be written as follows:

$$\{\phi_{,yy}\}\langle\phi_{,yy}\rangle = [C]\{H_{,yy}\}\langle H_{,yy}\rangle[C]^T$$

$$= \frac{16}{b^2}\,[C]\begin{Bmatrix} 0 \\ 0 \\ 2 \\ 6\zeta \\ 12\zeta^2 \\ 20\zeta^3 \end{Bmatrix} \langle 0\ 0\ 2\ 6\zeta\ \ 12\zeta^2\ 20\zeta^3\rangle[C]^T$$

$$= \frac{16}{b^2}\,[C]\begin{bmatrix} 0 & 0 & 0 & 0 & 0 & 0 \\ 0 & 0 & 0 & 0 & 0 & 0 \\ 0 & 0 & 4 & 12\zeta & 24\zeta^2 & 40\zeta^3 \\ 0 & 0 & 12\zeta & 36\zeta^2 & 72\zeta^3 & 120\zeta^4 \\ 0 & 0 & 24\zeta^2 & 72\zeta^3 & 144\zeta^4 & 240\zeta^5 \\ 0 & 0 & 40\zeta^3 & 120\zeta^4 & 240\zeta^5 & 400\zeta^6 \end{bmatrix}[C]^T \tag{3.30}$$

The integral of Equation A-48 may now be evaluated by integrating each term in the matrix of variables in Equation 3.30, to obtain the following:

$$\int_y \{\phi,_{yy}\}\langle\phi,_{yy}\rangle dy =$$

$$\frac{16}{b^2}[C]\begin{bmatrix} 0 & 0 & 0 & 0 & 0 & 0 \\ 0 & 0 & 0 & 0 & 0 & 0 \\ 0 & 0 & 4\zeta & 6\zeta^2 & 8\zeta^3 & 10\zeta^4 \\ 0 & 0 & 6\zeta^2 & 12\zeta^3 & 18\zeta^4 & 24\zeta^5 \\ 0 & 0 & 8\zeta^3 & 18\zeta^4 & 24\zeta^5 & 40\zeta^6 \\ 0 & 0 & 10\zeta^4 & 24\zeta^5 & 40\zeta^6 & (400/7)\zeta^7 \end{bmatrix}_{\ell_1}^{\ell_2} [C]^T \tag{3.31}$$

where the elements of the matrix of variables are to be evaluated for the integration limits, ℓ_1 and ℓ_2. This method permits the use of computer techniques to obtain the integral of functions between any limits of integration. This is important because, depending on the level of stress and the stress distribution, longitudinal strips of a flange or a web may be elastic, yielded, or strain-hardened. Therefore the integration over a cross-section of a plate component is performed in a piecewise fashion between the limits of these zones so that the differing material properties may be included in the evaluation of a stiffness matrix. In this way also, abrupt changes in stress distribution may be accommodated in evaluating a geometric stiffness matrix.

3.11 Integration of Longitudinal Shape Functions

As shown in the formulation of the analytical technique in

Appendix A, extensive integration is also required for longitudinal shape functions. For example, factor F_1 in Equation A-42 is expressed as:

$$F_1 = \int_x f,_{xx}^2 \, dx \tag{A-42}$$

As discussed in Section 3.9, the function, $f(\xi)$, may be of the form,

$$f(\xi) = P_o(\xi) \; Sin(m\pi\xi) \tag{3.32}$$

where $P_o(\xi)$ is a polynomial function. As a result, the functions to be integrated over the length of a member may be quite complicated expressions depending on the order of the polynomial, $P_o(\xi)$, and therefore a numerical integration technique is used. The length of a member is divided into a number of equal intervals over which Gaussian quadrature[50] is used to integrate a function. The total integral over a length is obtained by adding together these sub-integrals. The number of intervals used for a given length is equal to the number of half sine wavelengths along a member and a 6-point Gauss integration[50] technique is performed for each interval.

3.12 General Procedure for W shapes

The procedure described in Section 3.4 is used to develop a bending stiffness matrix and a geometric stiffness matrix for the web and each flange of a W shape. These represent stiffness submatrices that must be assembled into overall stiffness matrices for an entire member. In assembling the matrices, compatibility between the flanges and web at a cross-section is maintained by enforcing zero

relative rotation between the plate components at a web-to-flange junction.

Figure 3.9 illustrates the node numbering and coordinate displacements for a typical W shape cross-section. The notations of this figure will be used in describing the assembly of a stiffness matrix. Since a bending stiffness matrix and a geometric stiffness matrix are both assembled in exactly the same manner the procedure is illustrated for a bending stiffness matrix assembly only. In Section 3.4 it was shown that a plate buckling problem reduced to an eigenvalue form as shown by Equation A-52 which can be rewritten as follows:

$$[K]\{\theta\} = \lambda[K_G]\{\theta\} \tag{3.33}$$

The bending strain energy of a component plate during buckling results in the term on the left hand side of this equation Therefore, assembling the stiffness submatrices of the two flanges and the web of a W shape section to obtain the assembled stiffness matrix is, in effect, equivalent to adding together the plate bending strain energies of the individual component plates. Using the notation given in Figure 3.9, the left hand side of Equation 3.33 may be written as;

$$[K]\{\theta\} = [K_1]\begin{Bmatrix} u_1 \\ u_1' \\ u_2 \\ u_2' \\ u_3' \end{Bmatrix} \tag{3.34}$$

for a lower flange;

$$[K]\{\theta\} = [K_w]\begin{Bmatrix} u_3' \\ u_3'' \\ u_4'' \\ u_4' \\ u_5'' \\ u_5' \end{Bmatrix} \tag{3.35}$$

for a web; and

$$[K]\{\theta\} = [K_u]\begin{Bmatrix} u_5' \\ u_6 \\ u_6' \\ u_7 \\ u_7' \end{Bmatrix} \tag{3.36}$$

for an upper flange. The slopes u_3' and u_5' represent the rotations of the flanges and web at the web-to-flange junctions of a W shape cross-section. The fact that u_3' is common to Equations 3.34 and 3.35 and u_5' is common to Equations 3.35 and 3.36 ensures compatibility (in this case, rigidity of attachment) between the flanges and web. Therefore in assembling the stiffness submatrices, $[K_l]$, $[K_w]$, and $[K_u]$, to obtain the total stiffness matrix of a W shape, stiffness elements of the submatrices corresponding to u_3' and u_5' must be added directly. This procedure is illustrated schematically in Figure 3.10.

3.13 Iteration on the Number of Wavelengths

The vector of coordinate displacements, $\{\theta\}$, represents the amplitudes of the shape functions defining the buckled shape of a cross-section. This vector is automatically obtained as a natural part of the process of matrix iteration[50] for each assumed value of m, where m is the number of half sine wavelengths of buckling along the length of a member. The correct value of m is that value for which the energy of a system is a minimum since this represents the lowest energy state of the buckled configuration[2].

In an actual solution, a starting value of $m = 1$ is assumed. This value is successively incremented in steps of unity and at each increment a matrix iteration is performed to determine an eigenvalue and the corresponding critical buckled shape of a cross-section. As m is incremented, the critical eigenvalue continues to decrease until a point of minimum potential energy of a system is reached. Thereafter, increases in m cause an increase in the potential energy. The correct value of m is that value for which the potential energy of the system is a minimum and the corresponding eigenpair gives the critical stress and the buckled shape of a cross-section.

3.14 Effect of Residual Stresses

Residual stresses acting on a W shape section alter the characteristics of a geometric stiffness matrix and therefore influence the value of a critical stress. In order to include this effect in the analysis, a residual strain pattern, as shown in Figure 3.11, is assumed. Such a pattern allows for a fairly general representation and has been used successfully by other investigators[37,51,57,58,59] in

assessing the effects of residual stresses. At the outset of a problem, values must be specified for ε_2, the residual tension strain at the lower edge of a web, ε_3, the residual compressive strain at mid-depth of a web, and ε_4, the residual tension strain at the upper edge of a web. The values of ε_1 and ε_5, the residual strains at the lower and upper flange tips respectively, are then determined using the following conditions of equilibrium for a cross-section subjected to residual stresses:

$$\Sigma F = 0 \tag{3.37}$$

$$\Sigma M = 0 \tag{3.38}$$

Equation 3.37 is an expression of translational equilibrium of a cross-section in the longitudinal direction of a member, and Equation 3.38 expresses equilibrium of a cross-section with respect to rotation about an axis perpendicular to the web.

The residual strain pattern of Figure 3.11 may be transformed into a stress pattern using a simple stress - strain relationship as shown in Figure 3.2. The forces and moments due to the residual stresses are obtained by integrating the effects of the stresses over the web and each flange of a W shape. Performing this integration, Equations 3.37 and 3.38 may be written as follows:

$$\Sigma F = 2A_u(\sigma_5-\sigma_4) + 2A_1(\sigma_1-\sigma_2) + A_w(2\sigma_3-\sigma_4-\sigma_1) = 0 \tag{3.39}$$

and,

$$\Sigma M = \frac{A_w h}{24}(6\sigma_3-5\sigma_4-\sigma_2) + \frac{h}{A_2}(\sigma_5-\sigma_4) = 0 \tag{3.40}$$

where, $\sigma_i (i=1,2,3,4,5)$ are stresses corresponding to the strains $\varepsilon_i (i=1,2,3,4,5)$, A_l is the area of a lower flange, A_u is the area of an upper flange, A_w is the web area, and h is the web height.

Solving Equations 3.39 and 3.40 simultaneously and using Figure 3.2 to transform from stress to strains, results in the following values:

$$\varepsilon_1 = \varepsilon_4 - \frac{A_w}{12A_u} (\varepsilon_2 - 6\varepsilon_3 + 5\varepsilon_4) \tag{3.41}$$

$$\varepsilon_5 = \varepsilon_2 - \frac{A_w}{12A_l} (5\varepsilon_2 - 6\varepsilon_3 + \varepsilon_4) \tag{3.42}$$

In subsequent formulations, residual strains are added to applied strains so that their effects on yielding and strain-hardening as well as their effects on decreasing a geometric stiffness matrix are included directly in the analytical technique.

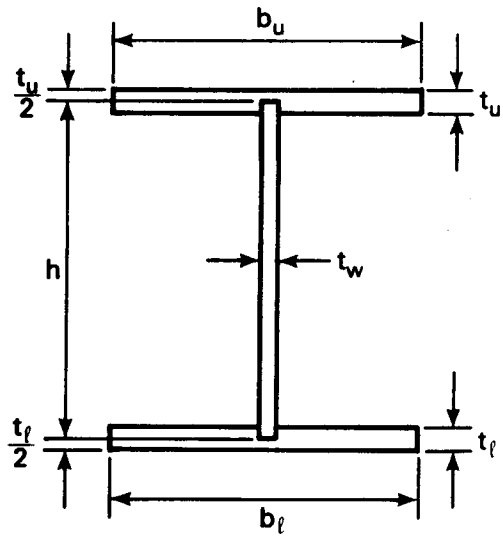

Figure 3.1 Idealized Cross-section

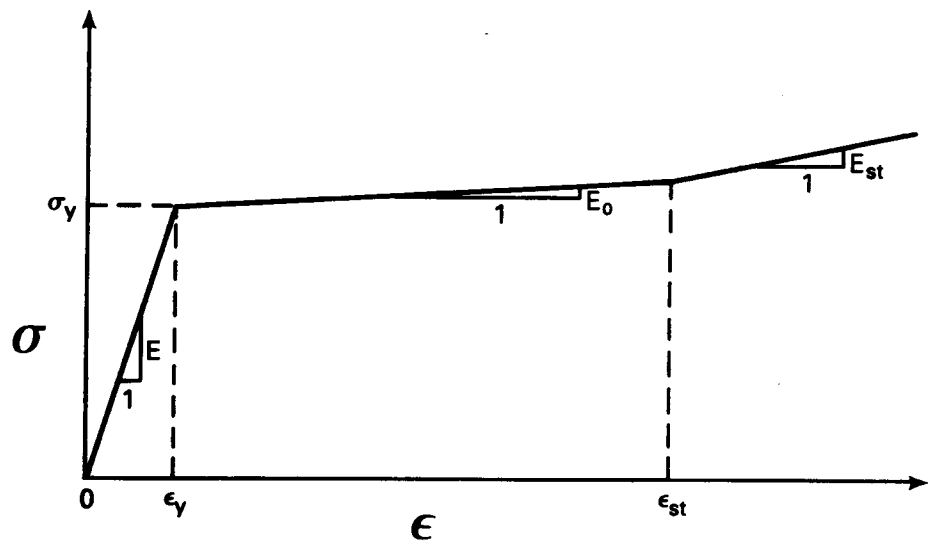

Figure 3.2 Idealized Tri-linear Stress-Strain Curve

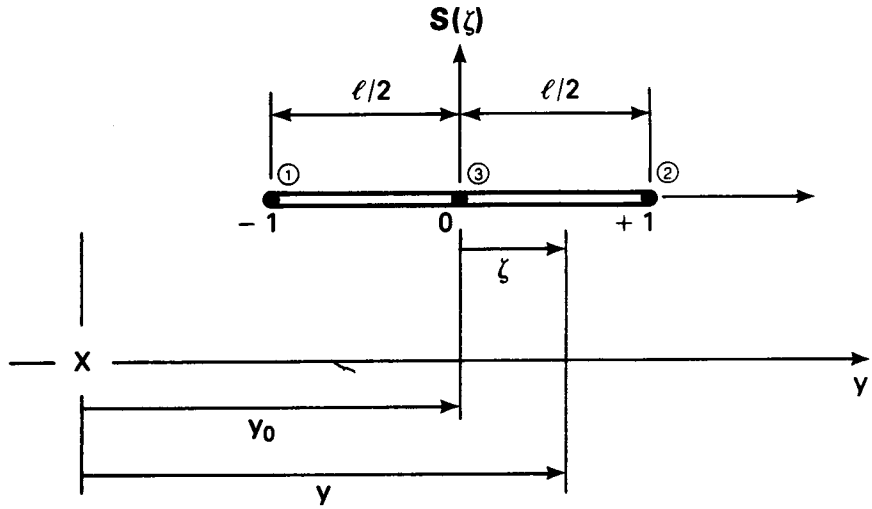

Figure 3.3 Relationship Between Cartesian and Natural Coordinates

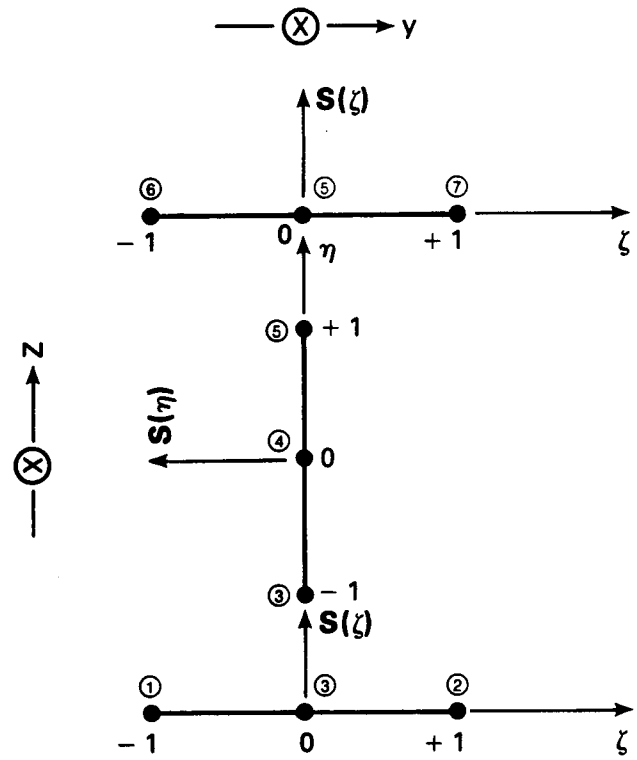

Figure 3.4 Local Coordinates and Numbering System

1. $U_1 = +1$

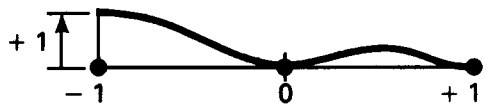

$$\phi_1 = \frac{1}{4}\zeta^2(\zeta - 1)^2(3\zeta + 4)$$

2. $U_1' = +1$

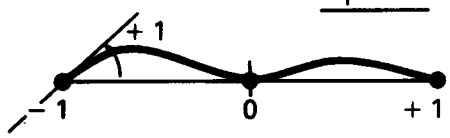

$$\phi_2 = \frac{b}{8}\zeta^2(\zeta + 1)(\zeta - 1)^2$$

3. $U_2 = +1$

$$\phi_3 = -\frac{\zeta^2}{4}(\zeta + 1)^2(3\zeta - 4)$$

4. $U_2' = +1$

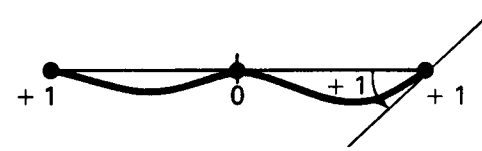

$$\phi_4 = \frac{b}{8}\zeta^2(\zeta - 1)(\zeta + 1)^2$$

5. $U_3' = +1$

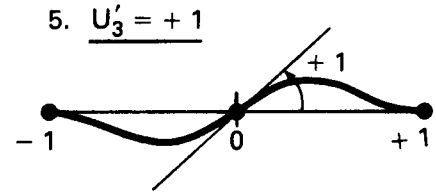

$$\phi_5 = \frac{b}{2}\zeta(\zeta^2 - 1)^2$$

$$\zeta = \frac{2y}{b}$$

b – flange width

Figure 3.5 Shape Functions for Flanges

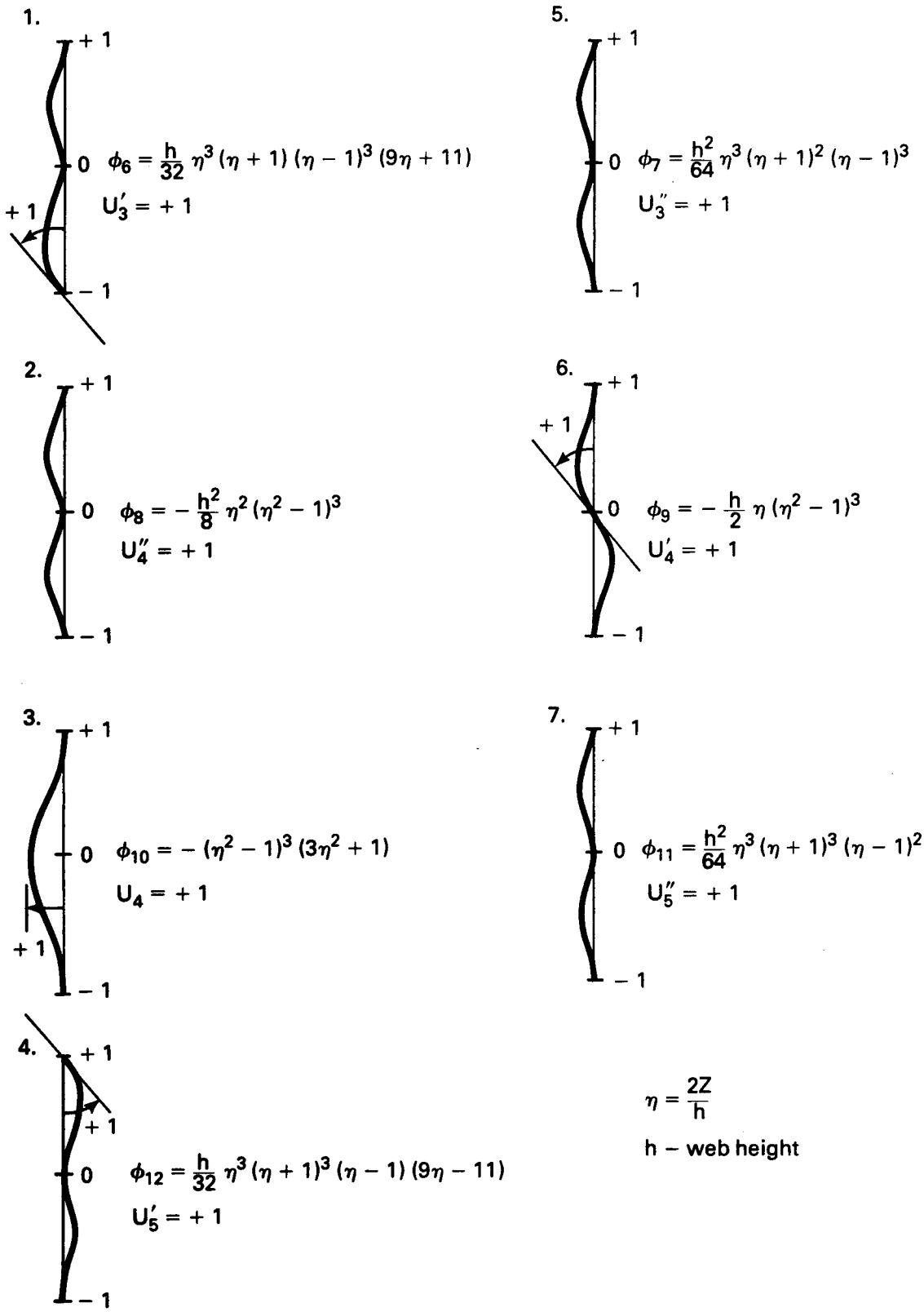

Figure 3.6 Shape Functions for Webs

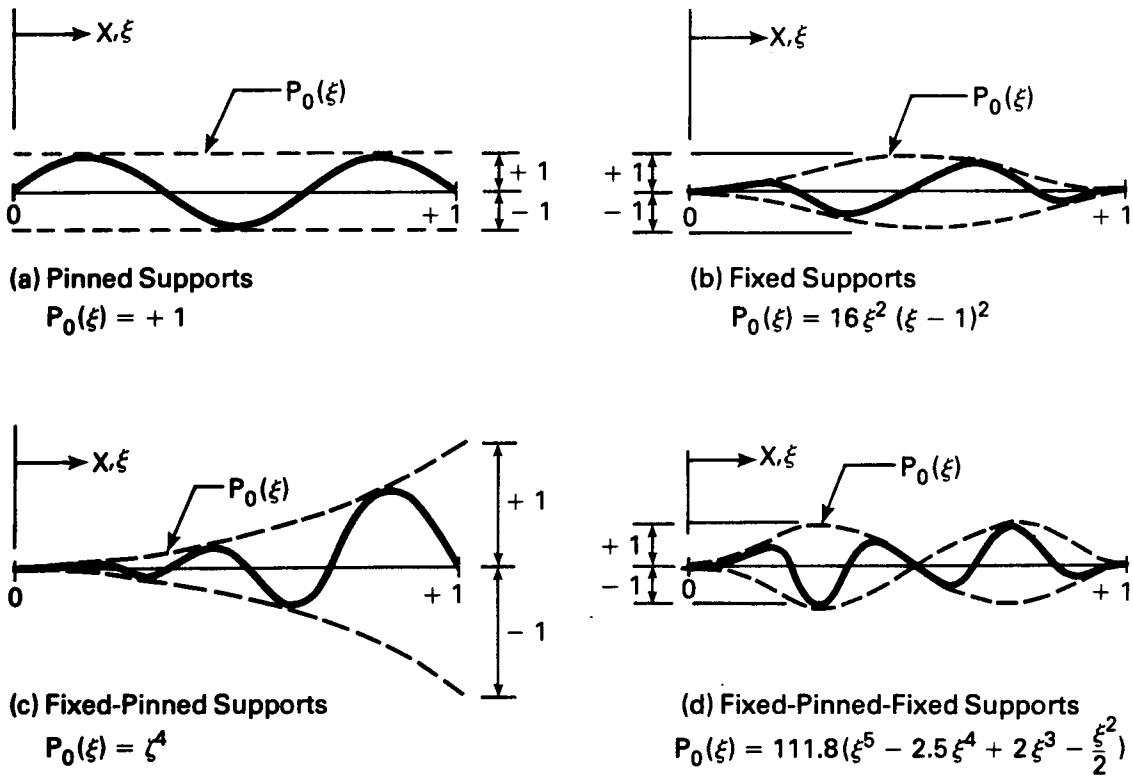

(a) Pinned Supports
$P_0(\xi) = +1$

(b) Fixed Supports
$P_0(\xi) = 16\xi^2(\xi - 1)^2$

(c) Fixed-Pinned Supports
$P_0(\xi) = \zeta^4$

(d) Fixed-Pinned-Fixed Supports
$P_0(\xi) = 111.8(\xi^5 - 2.5\xi^4 + 2\xi^3 - \frac{\xi^2}{2})$

$\xi = \frac{X}{L}$, L = member length

Figure 3.7 Longitudinal Shape Functions

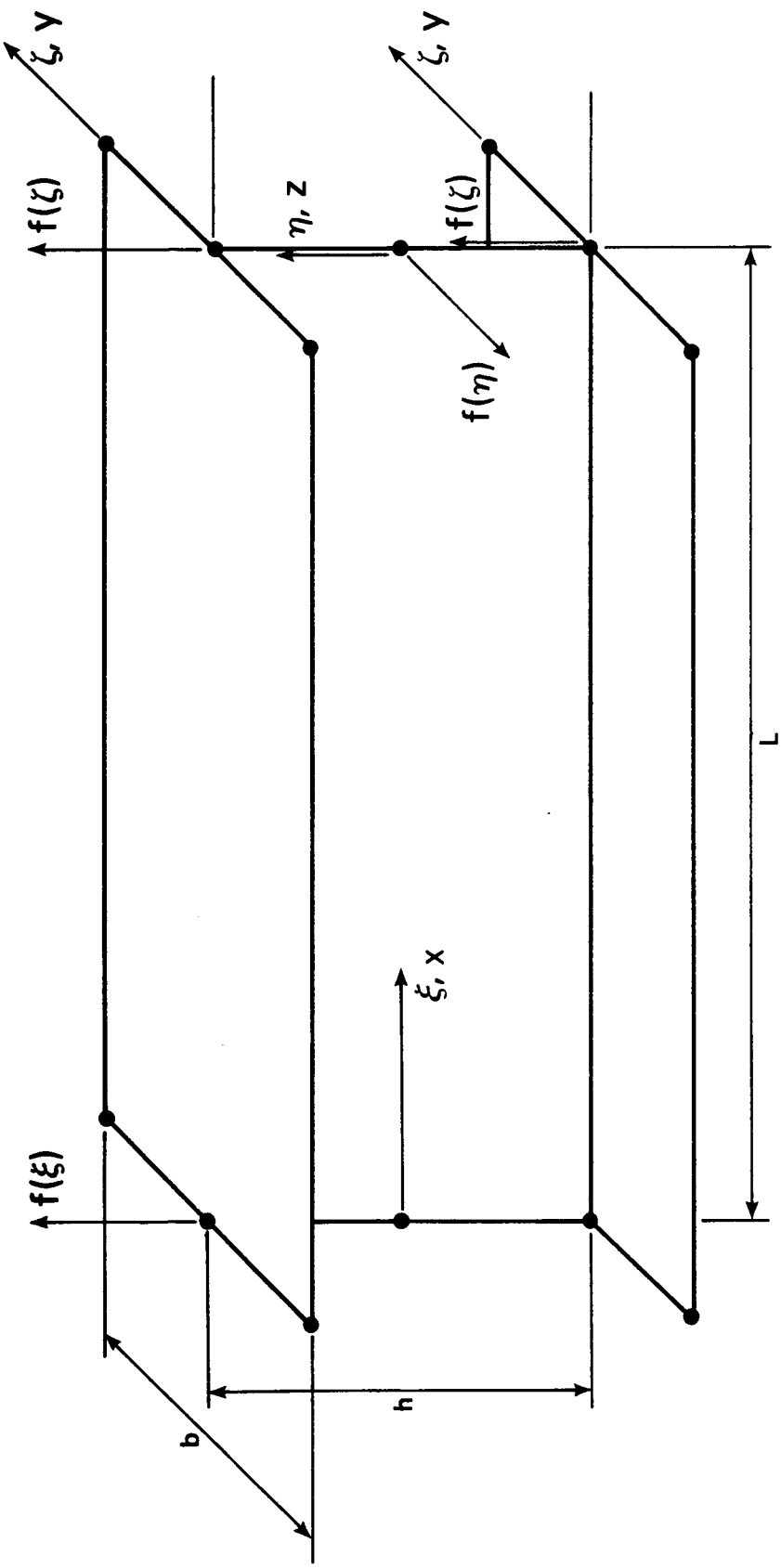

$\xi = X/L$
$\zeta = 2y/b$
$\eta = 2z/h$

Figure 3.8 Natural Coordinate Systems for a W shape

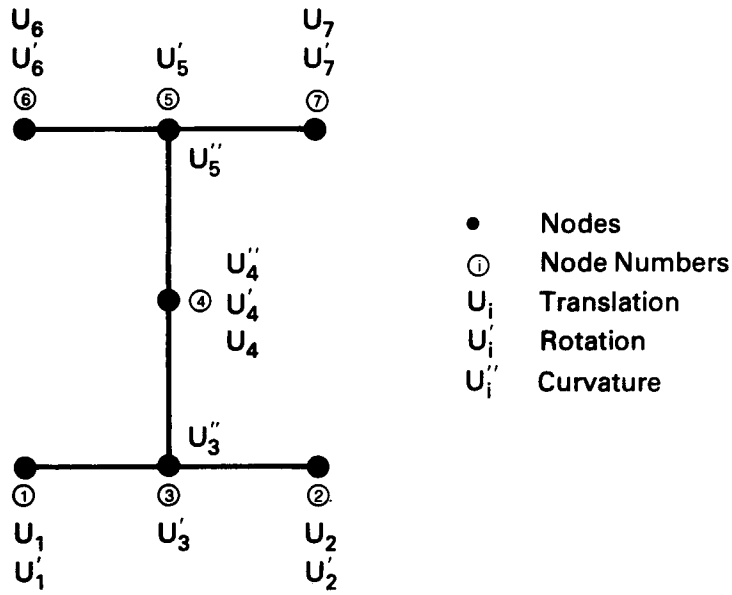

Figure 3.9 Node Numbering and Coordinate Displacements

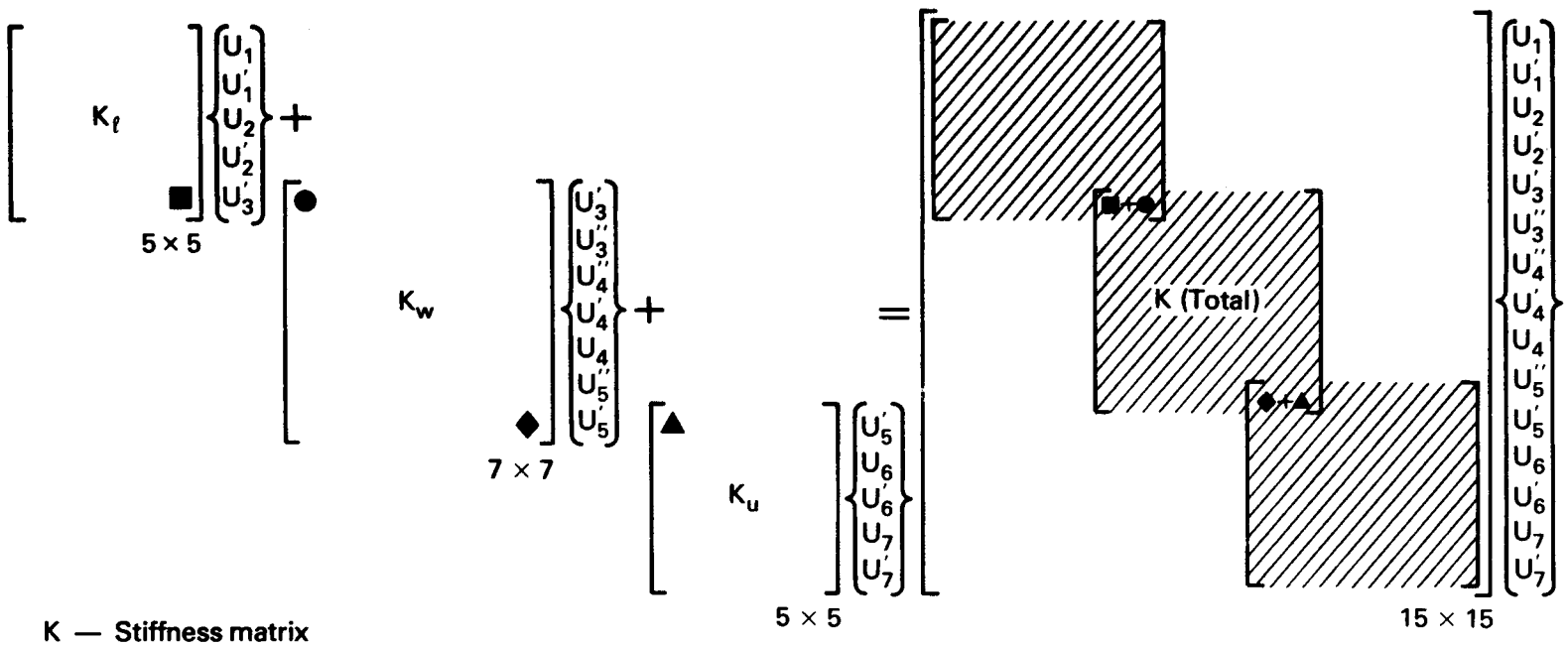

Figure 3.10 Schematic Stiffness Assembly

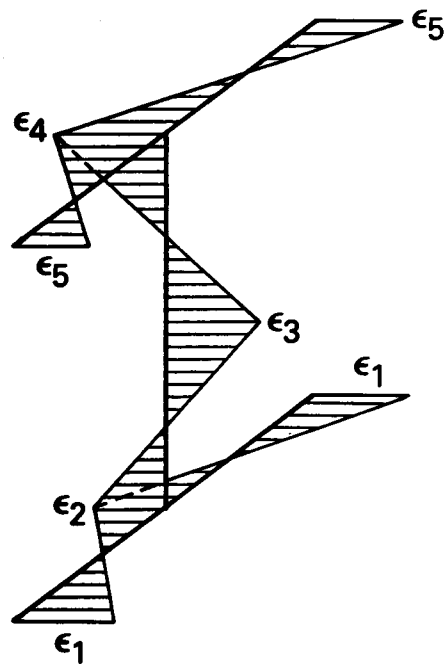

Figure 3.11 Residual Strain Distribution

Chapter 4

ANALYSIS FOR COMBINED AXIAL COMPRESSION AND BENDING

4.1 Introduction

In Chapter 3 a general formulation was presented for the analysis of buckling of plates subjected to piecewise linearly varying uniaxial stresses. The inclusion of residual stresses was also discussed and it was stated that the method could be applied to buckling in the elastic as well as the inelastic range. A W shape subjected to combined axial compression and strong-axis bending is composed of three uniaxially stressed plates (two flanges and a web). Because of the presence of residual stresses, uniaxial stresses on a component plate are piecewise linear at a section. The problem of local buckling of a W shape section is formulated by combining the effects of the individual component plates to obtain the total stiffness matrices for a member. In this chapter the procedure is explained in detail for the general loading case of a W shape section subjected to axial compression and strong axis bending combined. The formulation for the general case may be applied to a particular case of pure axial load or pure bending by setting the applied bending moment or the applied axial load equal to zero, respectively.

4.2 Assumptions

In Appendix A, a plate buckling condition is developed for a single uniaxially stressed rectangular plate. This buckling condition

is derived using the principle of virtual work and it is applicable to the elastic and inelastic ranges of stress. In addition to the usual assumptions of plate buckling presented in Appendix A, the following assumptions applicable to local buckling of a structural steel W shape section are made:

1. The member is loaded in such a way that all longitudinal fibres are subjected only to uniaxial stresses.
2. The idealized stress - strain response shown in Figure 3.2 applies for each longitudinal fibre in a cross-section.
3. The buckling condition expressed by Equation A-35 is applicable to material which is elastic, yielded, or strain-hardened.
4. Shape functions for a cross-section are continuous across boundaries between elastic and yielded material and between yielded and strain-hardened material.
5. Local buckling of component plates may occur when a cross-section is in any one of the following strain ranges:
   (a) fully elastic range
   (b) partly elastic and partly yielded range
   (c) fully yielded range
   (d) partly yielded and partly strain-hardened range
   (e) fully strain-hardened range
6. Member failure occurs when a plate component of a cross-section buckles locally.

4.3 Stiffness Matrix Formulations

4.3.1 Introduction

In the following sections, stiffness submatrices are formulated for individual plate components of a W shape. An applied uniform axial strain is superimposed on a general residual strain distribution such as that shown in Figure 4.1 where ε_i (i=1,2,3,4,5) are residual strains, and ε_a is an axial strain. A bending moment strain, ε_b, is then added. The resulting total strain distribution is used to determine the stresses on each component plate as well as the extent of yielded and strain-hardened regions within a plate. Stiffness submatrices are formulated for each plate component for a general case of material being partly elastic, partly yielded, and partly strain-hardened. The component plate stiffness submatrices are then combined as described in Chapter 3.

As previously mentioned, it is assumed for the purpose of clarity, that a section is oriented with its web in a vertical plane. Furthermore, it is assumed that the direction of an applied moment is such that it tends to place the upper flange in compression and the lower flange in tension. As a result of this assumption, the upper flange will always be in compression under the actions of the applied axial compression and bending loads combined. The lower flange, however, may be in tension when the axial load is low compared to the flexural load or in compression when the flexural load is low compared to the axial load. In the latter case, the general analysis of a lower flange is identical to that of an upper flange in compression.

4.3.2 Application of Incremental Bending Strains

In this analysis of local buckling of beam-columns, it is necessary to apply additional increments of bending strains to a cross-section. Before an increment is applied, a cross-section may be partially yielded or strain-hardened as a result of previously applied strains. Before additional bending strain increments can be applied it is therefore necessary to update the location of the neutral axis.

Figure 4.2(a) shows a cross-section which is partially elastic and partially yielded as a result of a total strain distribution such as that shown in Figure 4.1. The neutral axis is located at a distance, y_1, from the mid-depth of a web. This location is determined from the requirement that a cross-section must be in equilibrium under the action of applied loads. Once the neutral axis has been located the bending strains, ε_c, at mid-depth of a web, and ε_b', at the lower edge of a web may be determined from the strain geometry.

Referring to Figure 4.2(b), the following expressions for ε_c and ε_b' may be obtained:

$$\varepsilon_c = \left(\frac{2y_1}{2y_1-h}\right)\varepsilon_b \tag{4.1}$$

where h is the web depth and ε_b is the applied compressive bending strain, and

$$\varepsilon_b' = \left(\frac{h+2y_1}{h-2y_1}\right)\varepsilon_b . \tag{4.2}$$

In these relationships ε_c and ε_b' are given as functions of the applied compressive bending strain, ε_b. Thus the distribution of incremental bending strains is completely specified when a value of the applied strain, ε_b, is specified. In subsequent formulations an analytical technique is set up so that ε_b is an eigenvalue which corresponds to a critical buckling strain.

4.3.3 Stiffness Submatrices

In this section, bending and geometric stiffness submatrices are formulated for individual plate components of a W shape. The stiffness matrices, [K] and $[K_G]$, are formulated separately for a compression flange, a tension flange, and a web. For the purpose of analysis only, a web is considered to consist of two parts; the lower half of a web between nodes 3 and 4, and the upper half between nodes 4 and 5 as shown in Figure 3.9, Chapter 3. Because the origin of local coordinates is at node 4 of a web, this particular division simplifies the analysis somewhat with regard to integration of piecewise continuous functions along its height.

Equations A-53 and A-54 are expressions for bending and geometric plate stiffness matrices, respectively. These expressions are repeated below for ease of reference:

$$[K] = F_i[\Phi_i] \tag{A-53}$$

$$[K_G] = F_5[\Phi_5] \tag{A-54}$$

where i = 1,2,3,4 and repeated subscripts indicate summation in Equation A-53. In this expression, $[\Phi_i]$ are integral matrices as

defined by Equations A-47 to A-50, and F_i are material constants as defined by Equations A-42 to A-45. The values of F_i depend on whether the material is elastic, yielded, or strain-hardened. In Equation A-54, F_5 is a constant depending on the material thickness and is given by Equation A-46, and $[\Phi_5]$ is an integral matrix as defined by Equation A-51.

Partial yielding or strain-hardening of a cross-section results in non-uniform material properties and stresses defined piecewise over a section. Therefore, the integral expressions of Equations A-53 and A-54 are also defined piecewise over a section. The limits of integration correspond to the locations of material boundaries between elastic and yielded material and between yielded and strain-hardened material within a plate cross-section. Therefore, in order to carry out the integration required to determine [K], it is necessary to locate boundaries corresponding to material discontinuities within a plate cross-section. The evaluation of $[K_G]$ can be made once the stress discontinuities and stress distributions are determined for a plate cross-section. In the following sections these quantities are evaluated and explicit values of [K] and $[K_G]$ are determined for each plate component of a W shape.

4.3.3.1 Compression Flange

The distributions of strain and stress for a compression flange subjected to combined residual, axial, and flexural stresses are shown in Figure 4.3. In Figure 4.3(a), ε_a is an axial strain, ε_b is a bending strain, ε_4 is a residual tensile strain, ε_5 is a residual compressive strain, ε_y is a yield strain, and ε_{st} is a strain-hardening

strain. The corresponding stresses shown in Figure 4.3(b) are derived from the strain diagram according to the stress - strain relationship defined in Figure 3.2. In Figure 4.3(b), s_i(i = 1,2,3,4,5,6) are stress components and α_t and α_t', in natural coordinates, are the locations of the material boundaries between elastic and yielded and between yielded and strain-hardened material.

The values of α_t and α_t' are listed in Table 4.1(a) for various levels of strain. The second column of this table indicates the material condition for the corresponding range of strain indicated in the first column. For example, for the second strain range indicated the material is partially elastic (e) and partially yielded (y), and for the fifth strain range indicated the material is fully strain-hardened (s). The stresses defined piecewise for the various stress regions of Figure 4.3(b) are defined in Table 4.1(b). In this table, ζ is a natural coordinate as indicated in Figure 4.3, E is the elastic modulus, E_o is the slope of the yield portion of a stress - strain curve, and E_{st} is the strain-hardening modulus.

Using the limits of integration, α_t and α_t', as given in Table 4.1(a), and expanding the expression in Equation A-53 over the non-uniform material regions, the stiffness matrix for a flange in compression is given as:

$$[K] = F_{ie}\left[\Phi_i\right]_{-\alpha_t}^{\alpha_t} + F_{iy}\left[\left[\Phi_i\right]_{-\alpha_t'}^{-\alpha_t} + \left[\Phi_i\right]_{\alpha_t}^{\alpha_t'}\right]$$

$$+ F_{is}\left[\left[\Phi_i\right]_{-1}^{-\alpha_t'} + \left[\Phi_i\right]_{\alpha_t'}^{1}\right] \qquad (4.4)$$

where subscripts, e, y, and s, indicate that material constants, F_i, have elastic, yielded, and strain-hardened values, respectively. The limits of integration are shown as subscripts and superscripts on each integral matrix, and double subscripts, i, indicate summation.

The geometric stiffness matrix for a compression flange is obtained by substituting the stresses, S_i, from Table 4.1(b) into Equation A-54 and integrating between the appropriate limits defined in column one of Table 4.1(b). The following expression is obtained:

$$[K_G] = F_5 \left\{ s_1 \left[\left[\Phi_5\right]_{-1}^{-\alpha_t'} + \left[\Phi_5\right]_{\alpha_t'}^{1} \right] - s_2 \left[\left[\zeta\Phi_5\right]_{-1}^{-\alpha_t'} - \left[\zeta\Phi_5\right]_{\alpha_t'}^{1} \right] \right.$$

$$+ s_3 \left[\left[\Phi_5\right]_{-\alpha_t'}^{-\alpha_t} + \left[\Phi_5\right]_{\alpha_t}^{\alpha_t'} \right] - s_4 \left[\left[\zeta\Phi_5\right]_{-\alpha_t'}^{-\alpha_t} - \left[\zeta\Phi_5\right]_{\alpha_t}^{\alpha_t'} \right]$$

$$\left. + s_5 \left[\Phi_5\right]_{-\alpha_t}^{\alpha_t} - s_6 \left[\left[\zeta\Phi_5\right]_{-\alpha_t}^{0} - \left[\zeta\Phi_5\right]_{0}^{\alpha_t} \right] \right\} \qquad (4.5)$$

where $[\zeta\Phi_5]$ is used to indicate that matrix, $[\Phi_5]$, is multiplied by natural coordinate, ζ, before integration is performed. This accounts for linearly varying stresses on a portion of a plate cross-section.

4.3.3.2 Tension Flange

The strain and stress distributions for a flange in tension are shown in Figure 4.4. In addition to the previously explained symbols, ε_1 is the residual compressive stress at the flange tips and

ε_2 is the residual tensile stress at the flange-to-web junction. The strain ranges and limits of integration corresponding to Figure 4.4(a) are listed in Table 4.2(a) and the corresponding stresses and stress regions illustrated in Figure 4.4(b) are listed in Table 4.2(b).

The stiffness matrix for a tension flange may now be obtained by performing the integration in Equation A-53 over the limits indicated by Figure 4.4 and Table 4.2(a) and using the appropriate material constants, F_i. The resulting expression is as follows:

$$[K] = F_{ie}\left[\left[\Phi_i\right]_{-1}^{-\alpha_b} + \left[\Phi_i\right]_{\alpha_b}^{1}\right] + F_{iy}\left[\left[\Phi_i\right]_{-\alpha_b}^{-\alpha_b'} + \left[\Phi_i\right]_{\alpha_b'}^{\alpha_b}\right]$$

$$+ F_{is}\left[\Phi_i\right]_{-\alpha_b'}^{\alpha_b'} \tag{4.6}$$

The geometric stiffness matrix is obtained from Equation A-54 by substituting the stresses given in Table 4.2(b) and integrating over the appropriate limits as indicated in Figure 4.4 and Table 4.2(b). The resulting expression is as follows:

$$[K_G] = F_5\Bigg\{S_1\left[\left[\Phi_5\right]_{-1}^{-\alpha_b} + \left[\Phi_5\right]_{\alpha_b}^{1}\right] - S_2\left[\left[\zeta\Phi_5\right]_{-1}^{-\alpha_b} - \left[\zeta\Phi_5\right]_{\alpha_b}^{1}\right]$$

$$+ S_3\left[\left[\Phi_5\right]_{-\alpha_b}^{-\alpha_b'} + \left[\Phi_5\right]_{\alpha_b'}^{\alpha_b}\right] - S_4\left[\left[\zeta\Phi_5\right]_{-\alpha_b}^{-\alpha_b'} - \left[\zeta\Phi_5\right]_{\alpha_b'}^{\alpha_b}\right]$$

$$+ S_5\left[\Phi_5\right]_{-\alpha_b'}^{\alpha_b'} - S_6\left[\left[\zeta\Phi_5\right]_{-\alpha_b'}^{0} - \left[\zeta\Phi_5\right]_{0}^{\alpha_b'}\right]\Bigg\} \tag{4.7}$$

4.3.3.3 Web - Tension Zone

The general strain and stress distributions for the lower half of a web (loaded in the orientation described previously) are shown in Figure 4.5. In this Figure, β_1, β_1', β_3, and β_3', in natural coordinates, locate the boundaries between elastic and yielded material and between yielded and strain-hardened material. These values are defined in Tables 4.3(a) and 4.3(b) for the various ranges of strain indicated. The stresses corresponding to the stress regions indicated, are listed in Table 4.3(c).

Referring to Figure 4.5 and Table 4.3 and proceeding in the manner described previously for the flanges, the bending stiffness and geometric stiffness matrices for the tension zone of a web are obtained as follows:

$$[K] = F_{ie}\left[\Phi_i\right]_{-\beta_1}^{-\beta_3} + F_{iy}\left[\left[\Phi_i\right]_{-\beta_1'}^{-\beta_1} + \left[\Phi_i\right]_{-\beta_3}^{-\beta_3'}\right] + F_{is}\left[\left[\Phi_i\right]_{-1}^{-\beta_1'} + \left[\Phi_i\right]_{-\beta_3'}^{0}\right] \tag{4.8}$$

and,

$$[K_G] = F_5\left\{s_1\left[\Phi_5\right]_{-1}^{-\beta_1'} + s_2\left[\left[\eta\Phi_5\right]_{-1}^{-\beta_1'} + \left[\eta\Phi_5\right]_{-\beta_3'}^{0}\right] + s_3\left[\Phi_5\right]_{-\beta_1'}^{-\beta_1} + s_4\left[\left[\eta\Phi_5\right]_{-\beta_1'}^{-\beta_1} + \left[\eta\Phi_5\right]_{-\beta_3}^{-\beta_3'}\right]\right.$$

... continued

$$+ s_5\left[\Phi_5\right]_{-\beta_1}^{-\beta_3} + s_6\left[\eta\Phi_5\right]_{-\beta_1}^{-\beta_3} + s_7\left[\Phi_5\right]_{-\beta_3}^{-\beta_3'}$$

$$+ s_8\left[\Phi_5\right]_{-\beta_3'}^{0} \Bigg\} \qquad (4.9)$$

4.3.3.4 Web - Compression Zone

Because of the complex yield pattern possible under the actions of residual, axial, and flexural stresses combined, three cases must be considered for the compression zone of a web. These three cases correspond to the material condition at the center of the web which may be elastic, yielded, or strain-hardened at the time the incremental bending strains are applied. Each of the three cases is considered separately.

The strain and stress distributions for the compression zone of a web when the center of the web is elastic are shown in Figure 4.6. In this case the total strain at a web center must not be greater than the yield strain, and therefore,

$$\varepsilon_a + \varepsilon_c + \varepsilon_3 \leq \varepsilon_y \qquad (4.10)$$

The material boundaries corresponding to the various ranges of strain possible are given in Table 4.4(a) and the stresses corresponding to the material zones indicated in Figure 4.6(b) are listed in Table 4.4(b). Referring to Figure 4.6 and Table 4.4, and proceeding as described for the previous cases, the bending and

geometric stiffness matrices may be written as follows:

$$[K] = F_{ie}\left[\Phi_i\right]_0^{\beta_2} + F_{iy}\left[\Phi_i\right]_{\beta_2}^{\beta_2'} + F_{is}\left[\Phi_i\right]_{\beta_2'}^{1} \tag{4.11}$$

and,

$$[K_G] = F_5 \left\{ s_1\left[\Phi_5\right]_0^{\beta_2} + s_2\left[\eta\Phi_5\right]_0^{\beta_2} + s_3\left[\Phi_5\right]_{\beta_2}^{\beta_2'} \right.$$

$$\left. + s_4\left[\Phi_5\right]_{\beta_2}^{\beta_2'} + s_5\left[\Phi_5\right]_{\beta_2'}^{1} + s_6\left[\Phi_5\right]_{\beta_2'}^{1} \right\} \tag{4.12}$$

The center of a web is yielded when,

$$\varepsilon_y < \varepsilon_a + \varepsilon_c + \varepsilon_3 \leq \varepsilon_{st} \tag{4.13}$$

and the corresponding strain and stress distributions as well as the limits of integration and various material zones are described in Figure 4.7 and Table 4.5. Using the appropriate values obtained therefrom, the bending and geometric stiffness matrices for this case may be written as follows:

$$[K] = F_{ie}\left[\Phi_i\right]_{\beta_2}^{\beta_2'} + F_{iy}\left[\Phi_i\right]_0^{\beta_2} + F_{is}\left[\Phi_i\right]_{\beta_2'}^{1} \tag{4.14}$$

and,

$$[K_G] = F_5 \left\{ s_1 \left[\Phi_5\right]_0^{\beta_2} + s_2 \left[\eta\Phi_5\right]_0^{\beta_2} + s_3 \left[\Phi_5\right]_{\beta_2}^{\beta_2'} \right.$$

$$\left. + s_4 \left[\eta\Phi_5\right]_{\beta_2}^{\beta_2'} + s_5 \left[\Phi_5\right]_{\beta_2'}^{1} + s_6 \left[\eta\Phi_5\right]_{\beta_2'}^{1} \right\} \tag{4.15}$$

The third and final case which must be considered for the compression zone of a web is that corresponding to the center of the web being in the strain-hardened condition. In this case,

$$\varepsilon_{st} < \varepsilon_a + \varepsilon_c + \varepsilon_3 \tag{4.16}$$

The corresponding distributions of strain and stress are shown in Figure 4.8 and the material boundaries and stress components for each region are given in Table 4.6. The resulting expressions for the bending and geometric stiffness matrices are as follows:

$$[K] = F_{ie} \left[\Phi_i\right]_{\beta_2}^{1} + F_{iy} \left[\Phi_i\right]_{\beta_2'}^{\beta_2} + F_{is} \left[\Phi_i\right]_0^{\beta_2'} \tag{4.17}$$

and,

$$[K_G] = F_5 \left\{ s_1 \left[\Phi_5\right]_0^{\beta_2'} + s_2 \left[\eta\Phi_5\right]_0^{\beta_2'} + s_3 \left[\Phi_5\right]_{\beta_2'}^{\beta_2} \right.$$

$$\left. + s_4 \left[\eta\Phi_5\right]_{\beta_2'}^{\beta_2} + s_5 \left[\Phi_5\right]_{\beta_2}^{1} + s_6 \left[\eta\Phi_5\right]_{\beta_2}^{1} \right\} \qquad (4.18)$$

4.4 Iterative Technique

In the solution of a particular problem, bending stiffness and geometric stiffness submatrices for each flange and a web are formulated as described in the previous sections. The global stiffness matrices are then assembled as explained in Chapter 3. In any problem of axial, bending, or combined loading, the required eigenvalue will be either ε_b, the bending strain, or ε_a the axial strain. However, because of material and stress non-linearities over a cross-section, the bending stiffness matrix, [K], and the geometric stiffness matrix, $[K_G]$, are implicit functions of the eigenvalue strain. Therefore at each successive value of an eigenvalue strain, it is necessary to reformulate [K] and $[K_G]$ for that particular value of strain. Thus an iterative technique is required.

As described in Chapter 3, an eigenvalue problem reduces to the form:

$$\left[[K] - [K_G]\right]\{\theta\} = \{0\} \qquad (4.19)$$

As stated previously, [K] and $[K_G]$ are implicit functions of $(\varepsilon_b + \varepsilon_a)$ when a material is non-linear. Equation 4.19 may be re-written as

follows:

$$\left[[K] - \lambda_o\left[K_{G_o}\right]\right]\{\theta\} = \{0\} \tag{4.20}$$

where,

$$\left[K_{G_o}\right] = \frac{1}{\varepsilon_b+\varepsilon_a}\left[K_G\right] \tag{4.21}$$

In the solution of Equation 4.20, a value of $(\varepsilon_b + \varepsilon_a)$ is assumed. Knowing this value, the elastic, yield, and strain-hardening material zones in a cross-section as well as the discontinuous stress distributions are fully defined. Therefore, [K] and $[K_{G_o}]$ are completely determinable and matrix iteration may be performed to determine λ_o. The solution to Equation 4.19 will be obtained when,

$$\frac{\lambda_o}{\varepsilon_b+\varepsilon_a} = 1.0 \tag{4.22}$$

In general, this will require the determination of several values of λ_o by matrix iteration. An exact solution is obtained when the eigenvalue, λ_o, is equal to the assumed value of $\varepsilon_b + \varepsilon_a$. In general, however, this will not be true, and,

$$\lambda_o = \lambda' + \lambda'' \tag{4.23}$$

where,

$$\lambda' = \varepsilon_b + \varepsilon_a \tag{4.24}$$

and λ'' is a residue which represents the amount by which λ_o deviates

from the exact value of $(\varepsilon_b + \varepsilon_a)$. Thus, the problem reduces to that of finding a value of λ_o such that,

$$|\lambda''| = |\lambda_o - \lambda'| \leq e \tag{4.25}$$

where e, is a small positive value which reflects the required precision of a solution.

For the purpose of illustration, Figure 4.9 shows a graph of $(\lambda_o - \lambda')$ vs. $(\varepsilon_b + \varepsilon_a)$. In the iteration technique, an initial value of $(\varepsilon_b + \varepsilon_a)$ is choosen so that $(\lambda_o - \lambda')$ is positive. Another value of $(\varepsilon_b + \varepsilon_a)$ is found so that the corresponding value of $(\lambda_o - \lambda')$ is negative. Once these two starting values have been found (by trial and error, if necessary) the method of bisection[31] is used to determine a value of $(\varepsilon_b + \varepsilon_a)$ for which $|\lambda_o - \lambda'| \leq e$. Once the convergence criterion is satisfied, the critical bending strain is given by:

$$\varepsilon_{b_{cr}} = \lambda_o - \varepsilon_a \tag{4.26}$$

This general technique may be used for pure bending when $\varepsilon_a = 0$, or for pure axial load when $\varepsilon_b = 0$. In the case of axial compression and bending combined, ε_a is a constant value of axial strain depending on the magnitude of applied axial load.

Strain Range	Material Condition	Location of Material Boundaries α_t	Location of Material Boundaries α'_t
$\varepsilon_b+\varepsilon_a \le \varepsilon_y-\varepsilon_5$	(e)	1.0	1.0
$\varepsilon_y-\varepsilon_5 < \varepsilon_b+\varepsilon_a \le \varepsilon_y+\varepsilon_4$	(e,y)	$\frac{\varepsilon_y+\varepsilon_4-\varepsilon_b-\varepsilon_a}{\varepsilon_4+\varepsilon_5}$	1.0
$\varepsilon_y+\varepsilon_4 < \varepsilon_b+\varepsilon_a \le \varepsilon_{st}-\varepsilon_5$	(y)	0.0	1.0
$\varepsilon_{st}-\varepsilon_5 < \varepsilon_b+\varepsilon_a \le \varepsilon_{st}+\varepsilon_4$	(y,s)	0.0	$\frac{\varepsilon_{st}+\varepsilon_4-\varepsilon_b-\varepsilon_a}{\varepsilon_4+\varepsilon_5}$
$\varepsilon_{st}+\varepsilon_4 < \varepsilon_b+\varepsilon_a$	(s)	0.0	0.0

(a) Strains

Stress Region		Stress	Stress Components
$-1.0 \le \zeta \le -\alpha'_t$	(s)	$s_1-s_2\zeta$	$s_1 = \sigma_y+(\varepsilon_{st}-\varepsilon_y)E_o+(\varepsilon_b+\varepsilon_a-\varepsilon_{st}-\varepsilon_4)E_{st}$
$-\alpha'_t \le \zeta \le -\alpha_t$	(y)	$s_3-s_4\zeta$	$s_2 = (\varepsilon_4+\varepsilon_5)E_{st}$
$-\alpha_t \le \zeta \le 0.0$	(e)	$s_5-s_6\zeta$	$s_3 = \sigma_y+(\varepsilon_b+\varepsilon_a-\varepsilon_y-\varepsilon_4)E_o$
$0.0 \le \zeta \le \alpha_t$	(e)	$s_5+s_6\zeta$	$s_4 = (\varepsilon_4+\varepsilon_5)E_o$
$\alpha_t \le \zeta \le \alpha'_t$	(y)	$s_3+s_4\zeta$	$s_5 = (\varepsilon_b+\varepsilon_a-\varepsilon_4)E$
$\alpha'_t \le \zeta \le 1.0$	(s)	$s_1+s_2\zeta$	$s_6 = (\varepsilon_4+\varepsilon_5)E$

(b) Stresses

Table 4.1 Stresses and Strains for a Compression Flange

Strain Range	Material Condition	Location of Material Boundaries	
		α_b	α_b'
$\varepsilon_b'-\varepsilon_a \leq \varepsilon_y-\varepsilon_2$	(e)	0.0	0.0
$\varepsilon_y-\varepsilon_2 < \varepsilon_b'-\varepsilon_a \leq \varepsilon_y+\varepsilon_1$	(e,y)	$\frac{\varepsilon_b'-\varepsilon_a-\varepsilon_y+\varepsilon_2}{\varepsilon_1+\varepsilon_2}$	0.0
$\varepsilon_y+\varepsilon_1 < \varepsilon_b'-\varepsilon_a \leq \varepsilon_{st}-\varepsilon_2$	(y)	1.0	0.0
$\varepsilon_{st}-\varepsilon_2 < \varepsilon_b'-\varepsilon_a \leq \varepsilon_{st}+\varepsilon_1$	(y,s)	1.0	$\frac{\varepsilon_b'-\varepsilon_a-\varepsilon_{st}+\varepsilon_2}{\varepsilon_1+\varepsilon_2}$
$\varepsilon_{st}+\varepsilon_1 < \varepsilon_b'-\varepsilon_a$	(s)	1.0	1.0

(a) Strains

Stress Region		Stresses	Stress Components
$-1.0 \leq \zeta \leq -\alpha_b$	(e)	$s_1-s_2\zeta$	$s_1 = (\varepsilon_a-\varepsilon_b'-\varepsilon_2)E$
$-\alpha_b \leq \zeta \leq -\alpha_b'$	(y)	$s_3-s_4\zeta$	$s_2 = (\varepsilon_1+\varepsilon_2)E$
$-\alpha_b' \leq \zeta \leq 0.0$	(s)	$s_5-s_6\zeta$	$s_3 = -\sigma_y+(\varepsilon_y-\varepsilon_2+\varepsilon_a-\varepsilon_b')E_o$
$0.0 \leq \zeta \leq \alpha_b'$	(s)	$s_5+s_6\zeta$	$s_4 = (\varepsilon_1+\varepsilon_2)E_o$
$\alpha_b' \leq \zeta \leq \alpha_b$	(y)	$s_3+s_4\zeta$	$s_5 = -\sigma_y-(\varepsilon_{st}-\varepsilon_y)E_o+(\varepsilon_{st}+\varepsilon_a-\varepsilon_b'-\varepsilon_2)E_{st}$
$\alpha_b \leq \zeta \leq 1.0$	(e)	$s_1+s_2\zeta$	$s_6 = (\varepsilon_1+\varepsilon_2)E_{st}$

(b) Stresses

Table 4.2 Stresses and Strains for a Tension Flange.

Strain Range	Material Condition	Location of Material Boundaries β_1	β_1'
$\varepsilon_b'-\varepsilon_a \leq \varepsilon_y-\varepsilon_2$	(e)	1.0	1.0
$\varepsilon_y-\varepsilon_2 < \varepsilon_b'-\varepsilon_a \leq \varepsilon_{st}-\varepsilon_2$	(e,y)	$\frac{\varepsilon_a+\varepsilon_c+\varepsilon_y+\varepsilon_3}{\varepsilon_b'+\varepsilon_c+\varepsilon_2+\varepsilon_3}$	1.0
$\varepsilon_{st}-\varepsilon_2 < \varepsilon_b'-\varepsilon_a$	(e,y,s)	$\frac{\varepsilon_a+\varepsilon_c+\varepsilon_y+\varepsilon_3}{\varepsilon_b'+\varepsilon_c+\varepsilon_2+\varepsilon_3}$	$\frac{\varepsilon_a+\varepsilon_c+\varepsilon_{st}+\varepsilon_3}{\varepsilon_b'+\varepsilon_c+\varepsilon_2+\varepsilon_3}$

(a) Strains Adjacent to Lower Edge of Web

Strain Range	Material Condition	Location of Material Boundaries β_3	β_3'
$\varepsilon_a+\varepsilon_c+\varepsilon_3 \leq \varepsilon_y$	(e)	0.0	0.0
$\varepsilon_y < \varepsilon_a+\varepsilon_c+\varepsilon_3 \leq \varepsilon_{st}$	(e,y)	$\frac{\varepsilon_a+\varepsilon_c+\varepsilon_3-\varepsilon_y}{\varepsilon_b'+\varepsilon_c+\varepsilon_2+\varepsilon_3}$	0.0
$\varepsilon_{st} < \varepsilon_a+\varepsilon_c+\varepsilon_3$	(e,y,s)	$\frac{\varepsilon_a+\varepsilon_c+\varepsilon_3-\varepsilon_y}{\varepsilon_b'+\varepsilon_c+\varepsilon_2+\varepsilon_3}$	$\frac{\varepsilon_a+\varepsilon_c+\varepsilon_3-\varepsilon_{st}}{\varepsilon_b'+\varepsilon_c+\varepsilon_2+\varepsilon_3}$

(b) Strains Adjacent to Middle of Web

Table 4.3 Stresses and Strains for the Tension Zone of a Web --

... cont'd.

Table 4.3 - continued

Stress Region		Stress	Stress Components
$-1 \le \eta \le -\beta_1'$	(s)	$s_1+s_2\eta$	$s_1 = -\sigma_y-(\varepsilon_{st}-\varepsilon_y)E_o+(\varepsilon_a+\varepsilon_c+\varepsilon_{st}+\varepsilon_3)E_{st}$
$-\beta_1' \le \eta \le -\beta_1$	(y)	$s_3+s_4\eta$	$s_2 = (\varepsilon_b'+\varepsilon_c+\varepsilon_2+\varepsilon_3)E_{st}$
$-\beta_1 \le \eta \le -\beta_3$	(e)	$s_5+s_6\eta$	$s_3 = -\sigma_y+(\varepsilon_a+\varepsilon_c+\varepsilon_y+\varepsilon_3)E_o$
$-\beta_3 \le \eta \le -\beta_3'$	(y)	$s_7+s_4\eta$	$s_4 = (\varepsilon_b'+\varepsilon_c+\varepsilon_2+\varepsilon_3)E_o$
$-\beta_3' \le \eta \le 0$	(s)	$s_8+s_2\eta$	$s_5 = (\varepsilon_a+\varepsilon_c+\varepsilon_3)E$
			$s_6 = (\varepsilon_b'+\varepsilon_c+\varepsilon_2+\varepsilon_3)E$
			$s_7 = \sigma_y+(\varepsilon_a+\varepsilon_c+\varepsilon_3-\varepsilon_y)E_o$
			$s_8 = \sigma_y+(\varepsilon_{st}-\varepsilon_y)E_o+(\varepsilon_a+\varepsilon_c+\varepsilon_{st}+\varepsilon_3)E_{st}$

(c) Stresses

Table 4.3 Stresses and Strains for the Tension Zone of a Web

Strain Range	Material Condition	Location of Material Boundaries β_2	Location of Material Boundaries β_2'
$\varepsilon_b+\varepsilon_a \le \varepsilon_y+\varepsilon_4$	(e)	1.0	1.0
$\varepsilon_y+\varepsilon_4 < \varepsilon_b+\varepsilon_a \le \varepsilon_{st}+\varepsilon_4$	(e,y)	$\frac{\varepsilon_y-\varepsilon_3-\varepsilon_c-\varepsilon_a}{\varepsilon_b-\varepsilon_c-\varepsilon_3-\varepsilon_4}$	1.0
$\varepsilon_{st}+\varepsilon_4 < \varepsilon_b+\varepsilon_a$	(e,y,s)	$\frac{\varepsilon_y-\varepsilon_3-\varepsilon_c-\varepsilon_a}{\varepsilon_b-\varepsilon_c-\varepsilon_3-\varepsilon_4}$	$\frac{\varepsilon_{st}-\varepsilon_3-\varepsilon_c-\varepsilon_a}{\varepsilon_b-\varepsilon_c-\varepsilon_3-\varepsilon_4}$

(a) Strains

Stress Region		Stresses	Stress Components
$0.0 \le \eta \le \beta_2$	(e)	$s_1+s_2\eta$	$s_1 = (\varepsilon_a+\varepsilon_c+\varepsilon_3)E$
			$s_2 = \varepsilon_b-\varepsilon_c-\varepsilon_3-\varepsilon_4$
$\beta_2 \le \eta \le \beta_2'$	(y)	$s_3+s_4\eta$	$s_3 = \sigma_y+(\varepsilon_a+\varepsilon_c-\varepsilon_y+\varepsilon_3)E_o$
			$s_4 = (\varepsilon_b-\varepsilon_c-\varepsilon_3-\varepsilon_4)E_o$
$\beta_2' \le \eta \le 1.0$	(s)	$s_5+s_6\eta$	$s_5 = \sigma_y+(\varepsilon_{st}-\varepsilon_y)E_o+(\varepsilon_a+\varepsilon_c-\varepsilon_{st}+\varepsilon_3)E_{st}$
			$s_6 = (\varepsilon_b-\varepsilon_c-\varepsilon_3-\varepsilon_4)E_{st}$

(b) Stresses

Table 4.4 Stresses and Strains in the Compression Zone of a Web (Case I - Center of Web Elastic)

Strain Range	Material Condition	Location of Material Boundaries β_2	Location of Material Boundaries β_2'
$\varepsilon_b+\varepsilon_a \le \varepsilon_y+\varepsilon_4$	(e)	$\frac{\varepsilon_y-\varepsilon_3-\varepsilon_a-\varepsilon_c}{\varepsilon_b-\varepsilon_c-\varepsilon_3-\varepsilon_4}$	1.0
$\varepsilon_y+\varepsilon_4 < \varepsilon_b+\varepsilon_a \le \varepsilon_{st}+\varepsilon_4$	(e,y)	1.0	1.0
$\varepsilon_{st}+\varepsilon_4 < \varepsilon_b+\varepsilon_a$	(y,s)	$\frac{\varepsilon_{st}-\varepsilon_3-\varepsilon_a-\varepsilon_c}{\varepsilon_b-\varepsilon_c-\varepsilon_3-\varepsilon_4}$	$\frac{\varepsilon_{st}-\varepsilon_3-\varepsilon_a-\varepsilon_c}{\varepsilon_b-\varepsilon_c-\varepsilon_3-\varepsilon_4}$

(a) Strains

Stress Region		Stress	Stress Components
$0.0 \le \eta \le \beta_2$	(y)	$s_1+s_2\eta$	$s_1 = \sigma_y+(\varepsilon_a+\varepsilon_c-\varepsilon_y+\varepsilon_3)E_o$
			$s_2 = (\varepsilon_b-\varepsilon_c-\varepsilon_3-\varepsilon_4)E_o$
			$s_3 = (\varepsilon_a+\varepsilon_c+\varepsilon_3)E$
$\beta_2 \le \eta \le \beta_2'$	(e)	$s_3+s_4\eta$	$s_4 = (\varepsilon_b+\varepsilon_c-\varepsilon_3-\varepsilon_4)E$
			$s_5 = \sigma_y+(\varepsilon_s-\varepsilon_y)E_o+$
			$(\varepsilon_a+\varepsilon_c-\varepsilon_{st}+\varepsilon_3)E_{st}$
$\beta_2' \le \eta \le 1.0$	(s)	$s_5+s_6\eta$	$s_6 = (\varepsilon_b-\varepsilon_c-\varepsilon_3-\varepsilon_4)E_{st}$

(b) Stresses

Table 4.5 Stresses and Strains for the Compression Zone of a Web (Case II - Center of Web Yielded)

Strain Range	Material Condition	Location of Material Boundaries β_2	Location of Material Boundaries β_2'
$\varepsilon_b+\varepsilon_a \le \varepsilon_y+\varepsilon_4$	(e,y,s)	$\frac{\varepsilon_y-\varepsilon_3-\varepsilon_a-\varepsilon_c}{\varepsilon_b-\varepsilon_c-\varepsilon_3-\varepsilon_4}$	$\frac{\varepsilon_{st}-\varepsilon_3-\varepsilon_a-\varepsilon_c}{\varepsilon_b-\varepsilon_c-\varepsilon_3-\varepsilon_4}$
$\varepsilon_y+\varepsilon_4 < \varepsilon_b+\varepsilon_a \le \varepsilon_{st}+\varepsilon_4$	(y,s)	1.0	$\frac{\varepsilon_{st}-\varepsilon_3-\varepsilon_a-\varepsilon_c}{\varepsilon_b-\varepsilon_c-\varepsilon_3-\varepsilon_4}$
$\varepsilon_{st}-\varepsilon_4 < \varepsilon_b+\varepsilon_a$	(s)	1.0	1.0

(a) Strains

Stress Region		Stress	Stress Components
$0.0 \le \eta < \beta$	(s)	$s_1+s_2\eta$	$s_1 = \sigma_y+(\varepsilon_{st}-\varepsilon_y)E_o+(\varepsilon_a+\varepsilon_c-\varepsilon_{st}+\varepsilon_3)E_{st}$
			$s_2 = (\varepsilon_b-\varepsilon_c-\varepsilon_3-\varepsilon_4)E_{st}$
$\beta_2' \le \eta \le \beta_2$	(y)	$s_3+s_4\eta$	$s_3 = \sigma_y+(\varepsilon_a+\varepsilon_c-\varepsilon_y+\varepsilon_3)E_o$
			$s_4 = (\varepsilon_b-\varepsilon_c-\varepsilon_3-\varepsilon_4)E_o$
$\beta_2 \le \eta \le 1.0$	(e)	$s_5+s_6\eta$	$s_5 = (\varepsilon_a+\varepsilon_c+\varepsilon_3)E$
			$s_6 = (\varepsilon_b-\varepsilon_c-\varepsilon_3-\varepsilon_4)E$

(b) Stresses

Table 4.6 Stresses and Strains for the Compression Zone of a Web (Case III - Center of Web Strain-hardened)

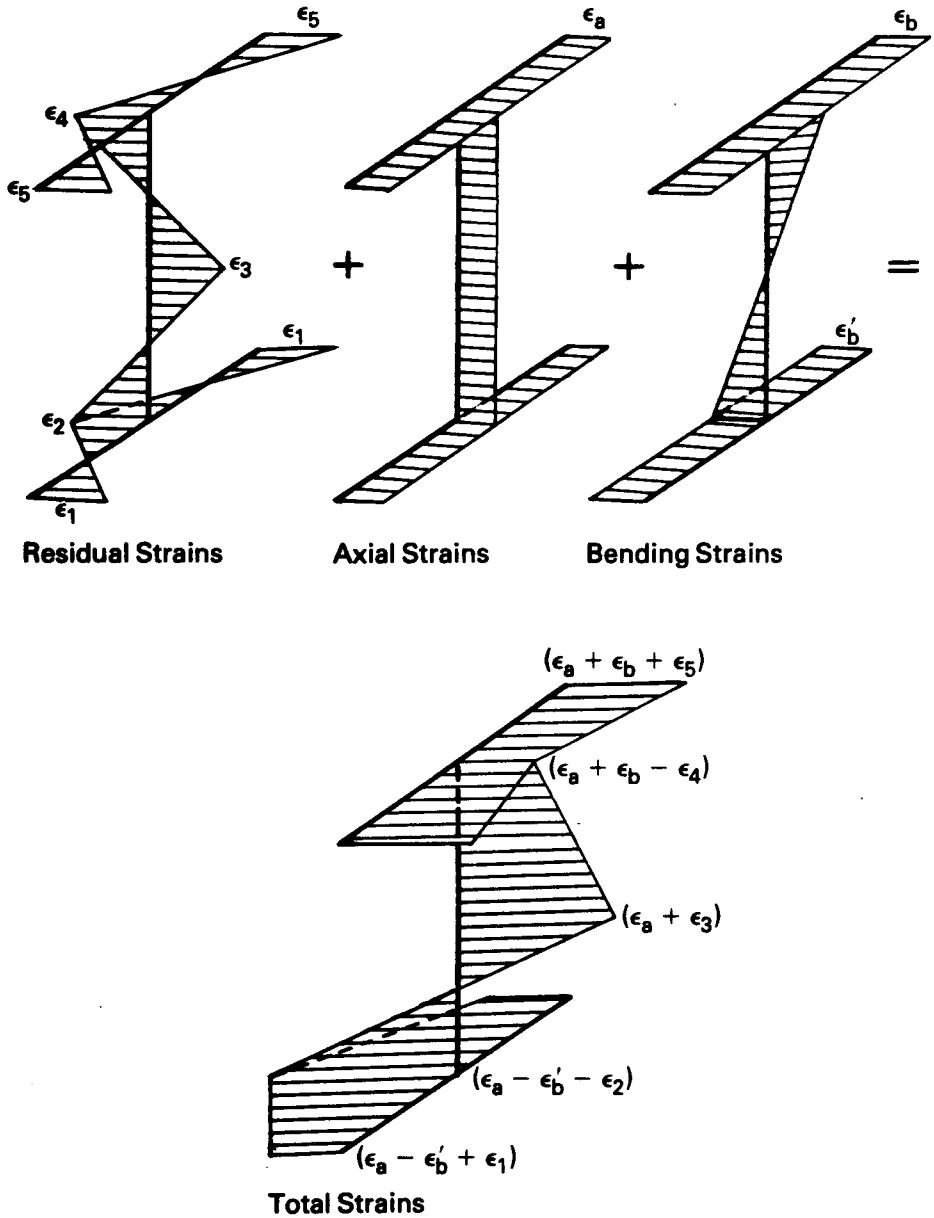

Figure 4.1 Superposition of Beam-Column Strains

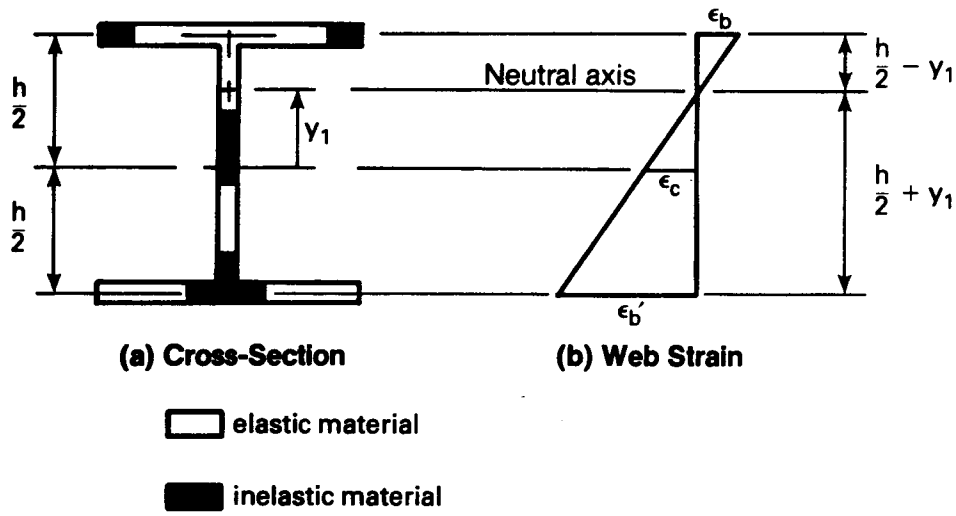

Figure 4.2 Flexural Strain on an Inelastic Section

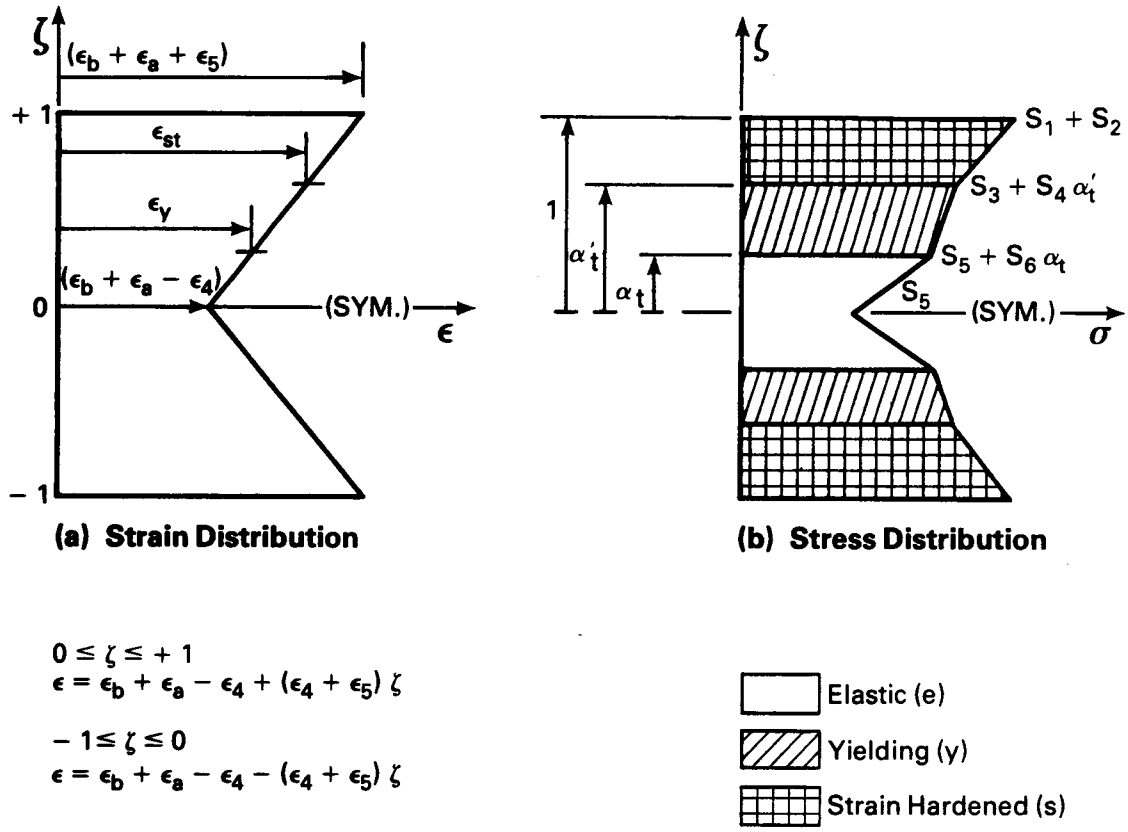

$0 \leq \zeta \leq +1$

$\epsilon = \epsilon_b + \epsilon_a - \epsilon_4 + (\epsilon_4 + \epsilon_5)\,\zeta$

$-1 \leq \zeta \leq 0$

$\epsilon = \epsilon_b + \epsilon_a - \epsilon_4 - (\epsilon_4 + \epsilon_5)\,\zeta$

Figure 4.3 Strain and Stress Distributions for a Flange in Compression.

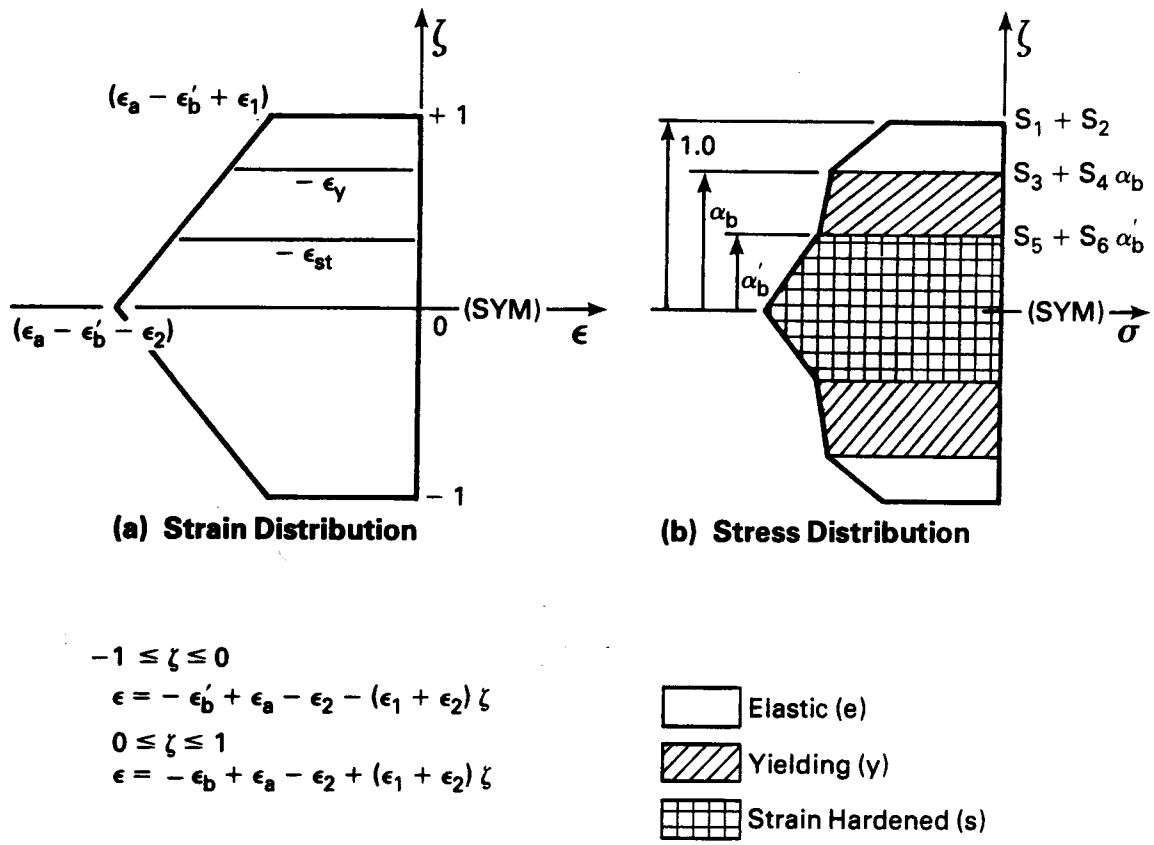

Figure 4.4 Strain and Stress Distributions for a Flange in Tension.

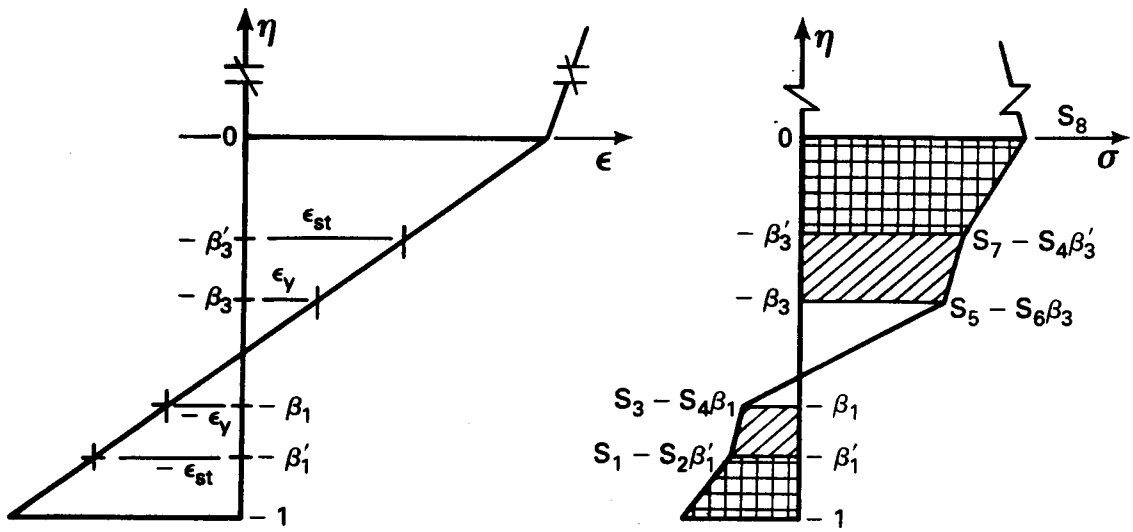

(a) Strain Distribution **(b) Stress Distribution**

$-1 \leq \eta \leq 0$

$\epsilon = \epsilon_a + \epsilon_c + \epsilon_3 + (\epsilon_b' + \epsilon_c + \epsilon_2 + \epsilon_3)\,\eta$

$\eta = -1$

$\epsilon = \epsilon_a - \epsilon_b' - \epsilon_2$

$\eta = 0$

$\epsilon = \epsilon_a + \epsilon_c + \epsilon_3$

Elastic (e)

Yielding (y)

Strain Hardened (s)

Figure 4.5 Strain and Stress Distributions for Tension Zone of a Web.

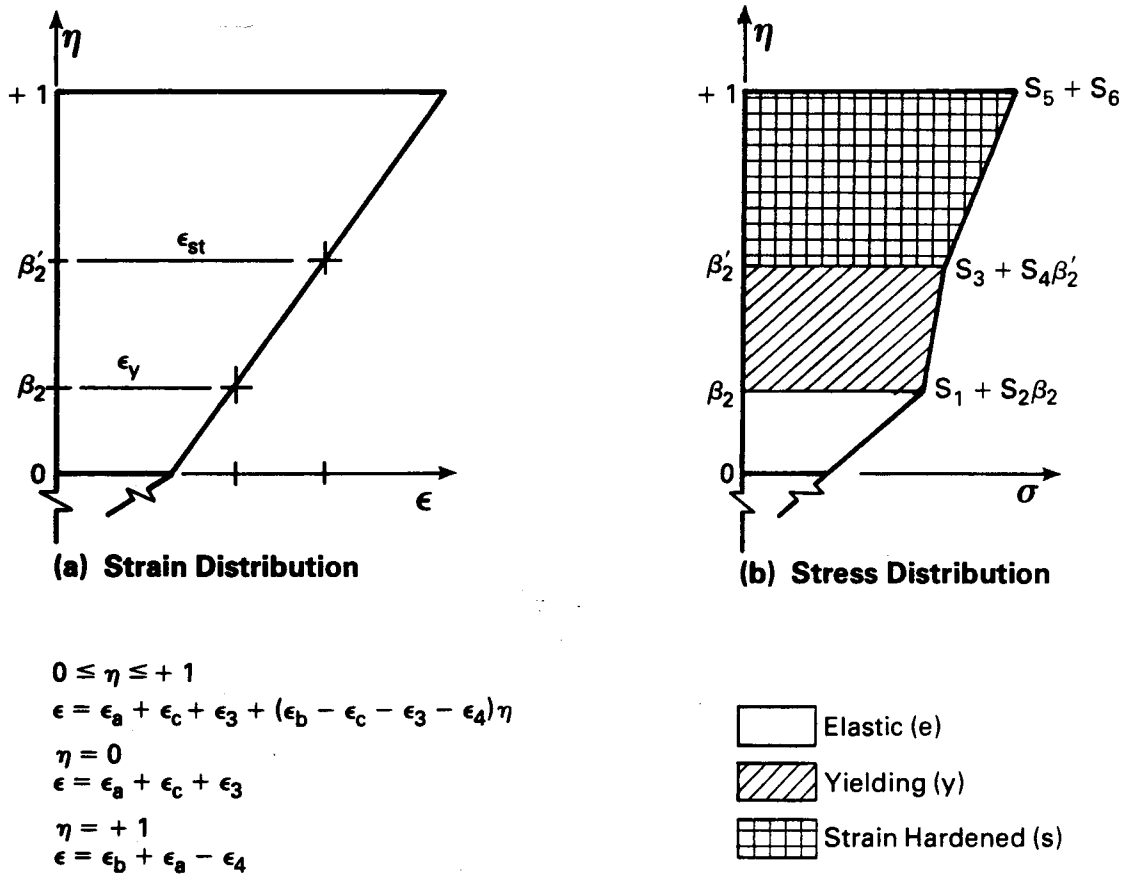

$0 \leq \eta \leq +1$

$\epsilon = \epsilon_a + \epsilon_c + \epsilon_3 + (\epsilon_b - \epsilon_c - \epsilon_3 - \epsilon_4)\eta$

$\eta = 0$

$\epsilon = \epsilon_a + \epsilon_c + \epsilon_3$

$\eta = +1$

$\epsilon = \epsilon_b + \epsilon_a - \epsilon_4$

Figure 4.6 Strain and Stress Distributions for Compression Zone of Web — (Case I - Center of Web Elastic)

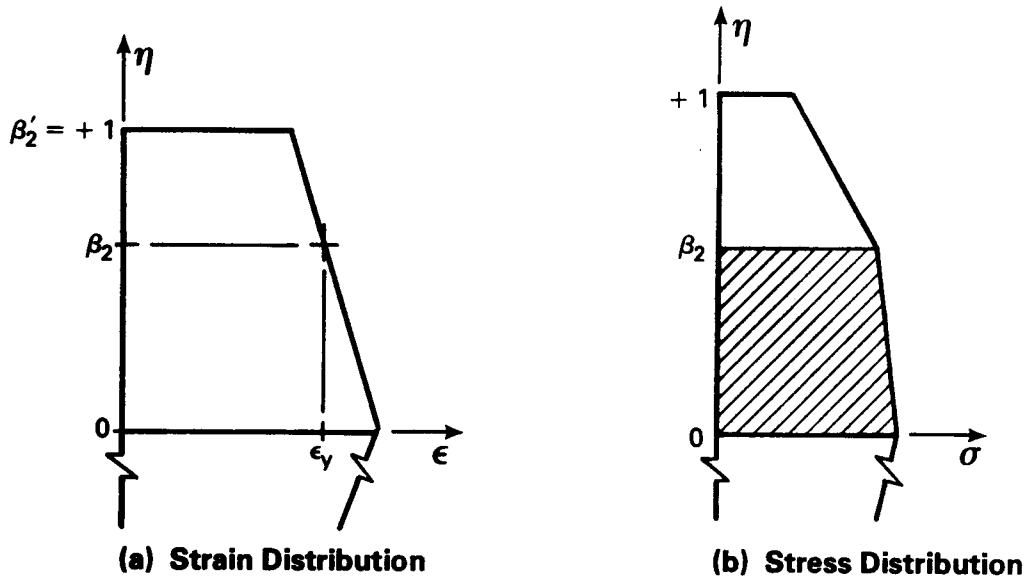

(a) Strain Distribution **(b) Stress Distribution**

Case (i) Strain at $\eta = +1 \leq$ Strain at $\eta = 0$

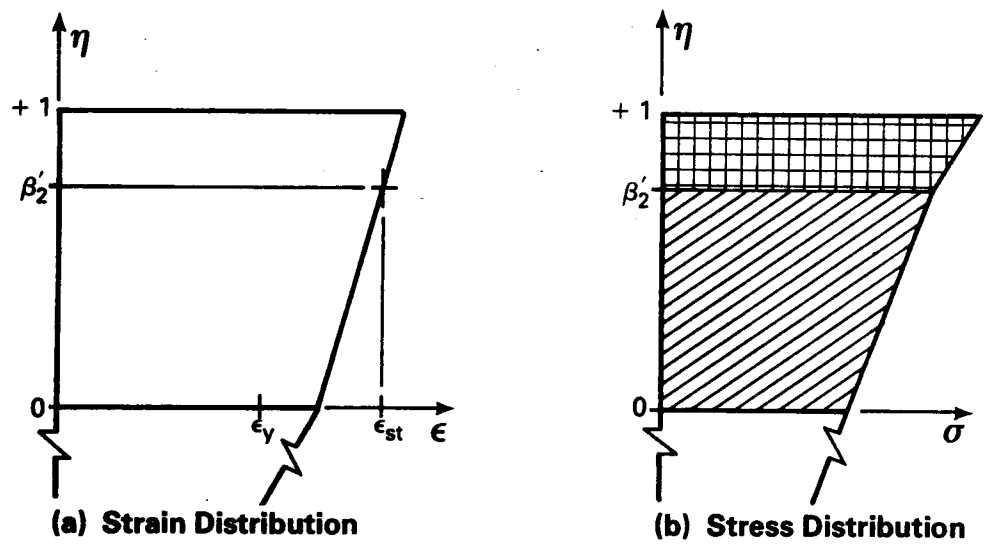

(a) Strain Distribution **(b) Stress Distribution**

Case (ii) Strain at $\eta = 1 >$ Strain at $\eta = 0$

$0 \leq \eta \leq 1$

$\epsilon = \epsilon_a + \epsilon_c + \epsilon_3 + (\epsilon_b - \epsilon_c - \epsilon_4 - \epsilon_3)\eta$

$\eta = 0$

$\epsilon = \epsilon_a + \epsilon_c + \epsilon_3$

$\eta = 1$

$\epsilon = \epsilon_b + \epsilon_a - \epsilon_4$

Elastic (e)

Yielding (y)

Strain Hardened (s)

Figure 4.7 Strain and Stress Distributions for Compression Zone of Web — (Case II - Center of Web Yielded)

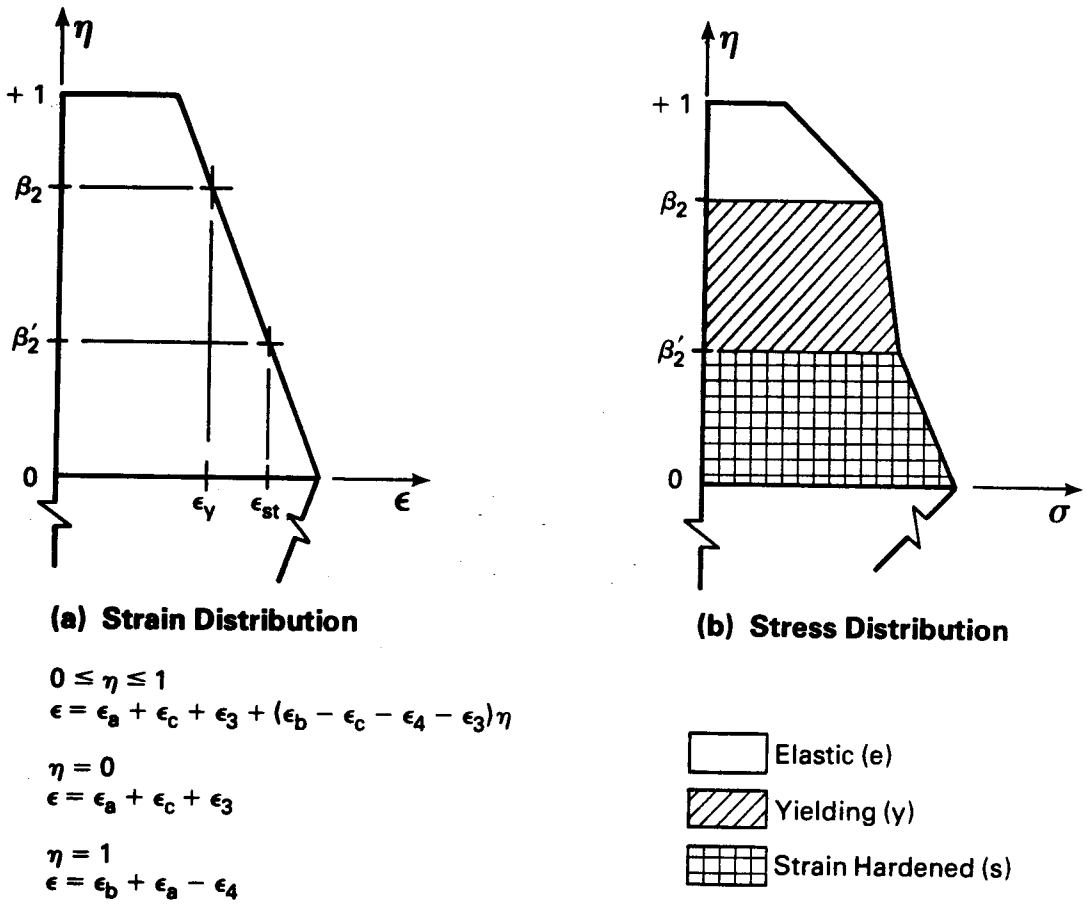

(a) Strain Distribution

(b) Stress Distribution

$0 \leq \eta \leq 1$

$\epsilon = \epsilon_a + \epsilon_c + \epsilon_3 + (\epsilon_b - \epsilon_c - \epsilon_4 - \epsilon_3)\eta$

$\eta = 0$

$\epsilon = \epsilon_a + \epsilon_c + \epsilon_3$

$\eta = 1$

$\epsilon = \epsilon_b + \epsilon_a - \epsilon_4$

Figure 4.8 Strain and Stress Distributions for Compression Zone of Web — (Case III - Center of Web Strain-hardened)

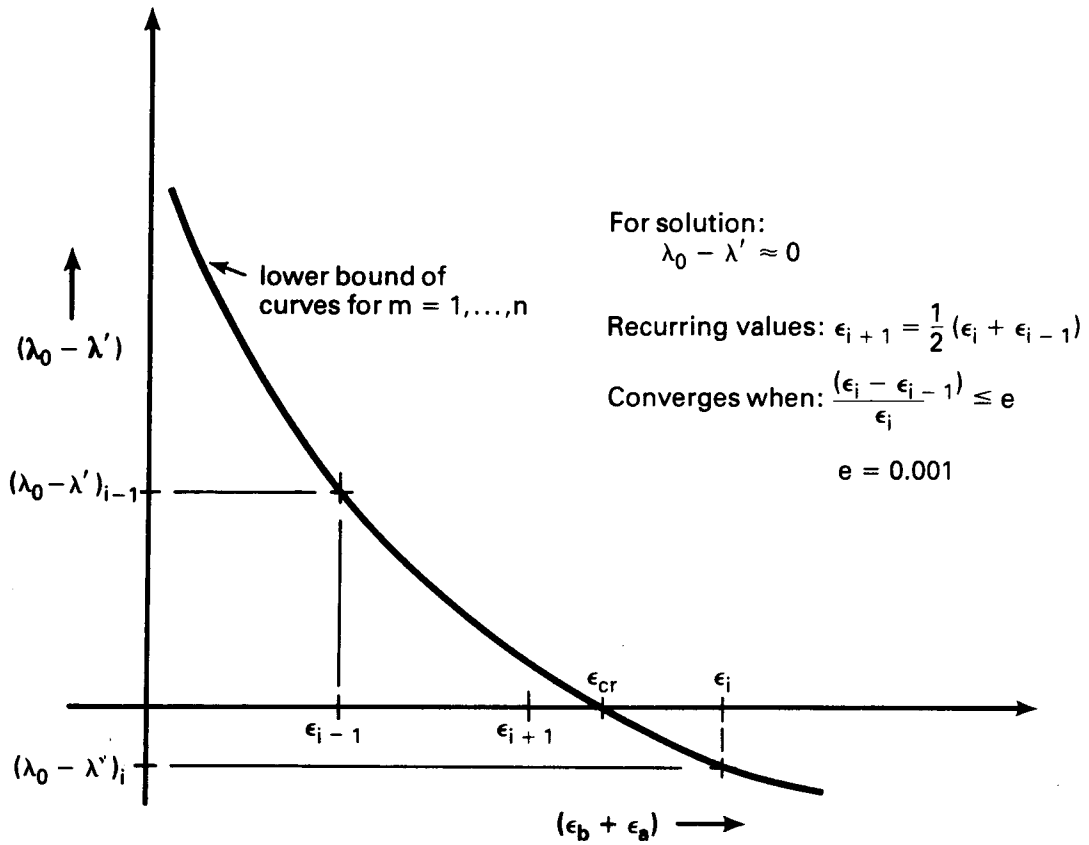

Figure 4.9 Iterative Technique for Critical Buckling Strain.

Chapter 5

COMPARISON OF THEORETICAL PREDICTIONS WITH TEST RESULTS

5.1 Introduction

An analytical procedure for the calculation of critical loads causing local buckling of plate components of W shapes has been presented in Chapters 3 and 4. This procedure uses matrix techniques to predict critical local buckling loads which may occur either in the elastic or inelastic load region. Because of the large number of iterative calculations required it was necessary to use a computer program which was written for this purpose. In this chapter, theoretical results are compared with the results of laboratory tests performed on 57 specimens. These tests include six column specimens and six beam specimens tested by Haaijer and Thurlimann[10]. Of the remaining 45 specimens, 4 were column specimens, 26 were beam specimens, and 15 were beam-column specimens all tested at the University of Alberta[11,12,13,36]. In all cases, local buckling of plate components of W shapes was the principal point of interest during testing.

5.2 Prediction of Buckling Loads

In the analysis of local plate buckling as presented herein, it is assumed that portions of a cross-section having strains higher than the yield strain, have effective material properties corresponding to those in the strain-hardening region. As mentioned previously, this assumption has also been used successfully by other investigators in

this area[25,34,51,53,54]. These material properties are presented in Appendix B and have values dependent on the elastic modulus, E, the strain-hardening modulus, E_{st}, and Poisson's ratio, ν. Where these values are not reported for a given laboratory specimen, values of E = 29,600 ksi., E_{st} = 800 ksi., and ν = 0.3 are assumed. In the case where a residual stress is not available, a value of 0.3 σ_y is assumed[3,5] as a maximum value of compressive and tensile residual stresses and the distribution configuration shown in Figure 3.11 is used. For the specimens tested by Haaijer and Thurlimann, specific values of D_x, D_y D_{xy} and G_t were reported for a value of E_{st} = 900 ksi. Consequently these values are used in the prediction of local buckling capacities for the specimens tested by Haaijer and Thurlimann.

5.3 Column Local Buckling Tests

Results of six column tests were published in 1958 by Haaijer and Thurlimann[7]. The specimens were designed to study the behaviour of W shape columns susceptible to local buckling beyond the elastic range. Each specimen was placed flat-ended between fixed plates in a testing machine and subjected to axial compression. During the tests, observations were made at each load increment to determine axial strains, web and flange deflections, and lateral movement. Column lengths varied between 23 and 32 inches while $b\sqrt{F_y}/2t$ varied between 40 and 56 for the flanges and $h\sqrt{F_y}/w$ varied between 147 and 265 for the webs.

The resulting critical column loads at the point of local buckling for these tests are shown in Table 5.1(a). The predicted loads as determined from the analytical procedure presented herein as

well as the ratios of the predicted to the experimentally determined loads are also shown in this table. The letters, F and W in brackets, indicate the plate component (flange or web) which initiated local buckling in each case.

In 1979 at the University of Alberta, G.L. Kulak tested four W shape column specimens for local buckling capacities. The end edges of the flanges and web of each specimen were rounded and fitted into grooved platens before being placed in a testing machine and subjected to axial compression. During the tests, local strains and plate deflections were recorded at various load levels so that a continuous monitoring of local, lateral and axial deflections was possible. The webs of all four specimens were proportioned to have a value of $h\sqrt{F_y}/w = 200$. Specimen numbers 1 to 3 were 36 inches long and had a value of $b\sqrt{F_y}/2t = 72$ for the flanges. Specimen number four was 24 inches long and the value of $b\sqrt{F_y}/2t$ for the flanges was set at 100 by milling the flanges to the required thickness. The results of these tests are presented in Table 5.1(b) where the values predicted by the analysis presented herein as well as the ratios of predicted to experimental values are also shown.

5.3.1 Discussion of Column Test Results

The ratios of predicted to experimental values of buckling loads presented in Table 5.1 vary between 0.97 and 1.08. It appears that there is better correlation of predicted and experimental values for Kulak's specimens than for those tested by Haaijer and Thurlimann. This difference in correlation for the two sets of test specimens is attributed to the fact that the test values for the specimens tested by

Haaijer and Thurlimann were scaled from published graphs whereas the measured values for the specimens tested by Kulak were directly available. Although this is considered to be the main source of error, other sources of error that are considered to be applicable to all test results presented herein are discussed in Section 5.6.

5.4 Beam Local Buckling Tests

Theoretical values of critical moments causing local buckling in W shapes are compared with corresponding test results for 32 beam specimens. Six beam specimen test results were obtained from the work of Haaijer and Thurlimann[10] and twelve results were obtained from tests carried out by Holtz and Kulak[11,12]. The remaining 14 test results were obtained from experiments carried out by Lukey and Adams[36].

The six beam sections tested by Haaijer and Thurlimann were identical to those tested in the column test series mentioned above. All beams were simply supported at the ends and loaded symmetrically by two concentrated loads so that local buckling could be expected to occur within the uniform moment region. Although the specimens were laterally braced failure was initiated by flange local buckling followed by some lateral movement between bracing points. It is to be expected that this combined failure mode affects the results predicted by the method presented herein although the extent of this effect is difficult to estimate.

In table 5.2(a) bending moments at failure for each of the six specimens tested by Haaijer and Thurlimann are compared with those predicted by the analysis presented herein. As before, the letter, F, in brackets indicates flange local buckling and in this case also, the

letter, L indicates the presence of lateral buckling. The ratios of experimental to predicted moment values are also shown.

In 1973, Holtz and Kulak[11] reported test results for a series of ten compact beam specimens. During testing, all specimens were simply supported and loaded symmetrically with equal concentrated loads so that a uniform moment region existed between load points. All specimens were laterally braced at the load and reaction points so that the possibility of lateral buckling was precluded. Similar tests were performed on a series of two non-compact beams in 1975[12].

Table 5.2(b) shows the critical buckling moments obtained for the bending tests performed by Holtz and Kulak. The corresponding moments as determined by the analysis presented herein are shown as well as the ratios of predicted to experimental values. The letters, F and W, indicate which element (either flange or web) precipitated the local failure.

The beam specimen tests performed by Lukey and Adams[36] were designed for the purpose of studying the relationship between flange slenderness ratios and rotation capacities of W shape beams subjected to a moment gradient. All specimens were simply supported and loaded with a concentrated load placed at mid-span with lateral bracing placed at reaction and load points. The analytical method presented herein was not developed to predict local buckling capacities of beams subjected to moment gradients. It was assumed, however, that a buckle would normally occur in a localized region at the location of maximum moment and that adjacent moment gradient regions would not significantly affect the critical buckling moment. For this reason it was decided to include the results of the beams tested under a moment gradient as

described above.

The critical buckling moments for the specimens tested by Lukey and Adams are presented in Table 5.2(c). The critical element initiating local failure and the ratio of experimental to predicted buckling moment values are also indicated for each specimen.

5.4.1 Discussion of Test Results

For the beam specimens tested by Haaijer and Thurlimann, the ratios of predicted to experimental values of the buckling moment vary between 0.97 to 1.13 as shown in Table 5.2(a). For five of the six specimens tested, the predicted values are within five per cent of the actual test values and for specimen number one the predicted value is slightly high. This slightly high value is not unacceptable, however, in view of the possible sources of error outlined in the next section.

The correlation between experimental and predicted buckling moments for the specimens tested by Höltz and Kulak is generally quite good as can be seen from Table 5.2(b). The ratios of experimental to predicted values vary between 0.89 and 1.12. For ten of the twelve specimens tested, the predicted values of buckling moment are within six per cent of the test values. For specimen numbers 5 and 9 the error is +12 per cent and -11 per cent respectively. Again, in view of the possible sources of error, as discussed in the next section for all test series, these values are considered to be acceptable.

For the specimens tested by Lukey and Adams, the ratios of predicted to experimental values of buckling moment vary between 0.87 and 1.08 for eleven of the fourteen specimens tested. For specimen numbers 2, 4, and 13, the ratios of predicted to experimental values

vary between 1.18 and 1.46 which must be considered as unacceptable correlation between test and theory for these three specimens. In attempting to explain this discrepancy between predicted and test values, it must be pointed out that all of the beam specimens tested eventually failed by a combination of local and lateral buckling. The laterally buckled shape, in plan view, was an S-shaped buckle symmetrically formed about the mid-span lateral brace. As a result, the final buckling mode was that of a combined local and lateral buckle. It is possible, therefore, that for specimen numbers 2, 4, and 13, additional lateral bracing placed at the quarter-points may have prevented lateral buckling thus permitting a failure by pure local buckling. Under such circumstances a higher test load would be obtained and a better correlation between test and theory would result. For the eleven remaining specimens, for which good correlation was obtained, it is assumed that this effect was not as significant presumably because the moment required to cause pure local buckling failure was either less than or equal to that required to cause a pure lateral buckling failure.

5.5 Beam-Column Local Buckling Tests

Local buckling tests on nine beam-columns using compact[4] sections were carried out by Perlynn and Kulak[12]. An additional series of tests consisting of six non-compact[4] beam-column specimens was carried out by Nash and Kulak[13]. Each specimen for both test series was aligned in a universal testing machine which was used to apply the principal concentric load through steel rockers at the top and bottom of a specimen. A moment was superimposed by using a center-hole jack acting between loading arms rigidly connected to the ends of a specimen.

As the eccentric load was increased to provide an increment of moment the principal load was decreased so that the total axial load remained constant and equal to a prescribed value. At each increment of moment, web and flange deflections were monitored locally at various points along the specimen, and overall rotations and deflections were also recorded. Each specimen was laterally braced at mid-span and adequate torsional restraint was provided at the ends by means of the rigidly connected loading arms.

The critical buckling moments for the compact beam-columns tested by Perlynn and Kulak are presented in Table 5.3(a). The ratio of the applied axial load to the yield load is also shown for each specimen. As mentioned previously, the critical element (either flange or web) which precipitates a local failure is indicated by the letter F or W. The predicted value of the local buckling moment as well as the ratio of predicted to experimental moment is also shown for each specimen. In a similar manner the results of the non-compact beam-columns tested by Nash and Kulak are presented in Table 5.3(b).

5.5.1 Discussion of Beam-Column Test Results

For the specimens tested by Perlynn and Kulak the predicted values of buckling moment are within 7 per cent of the test moment for seven of the nine specimens as shown in Table 5.3(a). For the remaining two specimens, the errors are +12 per cent and +13 per cent. In view of the possible sources of error as discussed in the next section, these values are considered to be acceptable.

As shown in Table 5.3(b), for the specimens tested by Nash and Kulak, the predicted values of buckling moment are in error with

respect to the test values by less than 5 per cent for three specimens and by +11 and -13 per cent for two of the remaining three specimens. These errors are considered to be acceptable in view of the possible sources of error as discussed in the next section. For specimen number six the predicted load was only 64 per cent of the maximum load recorded during the test. The validity of this test result is in doubt when compared to that obtained for specimen number five. This specimen was identical except for a 25 per cent increase in the $h\sqrt{Fy}/w$ term which is unlikely to result in a 40 per cent decrease in moment as is apparent from Table 5.3(b). Additional doubt is cast upon the validity of this test result since difficulty of specimen alignment at high axial loads ($P/P_y = 0.7$) was apparently evident during the testing procedure[60].

5.6 Sources of Error

In addition to the sources of error discussed in the previous sections for specific test series, the following sources of error are applicable as noted:

(a) Material Properties

This area is probably the most significant source of error as well as the least determinable. No investigator has as yet come up with an unquestionable evaluation of plate buckling properties that can be applied over the entire inelastic plate buckling range. Apparently, the most reliable guidance presently available for these values in the strain-hardening range is based on the works of Handelman and Prager[22], Haaijer and Thurlimann[7], and Lay[33]. In all cases these values are apparently closely related to the strain-hardening modulus, E_{st}, of a

simple tension coupon test and any error involved in determining E_{st} would doubtlessly be reflected in the theoretical values predicted. No estimate in the error involved in determining E_{st} values is available.

Because the specimens tested by Haaijer and Thurlimann and Lukey and Adams were proportioned so that failure in the plastic range was expected, an evaluation of E_{st} was made for each specimen. The specimens tested by Kulak et al on the other hand, were not proportioned as plastic design sections and therefore the effect of E_{st} was not expected to be as significant. In these cases the value of E_{st} was not available for each specimen. However, a value of E_{st} = 800 ksi. has been estimated from the available stress - strain curves.

Assuming that various material properties have been accurately determined from a simple tension test, it is generally accepted that these properties also apply to larger specimens of different shape subjected to compression. It is further assumed that the material is uniform throughout the test specimens. Local material discontinuities due to welding and forming specimens may contribute to error in this respect. No estimate of the error arising from the use of tension coupon material properties is available.

(b) Residual Stresses

The actual magnitudes and distributions of residual stresses were not available for the specimens tested by Haaijer and Thurlimann, and of the tests carried out by Kulak et al, residual stresses were available only for the column specimens. In these cases the residual stress distribution shown in Figure 3.11 with a maximum value of

residual stress of $0.3\sigma_y$ was assumed. Residual stresses vary in magnitude and distribution from specimen to specimen[32] and affect the local buckling capacity. The effect of changing residual stress values is studied parametrically in Chapter 6.

(c) End Conditions

The end conditions existing at the longitudinal extremities of a local buckle depend largely upon the method of testing and usually they will lie between the pinned and fixed end conditions. In the analysis presented herein, after careful consideration of the methods of testing used in each test series, it was decided that pinned end conditions best represent the end support conditions of the column specimens. Because of the elastic moment gradient region adjacent to either end of a local buckle developing in the beam specimens tested, fixed-end support conditions were assumed. The very rigid attachment of the loading arms to the beam-columns tested resulted also in the assumption of fixed ends for these specimens. The effects of end conditions vary with the length of a specimen[2] and therefore any resulting errors will be more significant for shorter members. With the reduction in plate bending stiffnesses due to inelastic action, it is expected that the affects of end conditions would be lessened. For these reasons it is felt that the effects of estimating degrees of end fixity are not likely to contribute significantly to error.

(d) Iterative Technique

All specimens buckled beyond the elastic range and therefore a considerable amount of iteration involving matrices was required to arrive at a solution for each specimen. Although tolerances were set at 0.1 per cent in the computer program, round-off error is expected to

contribute to the total error.

(e) Analytical Technique

The buckled shapes of the webs and flanges of specimens are approximated using polynomials which result in the least energy shapes for a given specimen. It has been shown[6,18] that this technique results in over-estimation of buckling loads when theoretical shapes do not exactly fit the true buckled shapes. The present technique and associated computer program were checked for this source of error by comparing elastic critical values of plates with values presented by Timoshenko[18] and Bleich[19]. It was found for rectangular plates with various boundary conditions and loadings that this error varied from zero per cent for simply supported plates to about 3.0 per cent for fixed boundary conditions. Since neither web plates nor flange plates of these specimens are fully fixed, it is expected this source of error would be below 2.0 per cent in the majority of cases.

(f) Scaling from graphs

The values reported by Haaijer and Thurlimann[7] and by Lukey and Adams[36] were presented in graphical form and the critical loads were scaled from these graphs. It is estimated that the error involved in this procedure would be about ±1.0 per cent.

(g) Test Measurements

No test difficulties, other than those mentioned above, were reported by the investigators. There are no other significant errors attributable to this source, although, as in all tests, some error, either human-related or machine-related, or both, is probable.

(h) Mode of Failure

It is apparent that in several tests, local buckling was

closely followed by, or in fact coupled with lateral buckling. Since the analytical method presented herein specifically excludes the occurrence of lateral buckling, such effects have not been evaluated. In any case, the degree to which lateral buckling was involved in the actual failure mechanism is not clearly known, and no estimate of the error involved is available.

5.7 Summary of Test Results

As explained previously, four of the 57 test results included herein, are not considered to be valid for the purpose of verifying a theoretical method which does not include the effects of lateral buckling. For the 53 specimens remaining, the predicted results were within 5 per cent of the test results for 60 per cent of the specimens, and within 10 per cent of the test values for 85 per cent of the specimens. The error was between ±10 percent and an overall maximum of ±13 per cent for only 15 per cent of the specimens. Overall, the ratio of theoretical to test values (of either critical load or critical moment) varies from -0.87 to +1.13 with a mean value of 1.00 and a standard deviation of 0.065. In all but four cases, the prediction of the critical component (either flange or web) which initiated the local buckling failure agreed with buckling observations made during the tests.

5.8 Summary

As outlined above, a comprehensive survey of available test data was used to substantiate the validity of the theoretical analysis presented herein as well as the associated computer program.

The comparison between predicted and experimental results has indicated satisfactory agreement between test and theory. In Chapter 6 this same technique is used to evaluate the effects of various parameters which are considered to be of some significance in affecting theoretical predictions.

Specimen Number	Load at Buckling: Experimental L_E-(kips)	Load at Buckling: Predicted L_T-(kips)	Ratio (L_T/L_E)
1	330 (F)	357 (F)	1.08
2	232 (F,W)	253 (F)	1.09
3	442 (F)	429 (F)	0.97
4	514 (F,W)	548 (F,W)	1.07
5	380 (F)	374 (F)	0.98
6	207 (W)	221 (W)	1.07

1 kip = 4.448 kN

(a) Results of G. Haaijer and B. Thurlimann

Specimen Number	Load at Buckling: Experimental L_E-(kips)	Load at Buckling: Predicted L_T-(kips)	Ratio (L_T/L_E)
1	1010 (F)	1015 (F)	1.01
2	1010 (F)	1018 (F)	1.01
3	1000 (F)	1019 (F)	1.02
4	680 (F)	693 (F)	1.02

1 kip = 4.448 kN

(b) Results of G.L.Kulak

5.1 Comparison of Experimental and Predicted Values for Columns.

Specimen Number	Moment at Buckling: Experimental M_E-(in.-kips)	Moment at Buckling: Predicted M_T-(in.-kips)	Ratio (M_T/M_E)
1	1325 (F)	1491 (F)	1.13
2	812 (F,L)	842 (F)	1.04
3	1825 (F,L)	1797 (F)	0.98
4	2951 (L)	2848 (F)	0.97
5	1280 (F,L)	1295 (F)	1.01
6	819 (F,L)	847 (F)	1.03

1 in.-kip = 112.98 N·M

(a) Results of Haaijer and Thurlimann

Specimen Number	Moment at Buckling: Experimental M_E-(in.-kips)	Moment at Buckling: Predicted M_T-(in.-kips)	Ratio (M_T/M_E)
1	3840 (F)	3851 (F)	1.00
2	4910 (F)	4893 (F)	1.00
3	5740 (W)	6091 (F,W)	1.06
4	6820 (W)	6796 (W)	1.00
5	3940 (W)	4400 (W)	1.12
6	3380 (F)	3571 (F,W)	1.06
7	3770 (W)	4005 (W)	1.06
8	3910 (F)	3790 (F)	0.97
9	4580 (F)	4092 (F)	0.89
10	4780 (F)	4588 (F)	0.96
11	5367 (W)	5452 (W)	1.02
12	5696 (W)	5939 (W)	1.04

1 in.-kip = 112.98 N·M

(b) Results of Holtz and Kulak

5.2 Comparison of Experimental and Predicted Values for Beams.

....cont'd

Specimen Number	Moment at Buckling: Experimental M_E-(in.-kips)	Moment at Buckling: Predicted M_T-(in.-kips)	Ratio (M_T/M_E)
1	2251 (F)	2324 (F)	1.03
2	1845 (F)	2698 (F)	1.46
3	549 (F)	476 (F)	0.87
4	463 (F)	548 (F)	1.18
5	487 (F)	491 (F)	1.01
6	488 (F)	463 (F)	0.95
7	390 (F)	423 (F)	1.08
8	701 (F)	628 (F)	0.90
9	656 (F)	643 (F)	0.98
10	659 (F)	645 (F)	0.98
11	698 (F)	639 (F)	0.92
12	679 (F)	647 (F)	0.95
13	391 (F)	525 (F)	1.34
14	440 (F)	403 (F)	0.92

1 in.-kip = 112.98 N·M

(c) Results of Lukey and Adams

5.2 Comparison of Experimental and Predicted Values for Beams.

Specimen Number	P/P_y	Moment at Buckling: Experimental M_E-(in.-kips)	Moment at Buckling: Predicted M_T-(in.kips)	Ratio (M_T/M_E)
1	0.2	2370 (F)	2376 (F)	1.00
2	0.2	2732 (F)	2534 (F)	0.93
3	0.2	2887 (W)	2796 (W)	0.97
4	0.4	1606 (F)	1808 (F)	1.13
5	0.4	1829 (F)	1781 (F)	0.97
6	0.4	2303 (F,W)	2157 (F,W)	0.94
7	0.8	738 (F)	825 (F)	1.12
8	0.8	694 (W)	660 (W)	0.95
9	0.8	582 (W)	588 (W)	1.01

1 in.-kip = 112.98 N·M

(a) Results of Perlynn and Kulak for Compact Sections

Specimen Number	P/P_y	Moment at Buckling: Experimental M_E-(in.-kips)	Moment at Buckling: Predicted M_T-(in.kips)	Ratio (M_T/M_E)
1	0.15	3704 (F)	3698 (F)	1.00
2	0.15	2622 (F)	2923 (F)	1.11
3	0.30	2827 (W,F)	2712 (W,F)	0.96
4	0.30	2488 (F)	2171 (F)	0.87
5	0.70	668 (W,F)	682 (W,F)	1.02
6	0.70	1095 (F)	705 (F)	0.64

1 in.-kip = 112.98 N·M

(b) Results of Nash and Kulak for Non-Compact Sections

5.3 Comparison of Experimental and Predicted Values for Beam-Columns.

Chapter 6

THEORETICAL STUDY AND EVALUATION OF PARAMETERS

6.1 Introduction

As presented in Chapter 5, test results are available for a limited number of local plate buckling specimens subjected to axial, flexural, and combined axial and flexural loadings. The number and variation of dimensions of these specimens are not sufficient in themselves to be able to establish general design parameters. Furthermore, the critical buckling loads may be significantly influenced by certain parameters which have not been specifically studied in the tests. In this chapter, analytical results in the form of critical plate buckling curves are presented and discussed for a wide variety of columns, beams, and beam-columns. Additionally, the effects of important parameters on local plate buckling capacities are evaluated and discussed. Unless specifically varied the following basic values are used in the parametric study: $E = 29{,}600$ ksi., $\sigma_y = 44$ ksi., $\varepsilon_y = \sigma_y/E$, $\varepsilon_{rc} = 0.3\varepsilon_y$, $E_{st} = 800$ ksi., flange aspect ratio = 4, and web aspect ratio = 2.

6.2 Columns

Figure 6.1 shows the variation of the critical load ratio (P_{cr}/P_y) with respect to the web width-to-thickness term $(h\sqrt{F_y}/w)$ for various values of the flange width-to-thickness term $(b\sqrt{F_y}/2t)$. The knee portion of each curve results from the presence of unavoidable

residual stresses. For the sake of comparison a curve corresponding to a theoretical value of zero residual stress is also shown. By this comparison it can be seen that the effects of residual stresses are most pronounced in the elastic and partially elastic regions. Assuming a residual compressive stress $\sigma_{rc} = 0.3\sigma_y$, yielding begins at $P_{cr}/P_y = 0.7$ and $h\sqrt{F_y}/w = 475$. As $h\sqrt{F_y}/w$ decreases, flange buckling becomes predominant as the yield load is approached, and at lower values strain-hardening occurs. The dashed curve respresents the elastic buckling solution.

The CSA S16.1-1975 Standard[4] specifies a flange slenderness value for column flanges of 100. As illustrated in Figure 6.1, the analysis presented herein predicts that this value is slightly unconservative. At the currently specified limitations[4] of $b\sqrt{F_y}/2t = 100$ and $h\sqrt{F_y}/w = 255$ for columns, the analysis presented herein predicts a value of $P_{cr}/P_y = 0.9$. Also, the figure shows that P_{cr}/P_y does not reach a value of 1.0 until $b\sqrt{F_y}/2t$ has been reduced to 72 and values of $h\sqrt{F_y}/w$ are less than 300.

This theoretical result for columns has been substantiated by the results of four column specimens tested by Kulak at the University of Alberta. As discussed in Section 5.3, three of the specimens had flange slenderness values of 72, and the fourth specimen had a flange slenderness value of 100. The value of web slenderness was 200 for all four specimens. The flanges of the three specimens having $b\sqrt{F_y}/2t = 72$ buckled at or slightly above $P_{cr}/P_y = 1.0$, while the flanges of the specimen having $b\sqrt{F_y}/2t = 100$ buckled at $P_{cr}/P_y = 0.9$. These test results as well as the theoretical analysis presented herein indicate that a value of $b\sqrt{F_y}/2t = 72$ (as opposed to the current

limitation[4] of $b\sqrt{F_y}/2t = 100$) should be used for columns. For this reason, subsequent parametric studies presented herein are based on a value of flange slenderness of 72 for columns.

In order to be able to later tie in column local buckling behaviour as one limiting case of beam-columns, the local buckling strength curves for axially loaded Class 1, Class 2, and Class 3 sections are shown in Figure 6.2. The rounded portion of each curve between values of $h\sqrt{F_y}/w$ of about 300 and 475 is due to gradual yielding in the presence of residual stresses. A curve corresponding to zero residual stresses as mentioned previously is also shown in Figure 6.2. For web slenderness values greater than 475, elastic buckling of the web occurs and for values between 475 and 300, web buckling occurs in the inelastic range. For values of web slenderness less than about 300, flange buckling in the yielded and strain-hardening ranges occurs at values of P_{cr}/P_y equal to or greater than 1.0.

A column local buckling curve is shown in Figure 6.2 for a value of $b\sqrt{F_y}/2t = 64$ corresponding to the present CSA-S16.1 specification[4] for a Class 2 section. For a Class 1 section with $b\sqrt{F_y}/2t = 54$, a similar column curve is shown in Figure 6.2. Although these two sections are not explicitly designated for use as columns, the corresponding column curves are presented here so that the effect of the $b\sqrt{F_y}/2t$ term for columns may be evaluated. Also, these sections subjected to column action, represent a limit of the corresponding beam-columns when bending moments are negligible.

The effect of the flange slenderness values can be seen by comparing the curves in Figure 6.2. For values of $h\sqrt{F_y}/w$ greater than

300, where web buckling is predominant, varying $b\sqrt{F_y}/2t$ from 54 to 72 has virtually no effect on the web buckling capacity. The effect of this term is most significant for values of $h\sqrt{F_y}/w$ less than 300 since that is the region wherein flange buckling is predominant. For $b\sqrt{F_y}/2t = 72$ strain-hardening of the section begins at a value of $h\sqrt{F_y}/w = 220$. As $b\sqrt{F_y}/2t$ is decreased, strain-hardening begins at progressively higher values of $h\sqrt{F_y}/w$, the upper limit being $h\sqrt{F_y}/w = 325$ for a Class 1 section with a flange slenderness value of 54.

6.2.1 Effects of Residual Stresses

The effects of residual stresses on the local buckling loads of columns is shown in Figure 6.1 for $b\sqrt{F_y}/2t$ ratios of 72, 80, 90, and 100, and in Figure 6.2 for $b\sqrt{F_y}/2t$ ratios of 54, 64, and 72. In these figures, column local buckling curves for a theoretical value of $\sigma_{rc} = 0$ are compared with those corresponding to a more practical value of $\sigma_{rc} = 0.3\sigma_y$ and a residual stress distribution as shown in Figure 3.11. The value of $\sigma_{rc} = 0.3\sigma_y$ is representative of values used by other investigators[3,5,61,62] for the purpose of including the effects of residual stresses when exact values are unknown.

By comparing the curves corresponding to $\sigma_{rc} = 0$ with those corresponding to $\sigma_{rc} = 0.3\sigma_y$, it can be seen that, in the range where elastic web buckling occurs (at values of $h\sqrt{F_y}/w$ greater than about 475), a residual stress of $0.3\sigma_y$ reduces the critical buckling load ratio by about 25 per cent. The influence of residual stresses diminishes as the value of P_{cr}/P_y approaches 1.0, and completely disappears as strain-hardening becomes imminent at lower values of $h\sqrt{F_y}/w$

According to the theoretical method presented herein, the

values of $b\sqrt{F_y}/2t = 100$ as presently specified for W shape columns[4] appears to be too liberal when a residual stress of $\sigma_{rc} = 0.3\sigma_y$ is assumed. In Figure 6.1, the curve corresponding to $b\sqrt{F_y}/2t = 100$ and $\sigma_{rc} = 0.3\sigma_y$ reaches a value of $P_{cr}/P_y = 0.9$ at the presently specified[4] web slenderness ratio of 255. The curve corresponding to $b\sqrt{F_y}/2t = 100$ and the theoretical value of $\sigma_{rc} = 0$ on the other hand, reaches a value of $P_{cr}/P_y = 1.0$ for values of web slenderness as high as 475. For this reason therefore, the analytical method presented herein suggests that the presently specified value of $b\sqrt{F_y}/2t = 100$ is too liberal because of the effects of residual stresses. The analytical method presented herein predicts that when a W shape column is proportioned so that $b\sqrt{F_y}/2t \leq 72$ and $h\sqrt{F_y}/w \leq 300$ a value of $P_{cr}/P_y \geq 1.0$ can be reached for an assumed residual stress of $\sigma_{rc} = 0.3\sigma_y$.

6.2.2 Effects of Strain-hardening Modulus

Figure 6.3 shows the effects of strain-hardening modulus values of 700, 800, and 900 ksi. on the local buckling capacity of columns. These values of strain-hardening moduli were chosen because they are representative of values that have been determined by several investigators in this area[5,7,36,54,59,61,62]. For columns proportioned so that $b\sqrt{F_y}/2t = 72$, variations in the values of the strain-hardening modulus are influential for values of $h\sqrt{F_y}/w$ less than about 200. In this region the curve separates into three branches corresponding to the three different values of the strain-hardening modulus investigated. As would be expected in this region, for a given value of web slenderness, the value of P_{cr}/P_y increases as the strain-hardening modulus increases. As can be seen from Figure 6.3, in the practical ranges of plate

proportions for W shape columns ($b\sqrt{F_y}/2t = 72$ and $h\sqrt{F_y}/w = 300$), the value of the strain-hardening modulus has negligible effect on column local buckling strength.

6.3 Beams

Figure 6.4 shows values of the ratio of critical local buckling moment to the yield moment plotted against the web width-to-thickness term ($h\sqrt{F_y}/w$), for various values of the flange width-to-thickness term ($b\sqrt{F_y}/2t$). Again, the effects of residual stresses are included as is evident from the rounded knee portions of these curves. For values of $h\sqrt{F_y}/w$ greater than about 1100, local buckling of the slender web occurs in the form of warping due to the presence of residual stresses.

6.3.1 Class 3 Beams

According to the CSA S16.1-1975 Standard[4], the flange width-to-thickness term for a Class 3 beam is set at 100 and is the same as that for a column. The currently specified web width-to-thickness ratio is 690. For these values, Figure 6.4 shows that $M_{cr}/M_y = 0.9$.

Comparing similar curves for various values of $b\sqrt{F_y}/2t$ in Figure 6.4, it is seen that M_{cr}/M_y attains a value of 1.04 at $b\sqrt{F_y}/2t = 72$ over a large range of web slenderness (up to about $h\sqrt{F_y}/w = 800$). Although M_{cr} slightly exceeds M_y (by only 4 per cent) for $b\sqrt{F_y}/2t = 72$, this value seems to be appropriate for a Class 3 beam in that it corresponds with the value suggested for columns. In this way, the same value may be used throughout for a Class 3 beam-column which has as its limits, pure axial load at one end of the loading spectrum, and pure flexure at the other. For $b\sqrt{F_y}/2t = 72$, Figure 6.4 shows that for curves

of web slenderness greater than 975 the web buckles elastically. For values of web slenderness between 800 and 975 the web buckles in the inelastic range as a consequence of the influence of residual stresses. The mode of failure changes from web buckling at a value of 800 to flange buckling for values less than 800. At a web slenderness value of 260 the curve begins to increase rapidly as strain-hardening becomes influential.

6.3.2 Class 2 Beams

The Standard[4] specifies that Class 2 beams have a flange slenderness value not exceeding 64 and a web slenderness value not exceeding 520. In Figure 6.5 values of the ratio of critical moment, M_{cr}, to the plastic moment, M_p, are plotted against the web width-to-thickness term, $h\sqrt{F_y}/w$, for a flange width-to-thickness value of 64. For values of $h\sqrt{F_y}/w$ greater than 1100, local buckling occurs in the form of warping of the slender web subjected to residual stresses. Referring to the curve corresponding to a value of $b\sqrt{F_y}/2t = 64$, local buckling of the web occurs in the inelastic range between values of $h\sqrt{F_y}/w$ of about 800 and 975. For values of $h\sqrt{F_y}/w$ less than 800, flange buckling occurs at a value of $M_{cr}/M_y = 1.0$, and at $h\sqrt{F_y}/w = 300$ strain-hardening of the section begins and strength increases rapidly as $h\sqrt{F_y}/w$ decreases further.

6.3.3 Class 1 Beams

For Class 1 beams the Standard[4] specifies a flange slenderness of 54 and a web slenderness limit of 420. Values of M_{cr}/M_p are plotted against $h\sqrt{F_y}/w$ for a value of $b\sqrt{F_y}/2t = 54$ as shown in Figure 6.5. For $h\sqrt{F_y}/w$ greater than 800, the behaviour of these beams is similar to

that described previously for Class 2 sections. Because of the increased sturdiness of the flanges however, web buckling continues to be the mode of failure for values of $h\sqrt{F_y}/w$ as low as 600. Below this value, flange buckling occurs. For values less than 800, M_{cr}/M_p is greater than 1.0 and this implies that the strain in the flanges can reach the strain-hardening range before local buckling occurs. Therefore, these sections can undergo sufficient rotation to permit redistribution of stresses while sustaining the plastic moment value, as required of Class 1 sections[2,3,4].

6.3.4 Effects of Residual Stresses

The critical buckling moment ratio is plotted against values of web slenderness for values of flange slenderness of 72, 80, 90, and 100 in Figure 6.4 and for values of flange slenderness of 54 and 64 in Figure 6.5. Again, the assumed residual stress value is $\sigma_{rc} = 0.3\sigma_y$ and the assumed residual stress distribution is similar to that shown in Figure 3.11. For the purpose of comparison, these curves are also plotted for the theoretical value of $\sigma_{rc} = 0.0$. In the range where web buckling is critical ($P_{cr}/P_y < 1.0$ and $h\sqrt{F_y}/w > 800$) residual stresses have their greatest effect in reducing the critical buckling moment capacity. For values of $h\sqrt{F_y}/w$ greater than about 1100, the residual stress causes web buckling in the form of warping of the very slender webs. As values of $h\sqrt{F_y}/w$ decrease below 800, the significance of residual stresses diminishes and as strain-hardening is approached their effects become negligible.

As discussed for columns, it appears here also that the presently specified flange slenderness[4] of 100 is too liberal for

Class 3 beams when a value of $\sigma_{rc} = 0.3\sigma_y$ is assumed. Referring to Figure 6.4, for a value of flange slenderness of 100 and $\sigma_{rc} = 0.3\sigma_y$, the critical local buckling moment is 90 per cent of the yield moment at the presently specified web slenderness[4] of 690. The theoretical curve for which $b\sqrt{F_y}/2t = 100$ and $\sigma_{rc} = 0$, on the other hand, shows that the critical local buckling moment reaches the yield moment for values of web slenderness as high as 800. This suggests, therefore, that the value of $b\sqrt{F_y}/2t = 100$ for Class 3 beams is too liberal because of the effects of residual stresses.

6.3.5 Effects of Strain-hardening Modulus

The effect of varying the strain-hardening modulus upon the local buckling behaviour of beams is shown in Figure 6.6 for a value of $b\sqrt{F_y}/2t = 72$ and in Figure 6.7 for a value of $b\sqrt{F_y}/2t = 54$. As for columns, the same three values of strain-hardening modulus are used here for beams. Figure 6.6 shows that for sections with $b\sqrt{F_y}/2t = 72$, the effect of strain-hardening is evident only for values of $h\sqrt{F_y}/w$ less than about 280. Although not explicitly shown herein, it has been determined that these same observations apply to compact sections[4] with a value of $b\sqrt{F_y}/2t = 64$. For plastic design sections[4], Figure 6.7 shows that the effect of strain-hardening is influential for values of $h\sqrt{F_y}/w$ less than 800. This is because the very sturdy flanges ($b\sqrt{F_y}/2t = 54$) enable these sections to reach strain-hardening strains at relatively high web slenderness values.

For the values of E_{st} examined, there are no significant differences in local buckling strength for beams having flange slenderness values of 72 and 64 when practical values of web slenderness

are used. The local buckling strength of plastic design sections, on the other hand, are significantly affected by changes in the strain-hardening modulus for all values of web slenderness less than about 800. As would be expected, this effect increases as web slenderness values decrease.

6.4 Beam-Columns

The previous section has indicated that suitable flange slenderness values for flexural members are $b\sqrt{F_y}/2t$ = 54, 64, and 72 for Class 1, 2, and 3 respectively. Further, a suitable value for axially loaded members is $b\sqrt{F_y}/2t = 72$. These will therefore be the values principally investigated for beam-columns. The analysis will be based on the assumption that an axial strain less than the critical one will be applied first. A flexural strain is then superimposed and gradually increased until local buckling occurs.

At each increment of flexural strain, equilibrium of a cross-section is satisfied and the position of the neutral axis is updated to account for yielding of a section. For a given flange width-to-thickness term, values of the ratio of applied load to yield load can then be plotted against values of the ratio of critical moment to yield moment or plastic moment for various web width-to-thickness terms. The web width-to-thickness term is varied from 300 to 800, corresponding to the limits determined previously for a pure column (zero flexural strain) and a pure beam (zero axial strain). In this way, for a given $b\sqrt{F_y}/2t$ value, a set of interaction curves is generated for various $h\sqrt{F_y}/w$ values.

6.4.1 Class 3 Beam-Columns

As discussed in Section 6.3.1, the present code value of $b\sqrt{F_y}/2t = 100$ for a Class 3 section appears to be too high according to the theory presented herein. Furthermore, a value of $b\sqrt{F_y}/2t = 72$ was found to be adequate for local buckling requirements of columns and for beams required to reach the yield moment, M_y, before local buckling occurs. In this section, therefore, interaction curves are generated for beam-columns corresponding to a $b\sqrt{F_y}/2t$ value of 72 and various values of $h\sqrt{F_y}/w$.

Ratios of applied load to yield load are plotted against the ratios of critical moment to yield moment for various $h\sqrt{F_y}/w$ values in Figure 6.8. Values along the vertical axis represent pure column behaviour and those along the horizontal axis represent pure beam behaviour. For each curve corresponding to a fixed $h\sqrt{F_y}/w$ value, as M_{cr}/M_y increases above zero, a point of tangency is approached on the line joining the points $P/P_y = 1.0$ and $M_{cr}/M_y = 1.04$. At the point of tangency the mode of failure changes from web local buckling to flange buckling and beyond this point each curve remains tangent to the line. The sloping dashed line, $M_{yc} = M_y\ (1-P/P_y)$, represents the strength interaction equation for a Class 3 beam-column .

6.4.1.1 Current Specifications

For Class 3 beam-columns the web limitations are currently specified as follows:

$$h\sqrt{F_y}/w = 690\ (1-2.60\ P/P_y) \qquad 0 \leq P/P_y \leq 0.15 \qquad (6.1)$$

$$h\sqrt{F_y}/w = 450\ (1-0.43\ P/P_y) \qquad 0.15 \leq P/P_y \leq 1.0 \tag{6.2}$$

These web limitations are based on test results obtained by Kulak and Nash[13]. Since the time of publication of these limitations, additional work in this area by Kulak and Nash[13] has indicated the following increases:

$$h\sqrt{F_y}/w = 690\ (1-1.69\ P/P_y) \qquad 0 \leq P/P_y \leq 0.15 \tag{6.3}$$

$$h\sqrt{F_y}/w = 535\ (1-0.28\ P/P_y) \qquad 0.15 \leq P/P_y \leq 1.0 \tag{6.4}$$

Although the theory presented herein indicates that a $b\sqrt{F_y}/2t$ value of 72 should be used for Class 3 sections, the specimens tested by Kulak and Nash were designed on the basis of the existing code value of $b\sqrt{F_y}/2t = 100$. Furthermore, the specimens were able to reach, and in some cases exceed the value of M_y reduced in the presence of axial load. The theory presented herein also predicts values in good agreement with these test results when the effects of the rigid plate boundary constraints (necessitated by the attachment of the loading arms to the test specimens) are included in the analysis. In practice, however, the effects of these rigid supports for longer members are negligible. Omitting the effects of these supports, the present method predicts that a value of $b\sqrt{F_y}/2t = 72$ is indicated for Class 3 sections. For this value, the web limitations as predicted by the theory presented herein are discussed in the following section.

6.4.1.2 Theoretical Limitations as Determined Herein

For a Class 3 section the beam-column interaction curves are

plotted in Figure 6.8 for various values of $h\sqrt{F_y}/w$. At various values of P/P_y each curve intersects the line described by:

$$M = M_y(1-P/P_y) \cdot \qquad (6.5)$$

In Figure 6.9 these values of P/P_y are plotted against the corresponding values of $h\sqrt{F_y}/w$. For pure beam action at $P/P_y = 0$, the predicted web limitation is $h\sqrt{F_y}/w = 850$. As P/P_y increases, the slope of the curve decreases rapidly and becomes constant in the region of P/P_y between 0.42 and 0.75. As P/P_y further increases the slope decreases slightly as pure axial strains are approached at $P/P_y = 1.0$ and a minimum value of $h\sqrt{F_y}/w = 300$ is reached.

A linear approximation to the curve described above is also shown in Figure 6.9 and it is given by the following relationship:

$$h\sqrt{F_y}/w = 725\ (1.0-0.59(P/P_y)) \qquad 0 \leq P/P_y \leq 1.0 \qquad (6.6)$$

This approximation deviates markedly on the conservative side from the theoretical curve for low values of P/P_y. In this region however, a conservative limitation is desirable in order to account for small residual axial loads occurring in service and as well to avoid the sensitivity of the steep theoretical gradient in this region. The relationship of Equation 6.6 as well as the limitations described by Equations 6.1 and 6.2 are also shown in Figure 6.9.

Referring to Figure 6.9, the theoretical method presented herein indicates a web limitation of $h\sqrt{F_y}/w = 725$ at $P/P_y = 0.0$ for beams. As P/P_y increases, a linear decrease in $h\sqrt{F_y}/w$ as a result of decreasing web flexural tension, is indicated. For pure column action, at $P/P_y = 1.0$, a minimum value of $h\sqrt{F_y}/w$ of 300 is reached. This theoretical

limitation differs from that presently specified by Equations 6.1 and 6.4 in the region of pure beam action ($P/P_y = 0.0$) by about +5 per cent. As P/P_y increases this difference reaches a maximum of about +60 per cent at $P/P_y = 0.15$ and from there it decreases to +18 per cent at $P/P_y = 1.0$. This comparison should be considered in light of the fact that the theoretical web limitations are based on the assumption of a flange slenderness ratio of $b\sqrt{F_y}/2t = 72$ (as previously explained), whereas the present limitations are based on the results of test specimens whose flange slenderness ratios were $b\sqrt{F_y}/2t = 100$.

6.4.2 Class 2 Beam-Columns

As already indicated, it will be assumed that a Class 2 beam-column is proportioned so that the flange width-to-thickness term is $b\sqrt{F_y}/2t = 64$. According to the theory presented herein, this value was found to be adequate for compact beam sections as illustrated in Figure 6.5. At the other extreme of beam-column action, namely pure axial load, these sections can reach a P_{cr}/P_y value of 1.0 for a value of $h\sqrt{F_y}/w = 300$, as shown in Figure 6.2. Accordingly, these beam-column sections were investigated for a range of P_{cr}/P_y ratios between zero and one, with the $h\sqrt{F_y}/w$ values varying from 300 to 800. The results of this investigation are presented in Figure 6.10.

In this figure, values of the ratio of applied load to yield load are plotted against ratios of critical moment to plastic moment for various values of $h\sqrt{F_y}/w$. The flange width-to-thickness term for all curves has a constant value of 64. For these curves, the same discussion as presented for Class 3 beam-columns in Section 6.4.1, is valid here for Class 2 beam-columns.

6.4.2.1 Current Specifications

The present limitations specified for web width-to-thickness terms for Class 2 beam-columns are as follows[4]:

$$h\sqrt{F_y}/w = 520\ (1-1.28\ P/P_y) \qquad 0 \le P/P_y \le 0.15 \tag{6.7}$$

$$h\sqrt{F_y}/w = 450\ (1-0.43\ P/P_y) \qquad 0.15 \le P/P_y \le 1.0 \tag{6.8}$$

These web limitations are based on test results from a series of nine compact beam-columns tested by Perlynn and Kulak[12]. As presented in Chapter 5, the analytical method presented herein substantiates these results when the effects of rigid supports necessary for testing purposes are included in the analysis. Conservatively omitting the effects of these rigid supports however, the analysis presented herein shows that the conventional value of plastic moment reduced for the presence of axial load[63,64],

$$M_{pc} = M_p \qquad 0 \le P/P_y \le 0.15 \tag{6.9(a)}$$

and,

$$M_{pc} = 1.18\ M_p\ (1-P/P_y) \qquad 0.15 \le P/P_y \le 1.0 \tag{6.9(b)}$$

cannot be attained by compact sections when $h\sqrt{F_y}/w$ is greater than 250. Such a limitation however would severely restrict the choice of web sizes available for use in compact sections. As shown in Figure 6.10, the analytical method presented herein predicts a maximum local buckling strength for compact sections of:

$$M_{pc} = M_p\ (1-P/P_y), \tag{6.10}$$

when the web slenderness ratio varies between 300 and 800. Therefore, in accordance with the analytical results presented in Figure 6.10, Equation 6.10 is suggested for use with compact sections and, in this way, all values of $h\sqrt{F_y}/w$ up to 800 can be utilized for Class 2 sections.

6.4.2.2 Theoretical Limitations as Determined Herein

As shown in Figure 6.10 the curves corresponding to various values of $h\sqrt{F_y}/w$ become tangent to the line described by Equation 6.10 at various values of P/P_y. In Figure 6.11 these values of $h\sqrt{F_y}/w$ are plotted against the corresponding values of P/P_y. The resulting curve has a value of $h\sqrt{F_y}/w = 800$ for pure beam action ($P/P_y = 0.0$). As P/P_y increases, the slope of the curve rapidly increases to a constant value in the region of P/P_y between 0.42 and 0.75. As P/P_y further increases, the slope decreases slightly as pure axial strains are approached at $P/P_y = 1.0$. At this value of P/P_y a minimum value of $h\sqrt{F_y}/w = 300$ is reached.

The curve described above may be approximated by a linear relationship given by:

$$h\sqrt{F_y}/w = 660\ (1-0.55\ (P/P_y)) \qquad 0 \leq P/P_y \leq 1.0 \tag{6.11}$$

This relationship as well as the relationships defined by Equations 6.7 and 6.8 as established by Kulak and Perlynn[12] are shown in Figure 6.11.

In establishing the above linear approximation a line was drawn from point A at the end of the curve at $P/P_y = 1.0$ to the point of tangency at B and extended to intersect the vertical axis at

$h\sqrt{F_y}/w = 660$. This approximation results in conservative limitations of $h\sqrt{F_y}/w$ for low values of P/P_y. This is desirable however in order to avoid the sensitivity of the steep theoretical gradient in this region as well as to recognize the possibility of small unavoidable axial loads that may occur in service.

As can be seen from Figure 6.11, the theoretical method presented herein predicts more liberal web limitations than those presently required for Class 2 sections. However, implicit in these limitations is the use of M_{pc} as defined by Equation 6.10 based on local buckling considerations rather than the use of M_{pc} as defined on a strength basis by Equations 6.9. Referring to Figure 6.11, the web limitation for pure beam action at $P/P_y = 0.0$ is $h\sqrt{F_y}/w = 660$. As P/P_y increases, the web is subjected to decreasing amounts of flexural tension. As a result, the $h\sqrt{F_y}/w$ limitation decreases linearly to a minimum value of 300 for pure column action at $P/P_y = 1.0$. In the region of pure bending ($P/P_y = 0.0$), this theoretical limitation differs by about +27 per cent from that presently specified by Equations 6.7 and 6.8. As P/P_y increases this difference increases to a maximum of about 45 per cent at $P/P_y = 0.15$ and decreases to a minimum of +18 per cent for pure column action at $P/P_y = 1.0$. As explained previously, the theoretical limitations are based on the assumption that the maximum moment in the presence of axial load is that given by Equation 6.10. The presently specified limitations, on the other hand, are based on the results of test specimens whose moment capacities equalled or exceeded that given by Equations 6.9. In addition to the above theoretical limitations, the analytical method presented herein also gives results in good agreement with these test

results when the effects of the rigid plate boundary constraints necessary for testing are included. The marked difference between the theoretical limitations and the presently specified limitations is therefore largely attributable to the effects of necessary constraints used during testing.

6.4.3 Class 1 Beam-Columns

A Class 1 beam-column is proportioned so that the flange width-to-thickness term $b\sqrt{F_y}/2t = 54$. As discussed in Sections 6.2 and 6.3.3, this value was found to be adequate at the two extremes of beam-column action, namely pure axial strain and pure flexural strain. The behaviour of Class 1 beam-columns was investigated for a range of values of P/P_y between zero and one, and for values of $h\sqrt{F_y}/w$ between 325 and 800. The results of this investigation are presented in the form of interaction curves in Figure 6.12, where values of P/P_y are plotted against values of M_{cr}/M_p for various values of $h\sqrt{F_y}/w$.

Unlike those for Class 2 and Class 3 sections, the interaction curves for Class 1 sections do not become tangential to a line joining the points at $P/P_y = 1.0$ and $M_{cr}/M_p = 1.0$. For Class 2 and Class 3 sections it was found that at a given value of P/P_y, the maximum critical moment value is determined by flange local buckling capacity. However, in the present case, local buckling is controlled by the web for values of M_{cr}/M_p less than about 1.05. Since web buckling controls, for a given value of P/P_y an increase in the sturdiness of the web (corresponding to a reduced $h\sqrt{F_y}/w$ value) will result in an increase in the value of M_{cr}/M_p. Thus the curves in Figure 6.12 do not become tangential but rather, they are separated to

the right of one another as $h\sqrt{F_y}/w$ decreases.

In the region of pure flexural strains, an upward sweep of the curves is evident for values of $h\sqrt{F_y}/w$ less than or equal to 600. This is apparently due to two factors. Firstly, as the region of pure flexural strain is approached in the vicinity of $M_{cr}/M_p = 1.05$, the mode of failure changes from web buckling to flange buckling. The second factor which contributes to this upward sweep is the effect of strain-hardening on the flange. (It is shown in Figure 6.15 that a reduction in the value of E_{st} reduces this upward sweep).

Referring again to Figure 6.12, the equation of the line joining the points, $P/P_y = 1.0$ and $M_{cr}/M_p = 1.0$ is given by Equation 6.10 and is restated here as follows:

$$M_{cr}/M_p = (1-P/P_y) \tag{6.10}$$

For all values of $h\sqrt{F_y}/w$ corresponding to the curves shown in the figure, the moment ratio given by Equation 6.10 is either equalled or exceeded for certain values of P/P_y. This implies that the strain-hardening strain may be reached or exceeded for these values and therefore the hinge rotation necessary for plastic design sections is attainable. For values of $h\sqrt{F_y}/w$ equal to 325 and 350, the effect of strain-hardening is more pronounced as indicated by the increased slopes of the corresponding curves.

The cross-sectional strength interaction equation commonly used for plastic design sections[63,64] is also shown in Figure 6.12. This is described by Equations 6.9 as stated previously and repeated here for convenience as follows:

$$M_{pc} = M_p \qquad 0 \leq P/P_y \leq 0.15 \qquad (6.9(a))$$

$$M_{pc} = 1.18\, M_p\, (1-P/P_y) \qquad 0.15 \leq P/P_y \leq 1.0 \qquad (6.9(b))$$

These values are applicable as long as local and overall instability do not occur. The validity of Equations 6.9 has been verified experimentally using W12 x 36, W8 x 31, W4 x 13, and W14 x 78 sections[5,63,64,66] with values of $b\sqrt{F_y}/2t$ of 38, 60, 39 and 53, and values of $h\sqrt{F_y}/w$ of 206, 153, 84 and 186, respectively. For these plate width-to-thickness terms the theory presented herein verifies that local buckling indeed is not critical in these sections and therefore does not interfere with the strength limitation as given by Equations 6.9. However, it should be noted that the specimens used for the experimental verification of the strength limitation are considerably sturdier than those presently designated as Class 1 sections.

6.4.3.1 Current Specifications

As mentioned previously, Class 1 sections are those for which the flange width-to-thickness term is presently limited to 54. Under pure axial loading the web width-to-thickness term for all W shapes is presently limited to 255 and for pure beam action the limit[4] is set at 420 . In the intermediate range where beam-column action is required, a bi-linear curve is applicable. This bi-linear relationship is presently expressed as follows[4]:

$$h\sqrt{F_y}/w = 255 \qquad 0.28 \leq P/P_y \leq 1.0 \qquad (6.12)$$

$$h\sqrt{F_y}/w = 420\ (1-1.4\ P/P_y) \qquad 0 \le P/P_y \le 0.28 \tag{6.13}$$

The current code width-to-thickness limitation for column webs is set at $h\sqrt{F_y}/w = 255$. This value is based upon the results of specimen D6, one of six tested by Haaijer and Thurlimann[7]. The current web limitations for Class 1 beam-columns are based on semi-empirical values obtained by Haaijer and Thurlimann. Although no beam-columns were tested, they used the test results of specimens D2, D4, and D6 in which the webs were uniformly compressed. It was then assumed that values obtained at the level of critical strain for these specimens could be applied at the level of mean strain in the compression zone of a beam-column. Although the analysis did not directly incorporate the effects of residual stresses, in the region of critical stress between the proportional limit and complete yield, a transition curve was fitted on the basis of geometric considerations.

According to the present theory, the current value of $b\sqrt{F_y}/2t = 54$ is an adequate limitation for Class 1 sections and no reduction or increase is indicated. It is apparent, however, that the present web width-to-thickness limitations for these sections are conservative. The present theory predicts that the value of $h\sqrt{F_y}/w$ can be increased for all values of P/P_y.

6.4.3.2 Theoretical Limitations as Determined Herein

Class 1 beam-columns are required to reach and sustain the reduced plastic moment capacity through a hinge rotation sufficient for the redistribution of stresses within a structure prior to collapse[4,33,63]. Because of the stricter requirements, these sections

should be expected to satisfy the strength limitations of Equations 6.9. In fact, the theoretical method presented herein predicts that this is so and that the present web limitations are somewhat conservative for Class 1 sections.

Values of P/P_y versus M_{cr}/M_p are plotted for various values of $h\sqrt{F_y}/w$ for Class 1 sections as shown in Figure 6.12. The strength relationship given by Equations 6.9 is also plotted in this figure. As shown in Figure 6.12 the local buckling capacity equals or exceeds the strength capacity of Equations 6.9 for some values of $h\sqrt{F_y}/w$. Values of P/P_y may be determined at the points of intersection of the local buckling curves with the strength curve of Equations 6.9. The corresponding values of $h\sqrt{F_y}/w$ are plotted against P/P_y values in Figure 6.13.

The resulting curve has a value of $h\sqrt{F_y}/w = 800$ for pure beam action ($P/P_y = 0.0$). For a relatively small increase of P/P_y from zero to about 0.08 the $h\sqrt{F_y}/w$ values decrease rapidly to a value of 430. As P/P_y increases, a sharp knee portion of the curve occurs and at $P/P_y = 0.23$ and $h\sqrt{F_y}/w = 370$ the curve becomes linear with a slight drop in $h\sqrt{F_y}/w$ to about 360 as P/P_y increases to 0.75. As P/P_y increases further, a slightly rounded portion of the curve occurs with a gradual decrease in slope. The $h\sqrt{F_y}/w$ term reaches a value of 325 for pure column action ($P/P_y = 1.0$). (This value of $h\sqrt{F_y}/w$ is in contrast to a value of 300 for Class 2 and 3 sections. The slightly higher value for Class 1 sections is due to the effect of the sturdier flanges).

The curve described above may be approximated by a bi-linear relationship given by:

$$h\sqrt{F_y}/w = 430\ (1-0.93(P/P_y)) \qquad 0 \leq P/P_y \leq 0.15 \tag{6.14}$$

and,

$$h\sqrt{F_y}/w = 382\ (1-0.22(P/P_y) \qquad 0.15 \leq P/P_y \leq 1.0 \tag{6.15}$$

This approximation as well as the present web limitations given by Equations 6.12 and 6.13 are also shown in Figure 6.13.

In arriving at the above approximation, point A is located at $P/P_y = 1.0$ and $h\sqrt{F_y}/w = 300$. This value of $h\sqrt{F_y}/w$ is used here so that for pure column action, the web limitations for Class 1, 2, and 3 beam-columns would coincide at a value of $h\sqrt{F_y}/w = 300$. (As explained previously, the value of $h\sqrt{F_y}/w = 325$ for Class 1 sections is due to the sturdier flanges). Point C on Figure 6.13 is located on the vertical axis opposite point D where the initial portion of the curve first deviates from the tangent to the curve at $P/P_y = 0$. Through points A and C, tangents to the curve are drawn and extended to intersect at point B ($P/P_y = 0.15$).

The reason for constructing line BC in this manner is twofold. In the region of low axial loads (corresponding to line CD) the web width-to-thickness term is very sensitive to small changes in the axial load. This is witnessed by the very steep gradient of the initial portion of the curve. Since a value of low axial load would be very difficult to pin-point with any great degree of accuracy (in a practical design case) line BC is constructed to eliminate the effect of this high sensitivity for practical applications. Furthermore, in practical cases, it is very likely that residual axial loads of low magnitudes will be present to some degree even in members

designed for pure bending. This effect is also accounted for by the above construction.

As seen from Figure 6.13, the theoretical method presented herein predicts more liberal web limitations than those presently required for Class 1 sections. For pure beam action at $P/P_y = 0.0$, the present theory indicates a web limitation of $h\sqrt{F_y}/w = 430$ which is about 2 per cent greater than the presently specified value of 420 (Equation 6.13). As P/P_y increases to 0.15, $h\sqrt{F_y}/w$ decreases to 370 and, as P/P_y further increases, the maximum difference between the presently specified value of $h\sqrt{F_y}/w$ and that predicted by the analysis presented herein occurs at $P/P_y = 0.28$. At this point, the presently specified value of $h\sqrt{F_y}/w$ is 255 whereas the theory presented herein predicts a value about 40 per cent higher. As P/P_y increases, this difference decreases and at $P/P_y = 1.0$ the theory presented herein indicates a value about 18 per cent higher than the presently specified value of $h\sqrt{F_y}/w = 255$.

6.4.4 Effects of Residual Stresses

The effects of residual stresses on the local buckling capacities of beam-column sections were investigated for values of $b\sqrt{F_y}/2t = 54$, 64, and 72. Since the effects are similar in all three cases, only one such case will be presented here. For a value of flange slenderness of 54 (corresponding to a Class 1 section) and various values of web slenderness, beam-column interaction curves are shown in Figure 6.12 for $\sigma_{rc} = 0.3\sigma_y$ and in Figure 6.14 for a theoretical value of $\sigma_{rc} = 0$.

The rounded knee portions of the curves in Figure 6.12 are

due to residual stresses which result in a gradual yielding within a cross-section. As shown in Figure 6.14, these rounded knee portions change to an abrupt transition in the absence of residual stresses. As can be seen, a Class 1 beam-column can perform adequately over a range of web slendernesses between 440 and 1000 where the residual stress has a theoretical value of zero. In the presence of a practical value of residual stress of $\sigma_{rc} = 0.3\sigma_y$, on the other hand, Figure 6.12 shows that these web slenderness values are reduced to 325 for pure column action and 800 for pure beam action.

6.4.5 Effects of Strain-hardening Modulus

The effect of varying the strain-hardening modulus on the local buckling capacities of beam-columns was studied for flange slenderness values of 54, 64, and 72. The same three values of strain-hardening modulus used in the study of column and beam local buckling were also used here. For $b\sqrt{F_y}/2t$ values of 72 and 64 and practical values of $h\sqrt{F_y}/w$ between 300 and 800 as used in the interaction diagrams and shown in Figures 6.8 and 6.10, the values of E_{st} investigated had no effect on local buckling capacities. For Class 1 sections ($b\sqrt{F_y}/2t$ = 54) and practical values of web slenderness between 325 and 800 (as used in Figure 6.12) the effect of varying the strain-hardening modulus is significant for certain values of $h\sqrt{F_y}/w$.

For the values of strain-hardening modulus considered, Figure 6.15 shows the interaction curves corresponding to $b\sqrt{F_y}/2t = 54$ and values of $h\sqrt{F_y}/w$ of 325, 500 and 800. These three values were chosen as being representative of the range of web slendernesses considered practical for Class 1 sections. When $h\sqrt{F_y}/w = 325$, the

effect of strain-hardening is present over the entire length of the curve. For pure beam action ($P/P_y = 0$), the effect of the strain-hardening modulus is quite significant. As P/P_y increases this effect diminishes and is least significant when pure column action ($P_{cr}/P_y = 1.0$) is approached. As $h\sqrt{F_y}/w$ is increased the significance of strain-hardening (for the values investigated) becomes less noticeable. At $h\sqrt{F_y}/w = 500$ the effect of varying E_{st} is noticeable at the point of pure beam action ($P/P_y = 0$). As P/P_y increases, this effect decreases and is no longer evident for values of P/P_y between 0.5 and the critical load ratio. As $h\sqrt{F_y}/w$ is further increased, the effect of varying the strain-hardening modulus over the range considered also decreases. At $h\sqrt{F_y}/w = 800$ no effect of changing the value of the strain-hardening modulus is evident. As can be seen from Figure 6.15, for the range of values of strain-hardening modulus considered, a Class 1 beam-column section has adequate performance with regard to local buckling capacity.

6.4.6 Effects of Specimen Length

It has been thoroughly demonstrated by several investigators[2,3,6,16,26] that critical plate buckling stresses approach relatively high values with decreasing values of aspect ratio (the ratio of the length of a plate in the direction of uniaxial stress to its transverse dimension). At a theoretical aspect ratio equal to zero, the critical buckling stress is infinite and as the aspect ratio increases for a given specimen, the predicted critical buckling stress rapidly decreases. At some point a value of the aspect ratio will be reached above which the predicted critical stress becomes stable. This

behaviour is illustrated in Figure 6.16 for a column having a flange slenderness value of 72 and a web slenderness value of 300. As the length, L, increases from zero, the critical load ratio drops rapidly and reaches a stable value for length values greater than 12. This corresponds to an aspect ratio of 2.4 for the flanges and 1.2 for the web for this particular specimen.

Investigations similar to the above have been carried out for additional columns, beams, and beam-columns of various dimensions. From this analysis it was determined that stable values of critical local buckling stress would be reached for all specimens having minimum aspect ratios of 4 for the flanges and 2 for the webs.

Figure 6.17 summarises the findings of this investigation by showing the length effects on the interaction diagrams of Class 1 beam-columns having web slenderness values of 325, 500, and 800. A Class 1 beam-column was chosen so that the length effect could be evaluated for a range of values of load ratio and moment ratio as well as a range of material conditions from elastic to fully strain-hardened. These include those values that occur: (1) at an elastic or partially yielded stress level ($h\sqrt{F_y}/w = 800$), (2) at an elastic, partially yielded, or a strain-hardened stress level ($h\sqrt{F_y}/w = 500$), and (3) at a strain-hardened stress level ($h\sqrt{F_y}/w = 325$).

Each curve in Figure 6.17 was plotted for values of the length, L, of 15, 20, 25, and 30. These values correspond to flange aspect ratios of 3, 4, 5, and 6, and to web aspect ratios of 1.5, 2.0, 2.5, and 3.0. For all specimens the length effect is negligible in the region for which $M_{cr} > M_p(1-P/P_y)$. This corresponds to the region where complete yielding has occurred and strain-hardening is imminent.

Presumably a negligible effect of the variation of aspect ratios investigated occurs in this region because of the reduced stiffness of the material in the strain-hardening region. In the elastic region (the initially flat portion of the curves corresponding to $h\sqrt{F_y}/w$ = 500 and 800) and the partially yielded region (the remaining portion of these curves up to the line $M_{cr} = M_p(1-P/P_y)$), the length effects are noticeable. For all cases considered however, the length effects are negligible for values of length of 20 or greater. A length value of 20 corresponds to a flange aspect ratio of 4 and a web aspect ratio of 2. As a result of this investigation, these aspect ratios were the minimum values used for all specimens in the parametric studies presented herein.

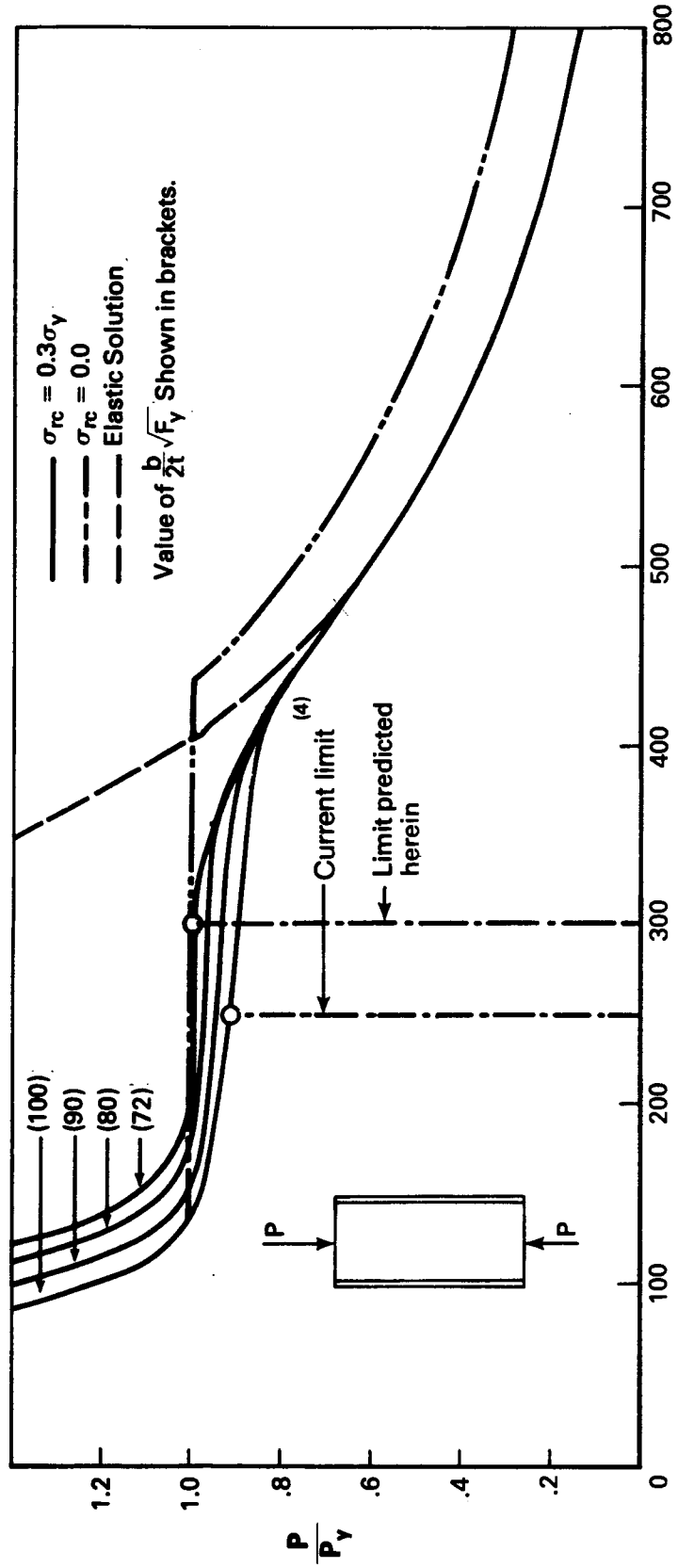

Figure 6.1 Effect of $\frac{h}{w}\sqrt{F_y}$ on $\frac{P}{P_y}$ for Various Values of $\frac{b}{2t}\sqrt{F_y}$

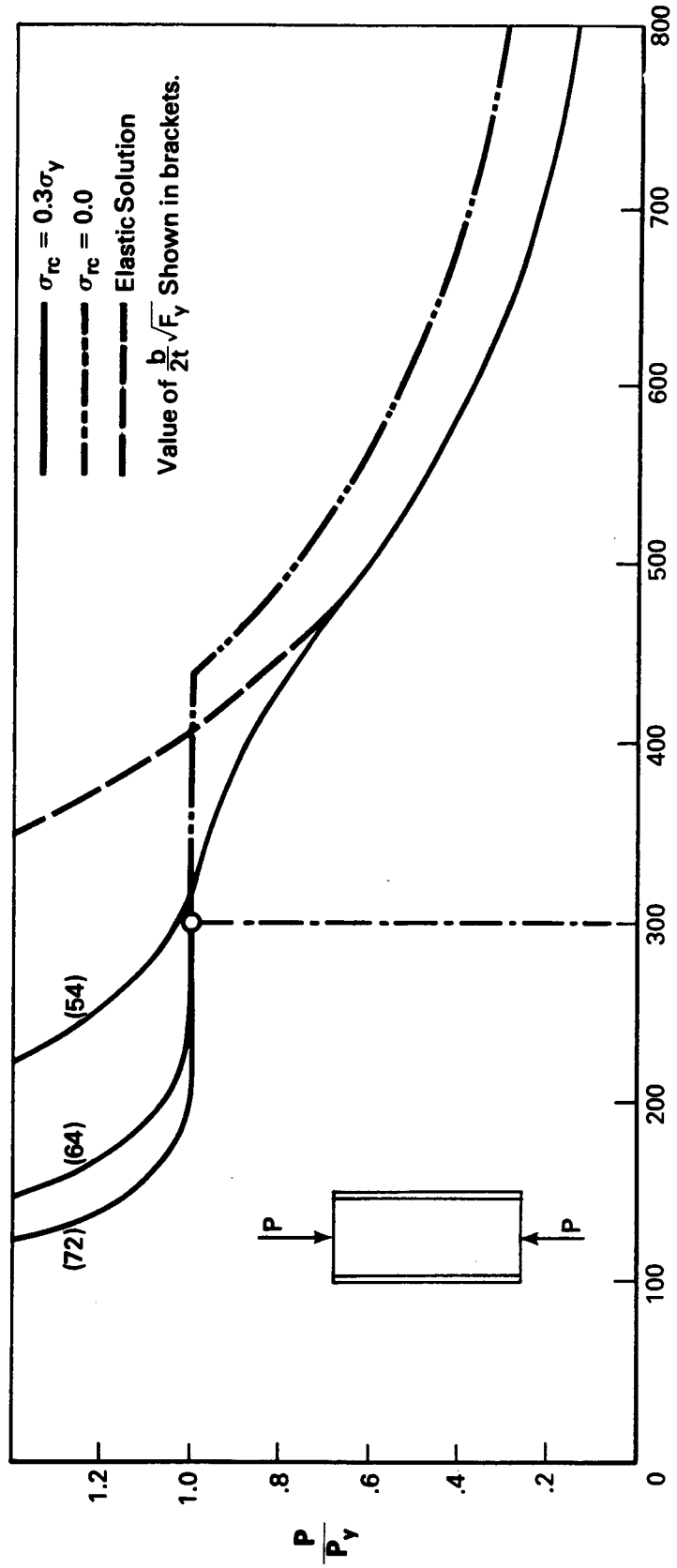

Figure 6.2 Effect of $\frac{h}{w}\sqrt{F_y}$ on $\frac{P}{P_y}$ for $\frac{b}{2t}\sqrt{F_y}$ Values of 54, 64, and 72.

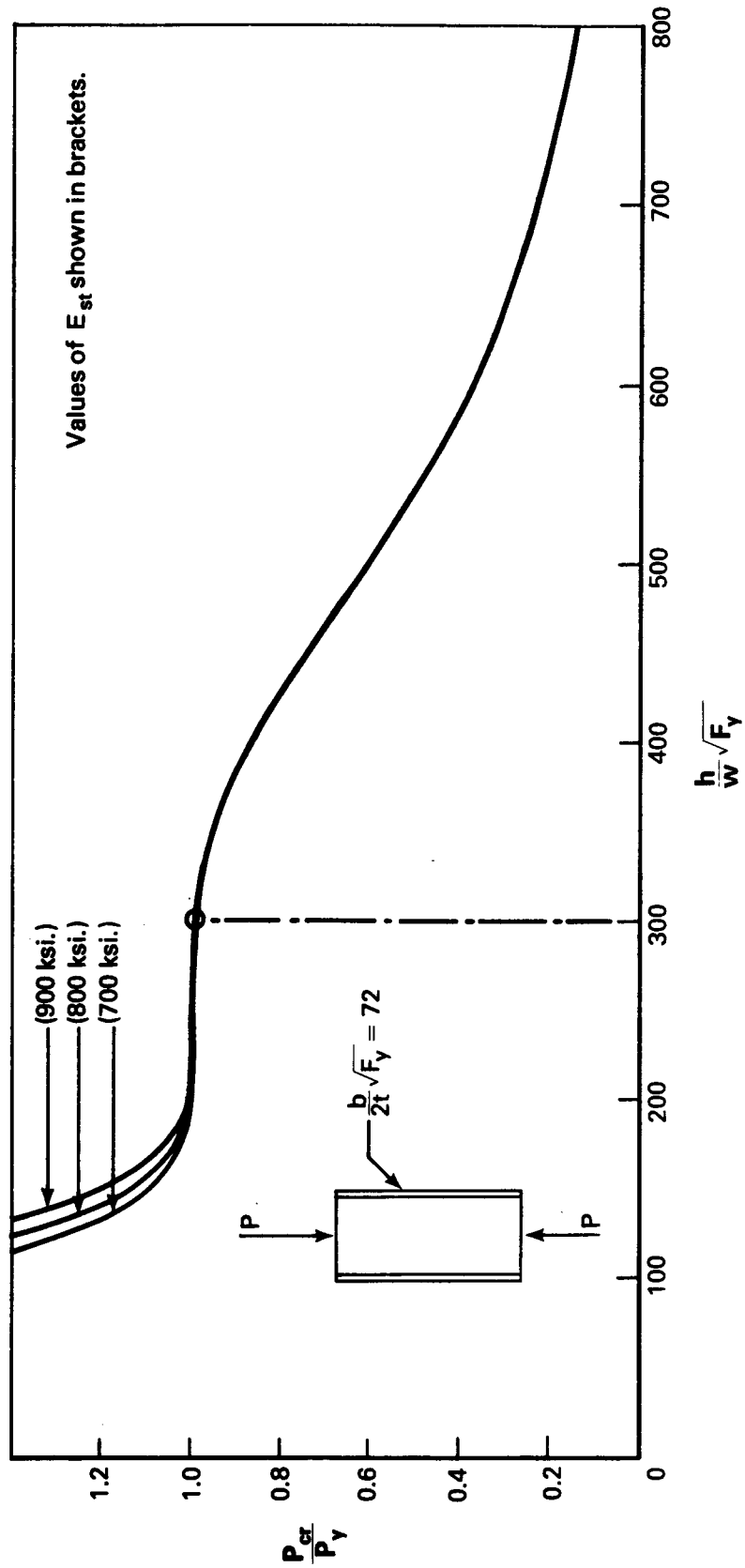

Figure 6.3 $\frac{P_{cr}}{P_y}$ vs. $\frac{h}{w}\sqrt{F_y}$ for Values of E_{st} = 700, 800, and 900 ksi.

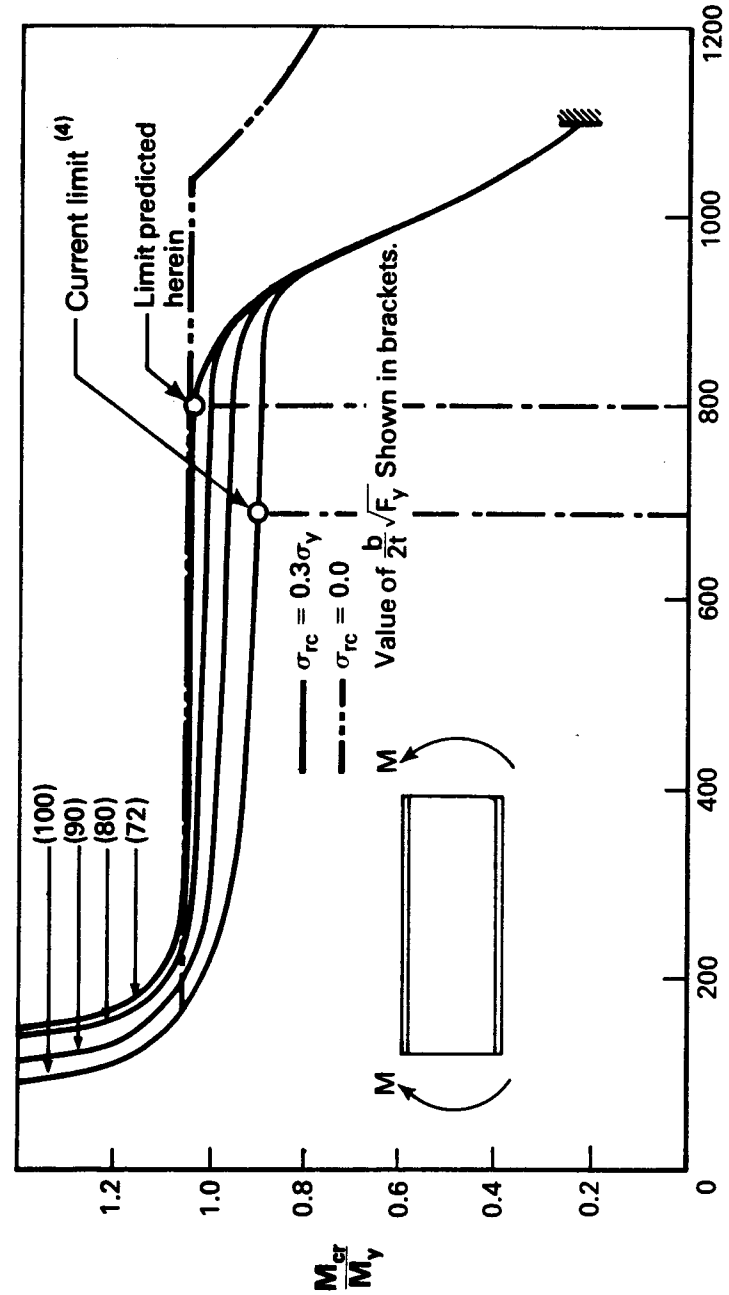

Figure 6.4 Effect of $\frac{h}{w}\sqrt{F_y}$ on $\frac{M_{cr}}{M_y}$ for Various Values of $\frac{b}{2t}\sqrt{F_y}$

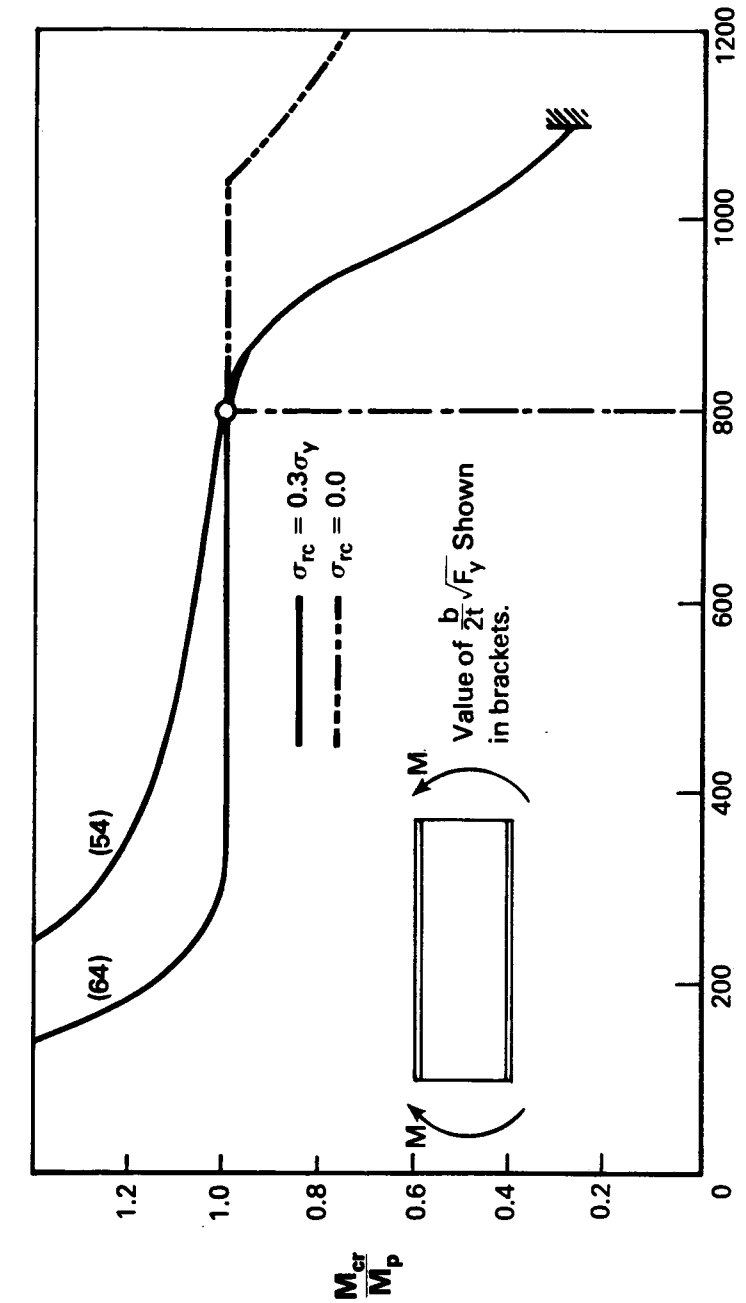

Figure 6.5 Effect of $\frac{h}{w}\sqrt{F_y}$ on $\frac{M_{cr}}{M_p}$ for Various Values of $\frac{b}{2t}\sqrt{F_y}$

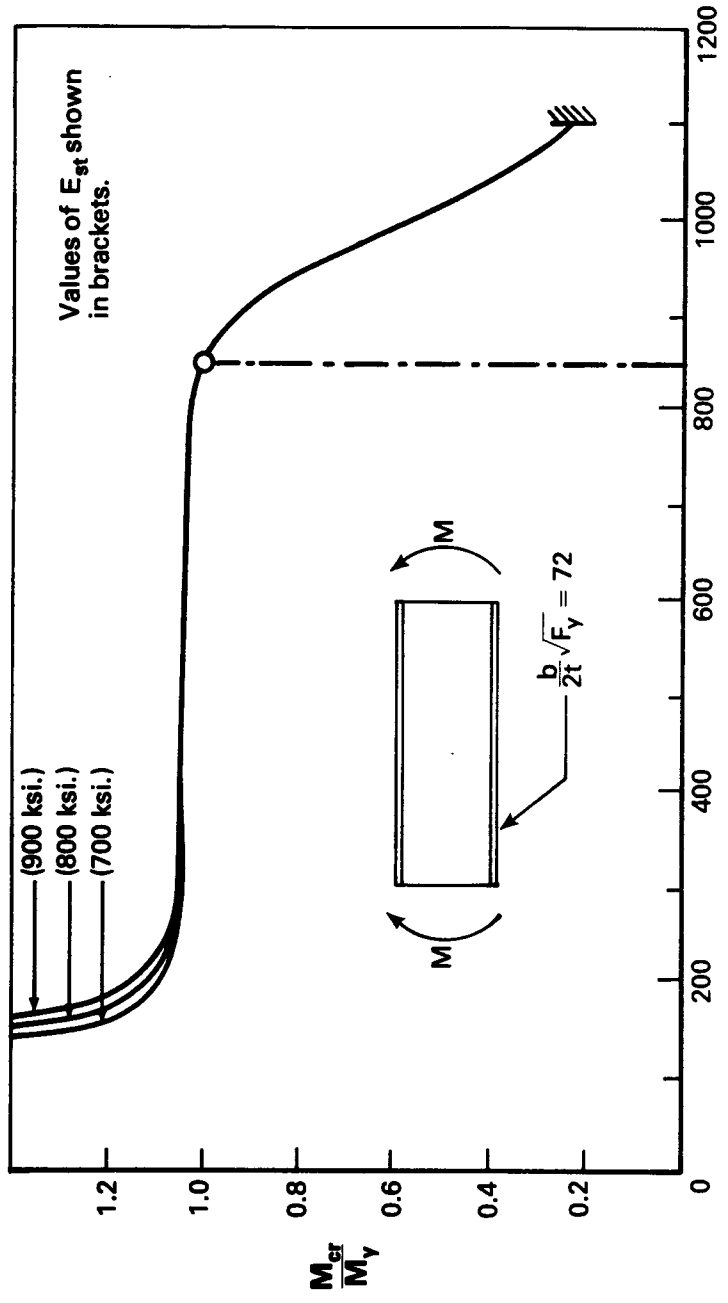

Figure 6.6 $\frac{M_{cr}}{M_y}$ vs. $\frac{h}{w}\sqrt{F_y}$ for Values of E_{st} = 700, 800, and 900 ksi.

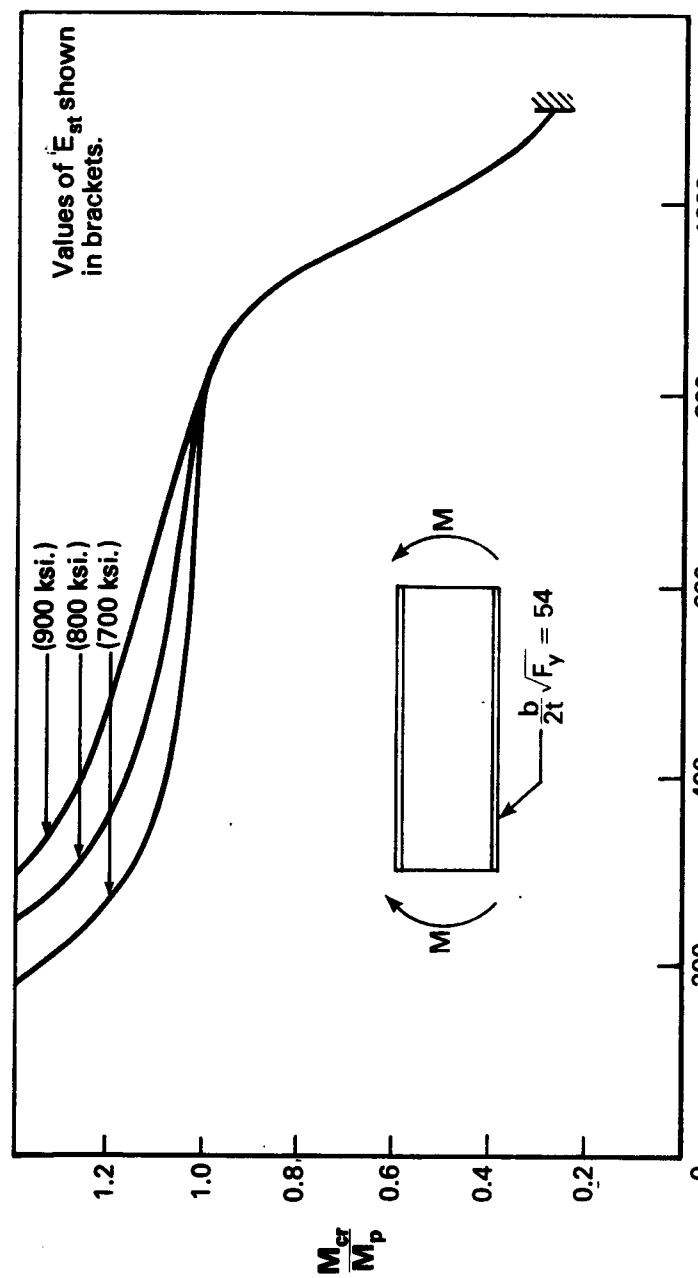

Figure 6.7 $\frac{M_{cr}}{M_p}$ vs. $\frac{h}{w}\sqrt{F_y}$ for Values of E_{st} = 700, 800, and 900 ksi.

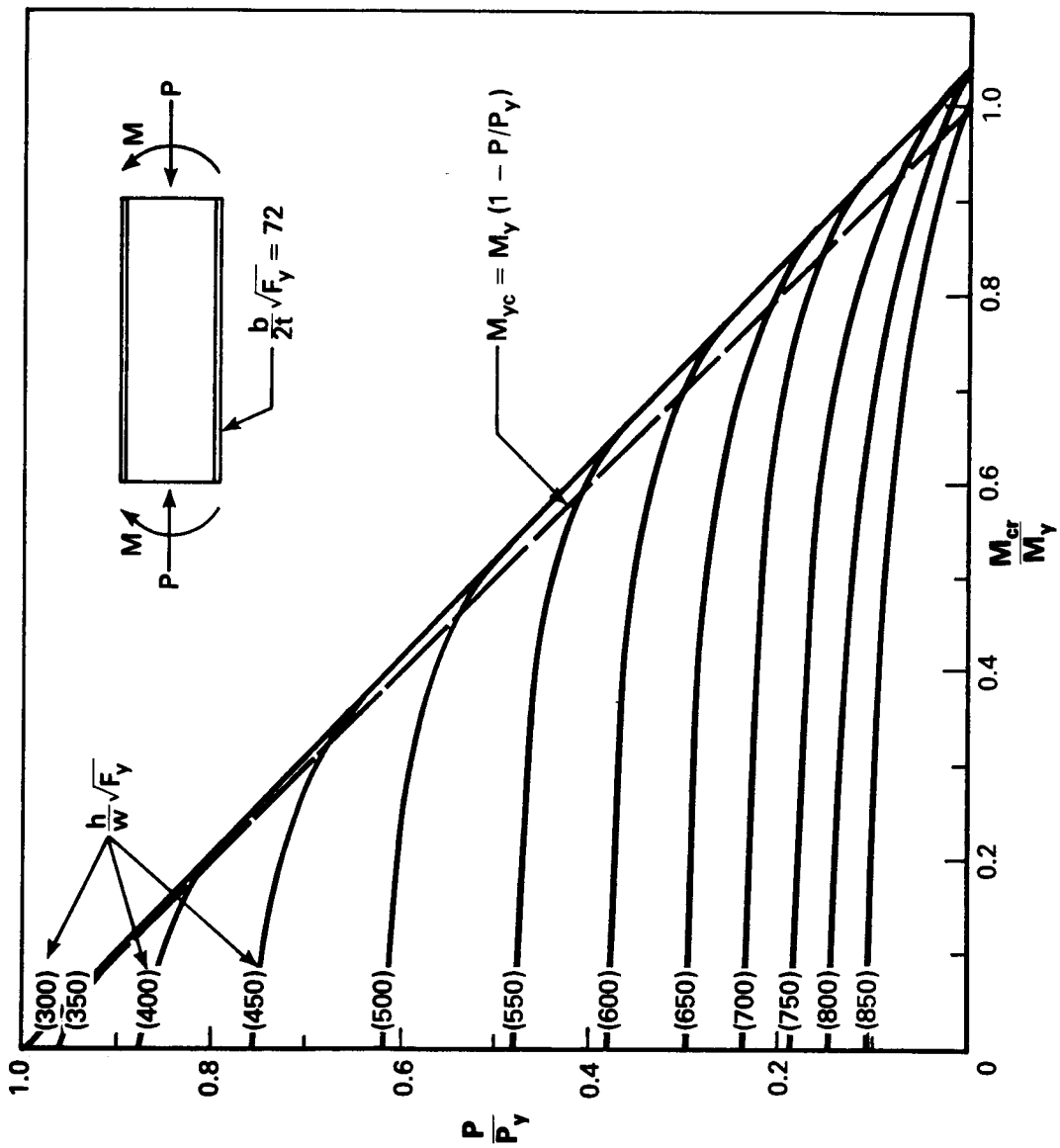

Figure 6.8 Effect of $\frac{P}{P_y}$ on $\frac{M_{cr}}{M_y}$ for Various Values of $\frac{h}{w}\sqrt{F_y}$

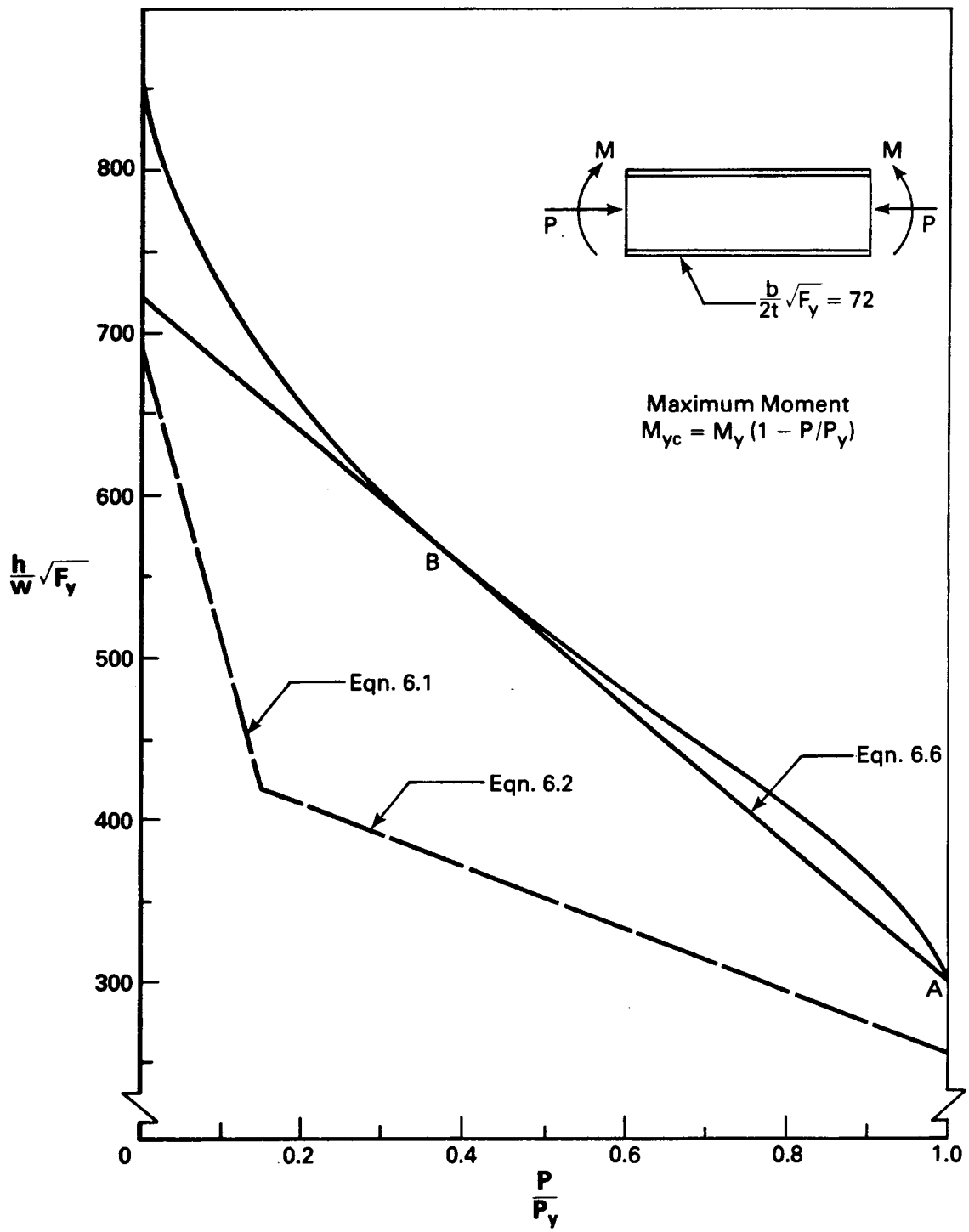

Figure 6.9 $\frac{h}{w}\sqrt{F_y}$ vs. $\frac{P}{P_y}$ for a Class 3 Section

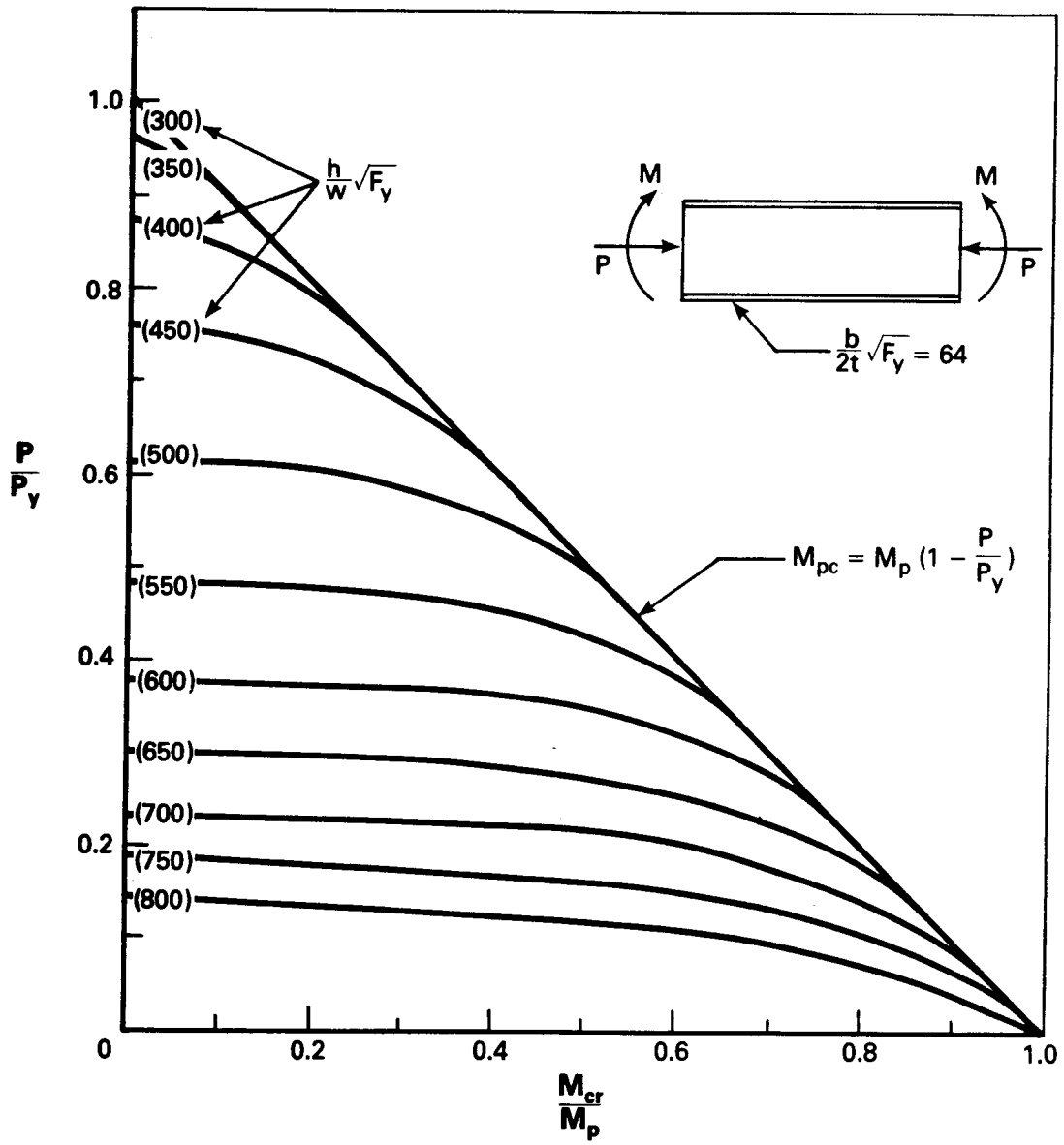

Figure 6.10 Effect of $\frac{P}{P_y}$ on $\frac{M_{cr}}{M_p}$ for Various Values of $\frac{h}{w}\sqrt{F_y}$

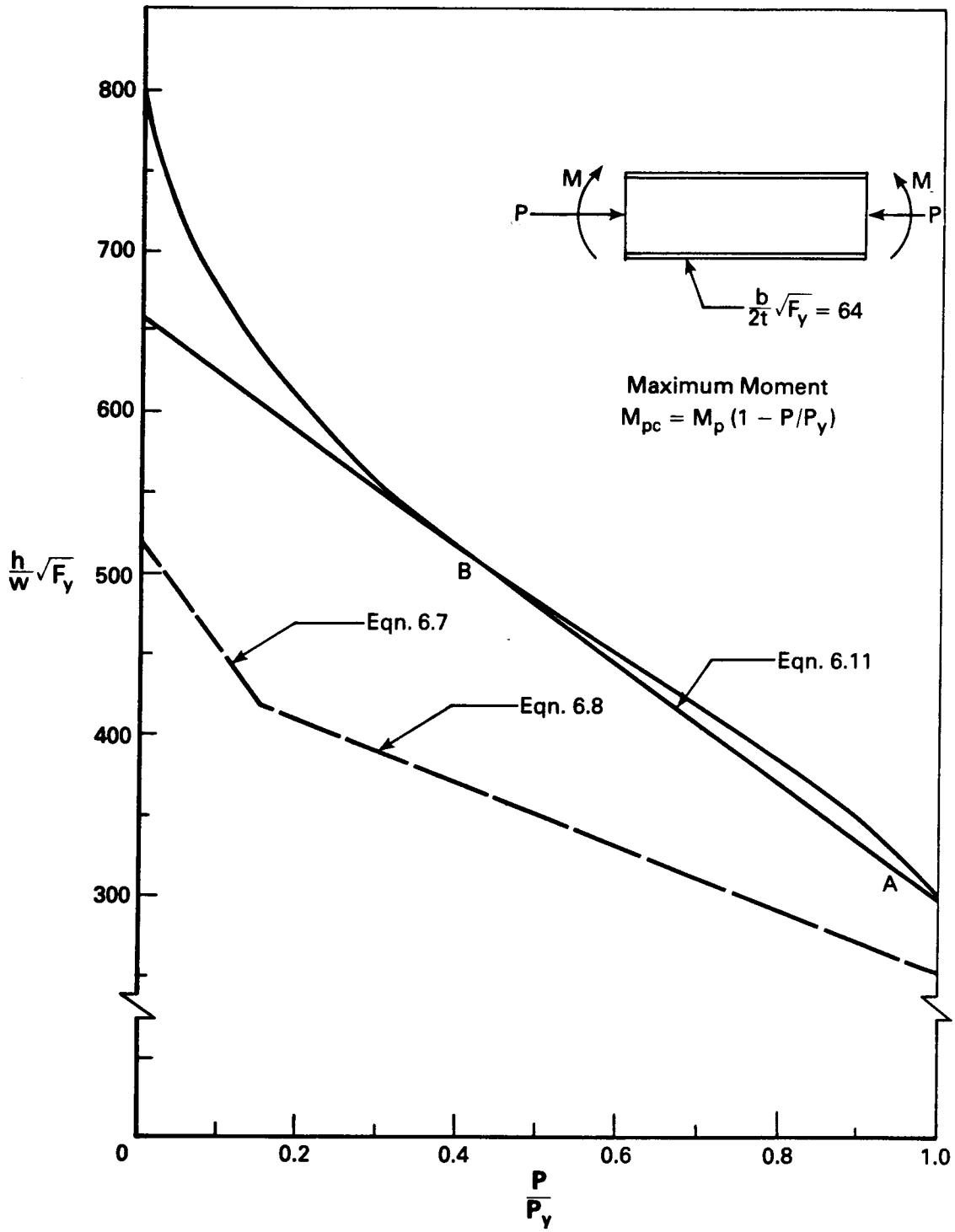

Figure 6.11 $\frac{h}{w}\sqrt{F_y}$ vs. P/P_y for a Class 2 Section

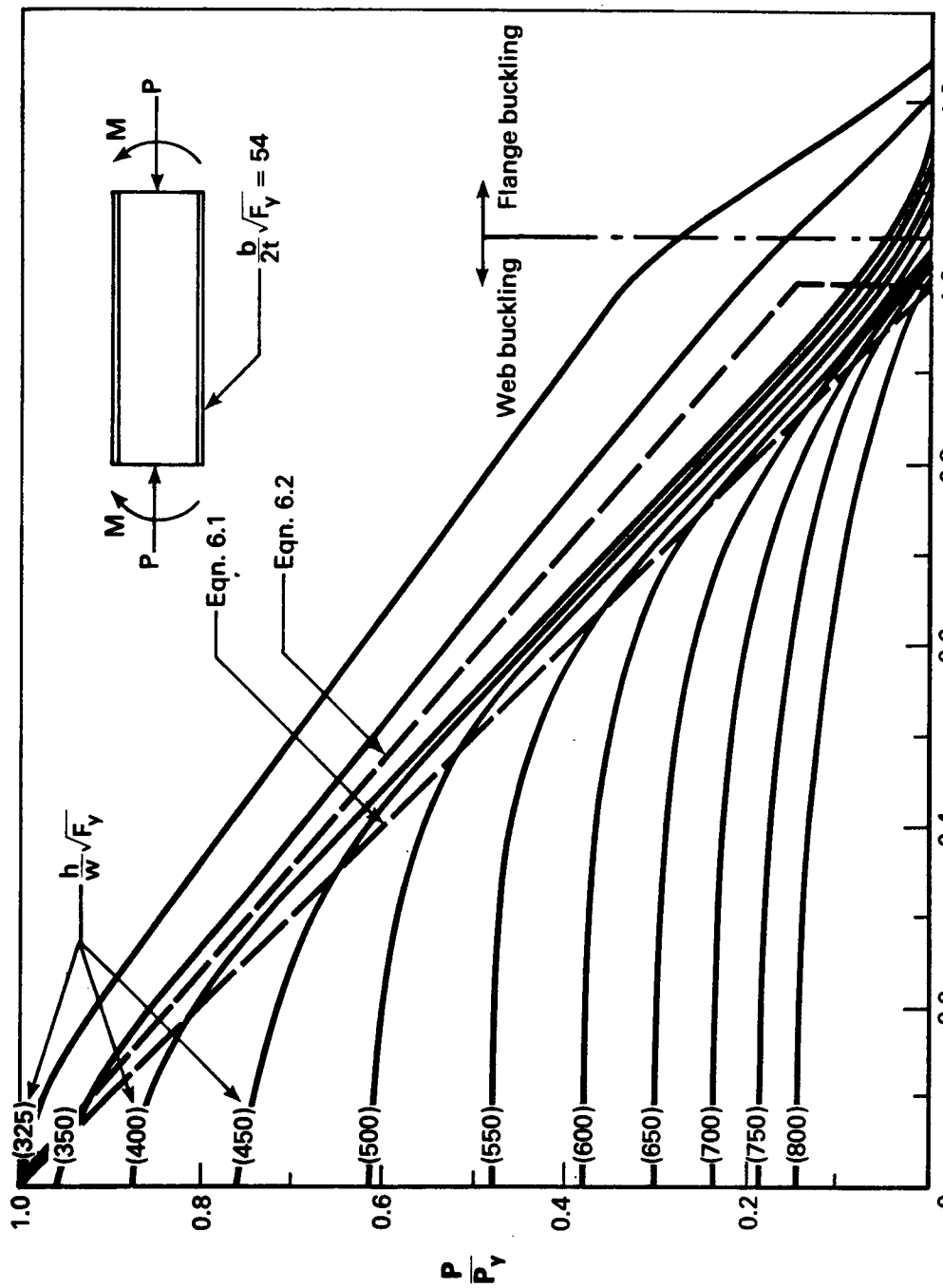

Figure 6.12 Effect of $\frac{P}{P_y}$ on $\frac{M_{cr}}{M_p}$ for Various Values of $\frac{h}{w}\sqrt{F_y}$

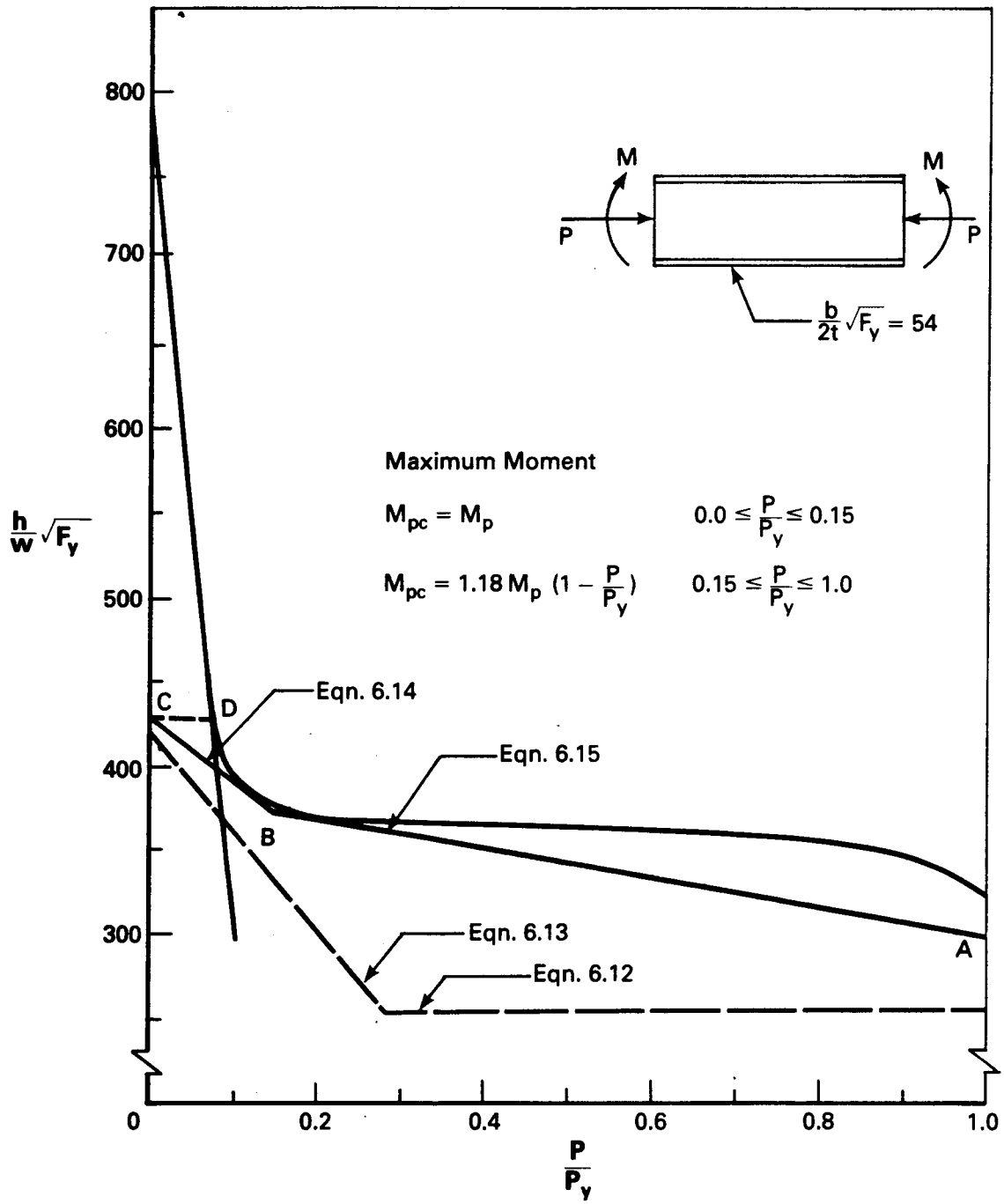

Figure 6.13 $\frac{h}{w}\sqrt{F_y}$ vs. $\frac{P}{P_y}$ for a Class 1 Section

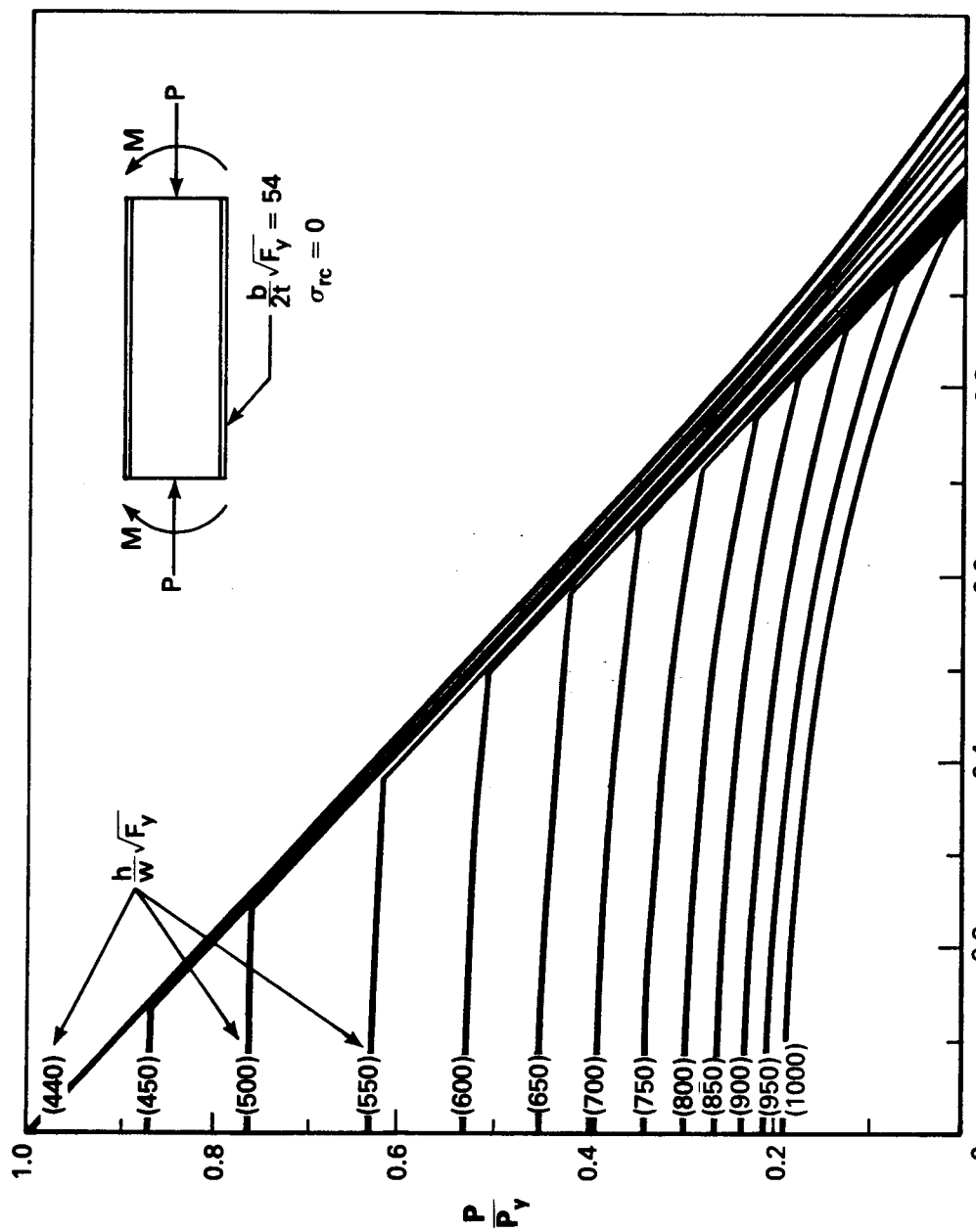

Figure 6.14 $\frac{P}{P_y}$ vs. $\frac{M_{cr}}{M_p}$ for Various Values of $\frac{h}{w}\sqrt{F_y}$ and $\sigma_{rc} = 0$

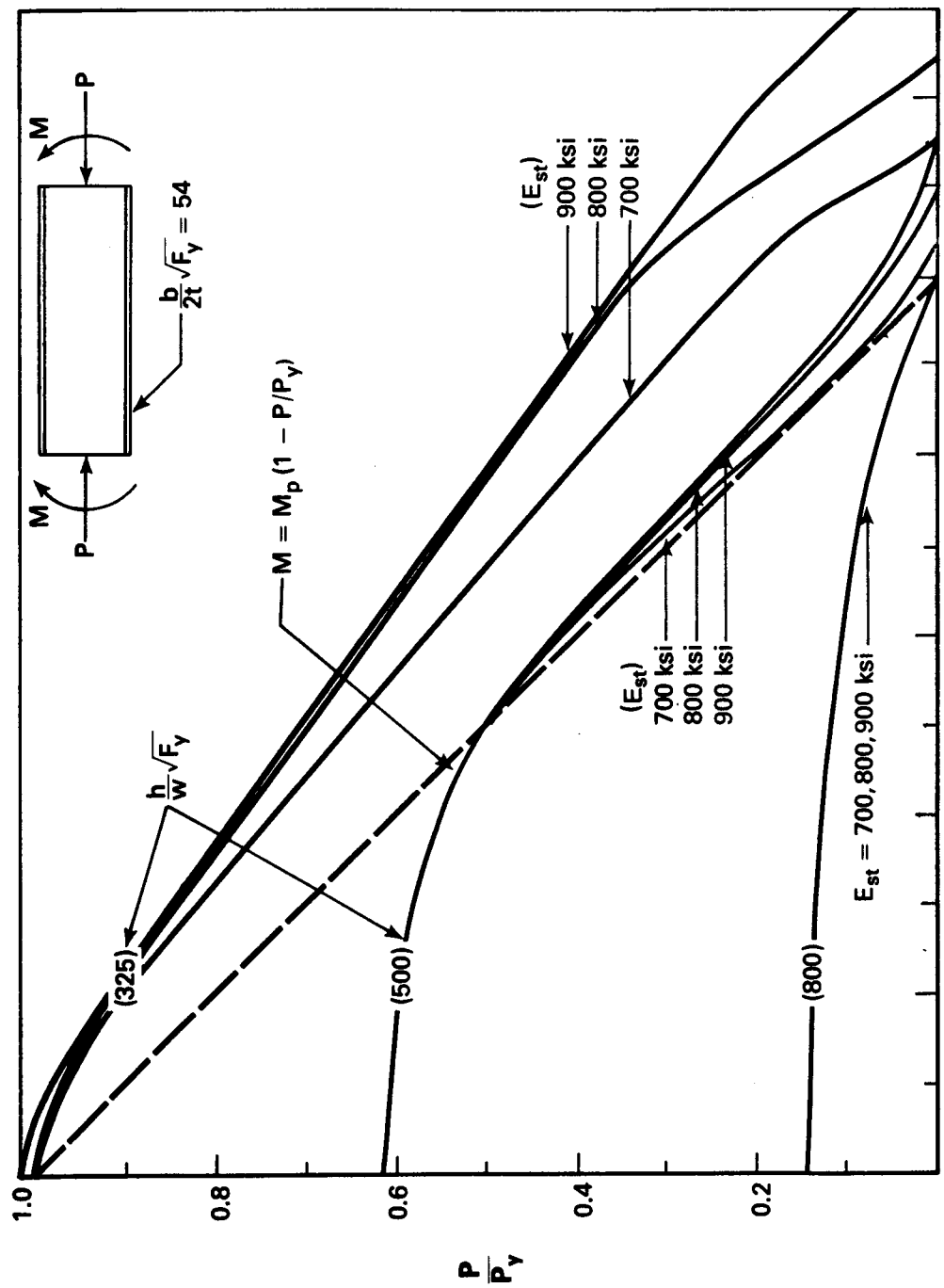

Figure 6.15 Effect of E_{st} on the Interaction of $\frac{P}{P_y}$ and $\frac{M_{cr}}{M_p}$

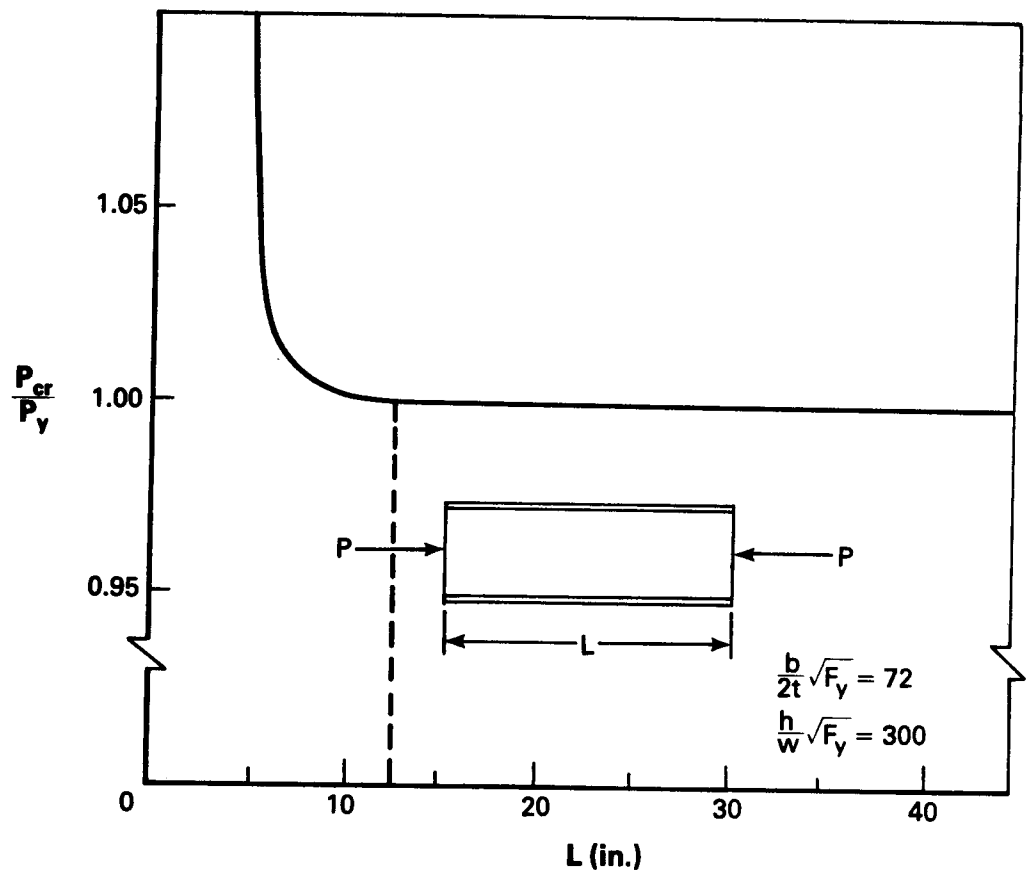

Figure 6.16 Effect of Length on Critical Load Prediction

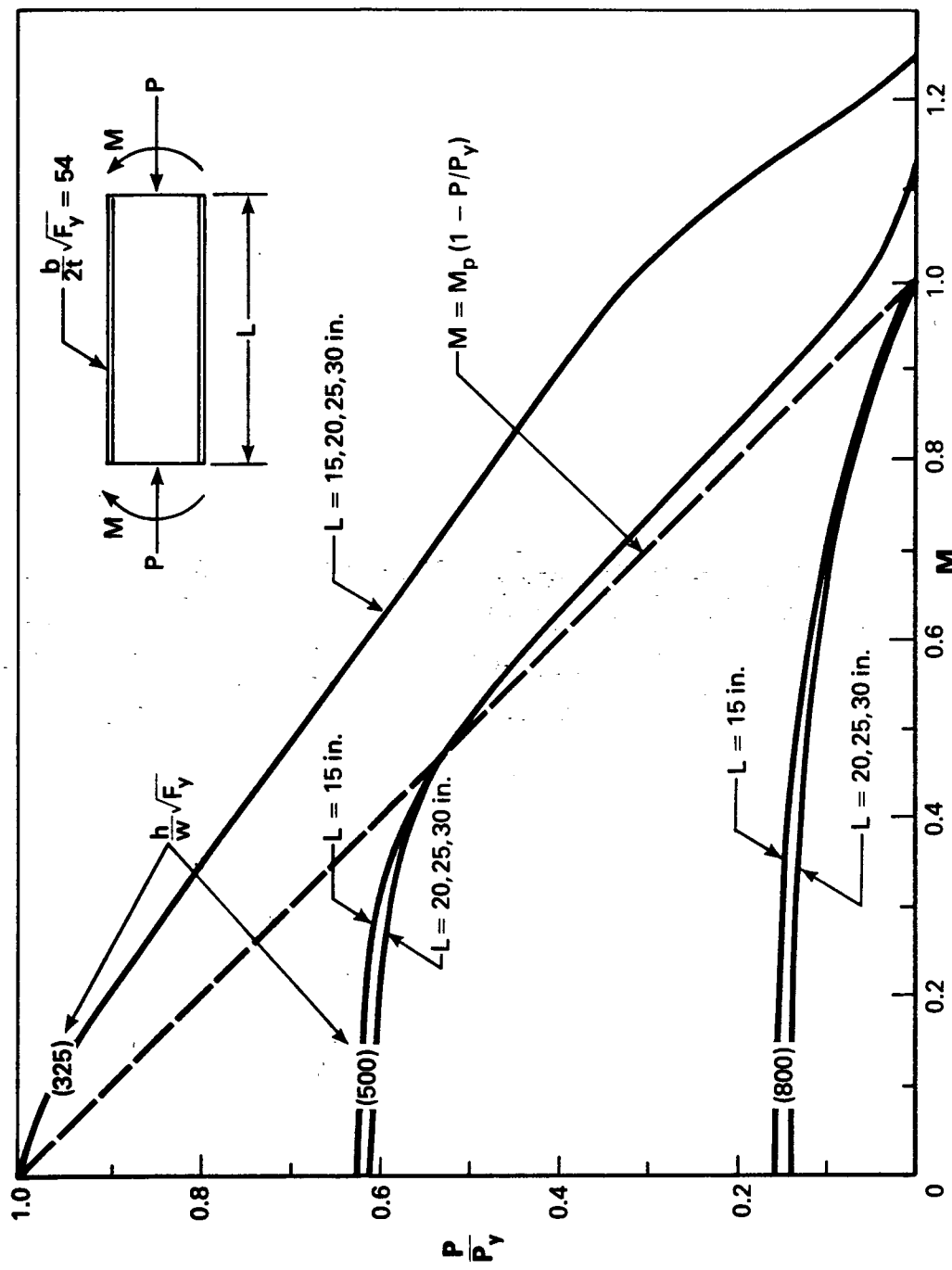

Figure 6.17 Effect of Length on the Interaction of $\frac{P}{P_y}$ and $\frac{M_{cr}}{M_p}$

Chapter 7

SUMMARY AND CONCLUSIONS

7.1 Introduction

The problem of local buckling of flange- and web-plate components of W-shapes subjected to axial compression, flexural compression, and axial and flexural compression combined has been extensively investigated. A review of the available literature in this area has revealed that a few investigators have previously attempted to deal with various aspects of this problem which is complex with respect to the practical difficulties of laboratory testing as well as with respect to theoretical modelling. At the present time, among the more notable contributions in this area are those of Haaijer and Thurlimann[7], Bleich[6], Timoshenko[2,26], and Kulak[10,11,12,13]. In all cases, however, the theoretical investigations have been either totally or partially empirical or semi-empirical in nature. Futhermore, only the latter investigator has attempted to include all aspects of the problem in an experimental program for Class 1, 2, and 3 sections subjected to the three types of loading mentioned above. The present investigation is an extension of this work and is primarily an attempt to formulate a sound theoretical basis for predicting both elastic and inelastic local buckling capacities of W shapes. In the following sections the scope of the theory is summarised, the findings are discussed with respect to existing design limitations and suggested modifications are indicated.

7.2 Summary of the Theoretical Method

The theoretical method presented herein has been formulated for the analysis of local buckling capacities of uniform members of W shape cross-sections. These members may be end-loaded in axial compression, flexural compression or combined axial and flexural compression. The flange - web restraint interaction is included directly in the formulation and the ends of a member may be rigidly supported or pinned with respect to plate buckling. The presence of residual stresses is accounted for by including their effects directly in the formulation of the local buckling geometric stiffness matrices of the plate components. Using an eigenvalue matrix iteration technique the elastic local buckling capacity is determined. If this value exceeds the proportional limit, an applied linear strain is gradually incremented above this limit and, at each level, gradual yielding of the section is evaluated and the position of the neutral axis is updated so that equilibrium conditions on the cross-section are satisfied. The member is then analysed for a critical eigenvalue strain. Essentially, when the critical eigenvalue strain is zero, the applied strain corresponds to the critical buckling strain. In this manner, the increase in strains and gradual yielding of a cross-section simulate actual conditions. Because of the flexibility of the shape functions used in the formulation, the method is capable of predicting separate flange or web buckling or a combination of both.

7.3 Summary of Findings

The present theoretical method has been verified by comparison of predicted results with the results of 53 test specimens of various dimensions and subjected to various load combinations.

Additionally, in the elastic range, the method gives results which agree with those predicted using widely acceptable classical methods[2,6]. A large number of hypothetical beams, columns, and beam-columns for each class of section has also been investigated. As a result of this study the analytical method presented herein indicates that the present code limitation for flanges of Class 3 sections is inadequate. This limitation is based on a purely theoretical torsional analysis of the flange[1]. For Class 1 and 2 sections, on the other hand, the analytical method presented herein substantiates the flange slenderness limitations of 54 and 64 which have been well established by experimental investigations. It is clear therefore, that the same theory which substantiates flange slenderness values of 54 and 64 based on experimental results for Class 1 and 2 sections, casts doubt upon the flange slenderness value of 100 based on an approximate torsional analysis of a Class 3 section flange. Assuming the above flange modification as indicated, presently specified web plate width-to-thickness limitations may be increased for columns, beams, and beam-columns.

7.4 Recommendations for Design

As a result of the theoretical investigation presented herein certain modifications of the present code values[4] of plate width-to-thickness limitations are indicated. These modifications apply to W shapes subjected to axial, flexural, and combined axial and flexural loadings that are uniform along the member lengths. Additionally, certain flange width-to-thickness limitations presently set by the code have been substantiated. These results, as summarised in Figure 7.1, are discussed in the following sections.

7.4.1 Class 1 Sections

The present theory substantiates the use of $b\sqrt{F_y}/2t = 54$ for the flanges of Class 1 sections. It is indicated that the present limitation of $h\sqrt{F_y}/w = 255$ for pure axial loading can be safely increased to 300. For pure flexural loading an increase of $h\sqrt{F_y}/w$ from the present code value of 420 to a value of 430 is indicated. In the intermediate range, where combined axial and flexural loadings occur, the following increases in $h\sqrt{F_y}/w$ are indicated:

$$h\sqrt{F_y}/w = 430\ (1-0.93\ (P/P_y)) \qquad 0 \leq P/P_y \leq 0.15 \tag{6.14}$$

$$h\sqrt{F_y}/w = 382\ (1-0.22\ (P/P_y)) \qquad 0.15 \leq P/P_y \leq 1.0 \tag{6.15}$$

For these values the present theoretical method indicates that the following maximum moments reduced for axial load, can be sustained for adequate plastic design behaviour:

$$M_{pc} = M_p \qquad 0 \leq P/P_y \leq 0.15 \tag{6.9(a)}$$

$$M_{pc} = 1.18\ M_p\ (1-P/P_y) \qquad 0.15 \leq P/P_y \leq 1.0 \tag{6.9(b)}$$

7.4.2 Class 2 Sections

According to the present theoretical method, the value of $b\sqrt{F_y}/2t = 64$, as presently set by the code for Class 2 sections, is adequate with respect to local buckling provided that the maximum reduced moment value is set at:

$$M_{pc} = M_p \ (1-P/P_y) \tag{6.10}$$

For pure axial loading it is indicated that the present web limitation of $h\sqrt{F_y}/w = 255$ can be increased to 300. For pure flexural loading the present value of $h\sqrt{F_y}/w = 520$ can be increased to 660. In the intermediate range of combined axial and flexural loading the following increases are indicated:

$$h\sqrt{F_y}/w = 660 \ (1-0.55 \ (P/P_y)) \quad 0 \leq P/P_y \leq 1.0 \tag{6.11}$$

7.4.3 Class 3 Sections

The present theoretical method indicates that the value of $b\sqrt{F_y}/2t = 100$ for flanges of Class 3 sections is too high. A reduction to a value of 72 is indicated. In the presence of pure axial loads the present value of $h\sqrt{F_y}/w = 255$ can be increased to 300 and, for beams, the present code value of $h\sqrt{F_y}/w = 690$ can be increased to 725. In the intermediate range where combined axial and flexural loadings occur the following increases are indicated:

$$h\sqrt{F_y}/w = 725 \ (1-0.59 \ (P/P_y)) \quad 0 \leq P/P_y \leq 1.0 \tag{6.6}$$

For these values a maximum moment value of

$$M_{yc} = M_y \ (1-P/P_y)) \tag{6.5}$$

can be reached in the presence of axial load. The above indicated modifications for Class 1, 2, and 3 sections are summarised in

Figure 7.1.

7.5 Further Recommendations

As a result of the tests performed by Kulak et al[10,11,12,13], increases in web limits for Class 2 and 3 sections have recently been implemented by the present code[4]. The theory presented herein indicates that these increases are also justified on a purely theoretical basis. Furthermore, according to this theoretical method, additional increases in web slendernesses are indicated with the reservations that Class 3 flange limits be set at $b\sqrt{F_y}/2t = 72$ and that M_{pc} for Class 2 beam-columns be limited to the value given by Equation 6.10. Increases in web limits for Class 1 sections are also indicated by the theoretical results presented herein.

Before these additional increases are implemented, however, it is suggested that further testing of laboratory specimens be carried out. These tests should be performed in the light of certain implications arising from the present theoretical analysis. The items of particular relevance to test specimens and testing procedure are listed below:

1. End Conditions

As nearly as possible, the end supports of test specimens should approximate simply-supported plate edges with respect to local buckling. For axially loaded members this is not a difficult problem. However, for members that must be subjected to axial and flexural loads combined, it would be necessary to use end-moment connections requiring very rigid support of the plate edges. A solution to this problem

would be to use members sufficiently long so that the effects of rigid edge restraints are reduced. An aspect ratio of at least 4 for webs and flanges is suggested.

2. Lateral Support

To ensure a local buckling mode of failure, adequate lateral support must be provided in order to preclude overall lateral-torsional instability. Lateral supports should be designed so as not to interfere with local buckling. It is suggested that knife-edge lateral supports be placed at web-to-flange junctions if possible.

3. Residual Stresses

If local buckling is expected to occur in the elastic or partially yielded regions, an exact determination of residual stress magnitude and distribution is especially important. In the present correlation of theoretical and test results this information was not available and therefore, typical values had to be assumed. As a result, partially due to this lack of information, discrepancies between theoretical predictions and test results are evident. Future experimental investigations of local buckling should incorporate the exact determination of residual stresses as part of the test program.

4. Material Properties

At the present time there are conflicting opinions[5,22,24,27,33] as to what values of material properties are applicable in the range of strain between the yield strain and the strain at the onset of strain-hardening. Further investigations in this area

would be desirable. Values of the strain at the onset of strain-hardening as well as values of the strain-hardening modulus were not available for several of the test specimens referred to in the present investigation. Therefore, typical values had to be assumed and this partially contributed to discrepancies between theoretical predictions and test results. In future testing, it is recommended that attempts be made to determine strain-hardening strains and moduli during standard tension coupon tests.

7.6 Conclusions

A sound theoretical analysis similar to a finite strip technique has been developed and verified for the purpose of determining critical local buckling loads for W shape structural members. These members may be end-loaded by axial loads, flexural loads, or axial and flexural loads combined. The method predicts local buckling of flanges and webs in the elastic and inelastic ranges and the interaction of the flanges and web is accounted for in the formulation of the problem. Also, the effects of residual stresses are included directly into the theoretical formulation. The calculations were performed by computer and the theoretical results were verified by comparison with available test results as well as with the predictions of classical analysis for elastic plate buckling.

A wide range of Class 1, 2, and 3 sections of varying dimensions were analysed for axial loadings, flexural loadings, and axial and flexural loadings combined. As a result, interaction diagrams were generated for each class of section and these diagrams were used to determine maximum web limitations for a range of axial loads varying

from zero to the yield load. It was generally indicated that present web limitations are too restrictive and appropriate increases have been suggested. Additionally, it has been suggested that more testing of laboratory specimens be carried out and appropriate recommendations have been made regarding the design of such tests.

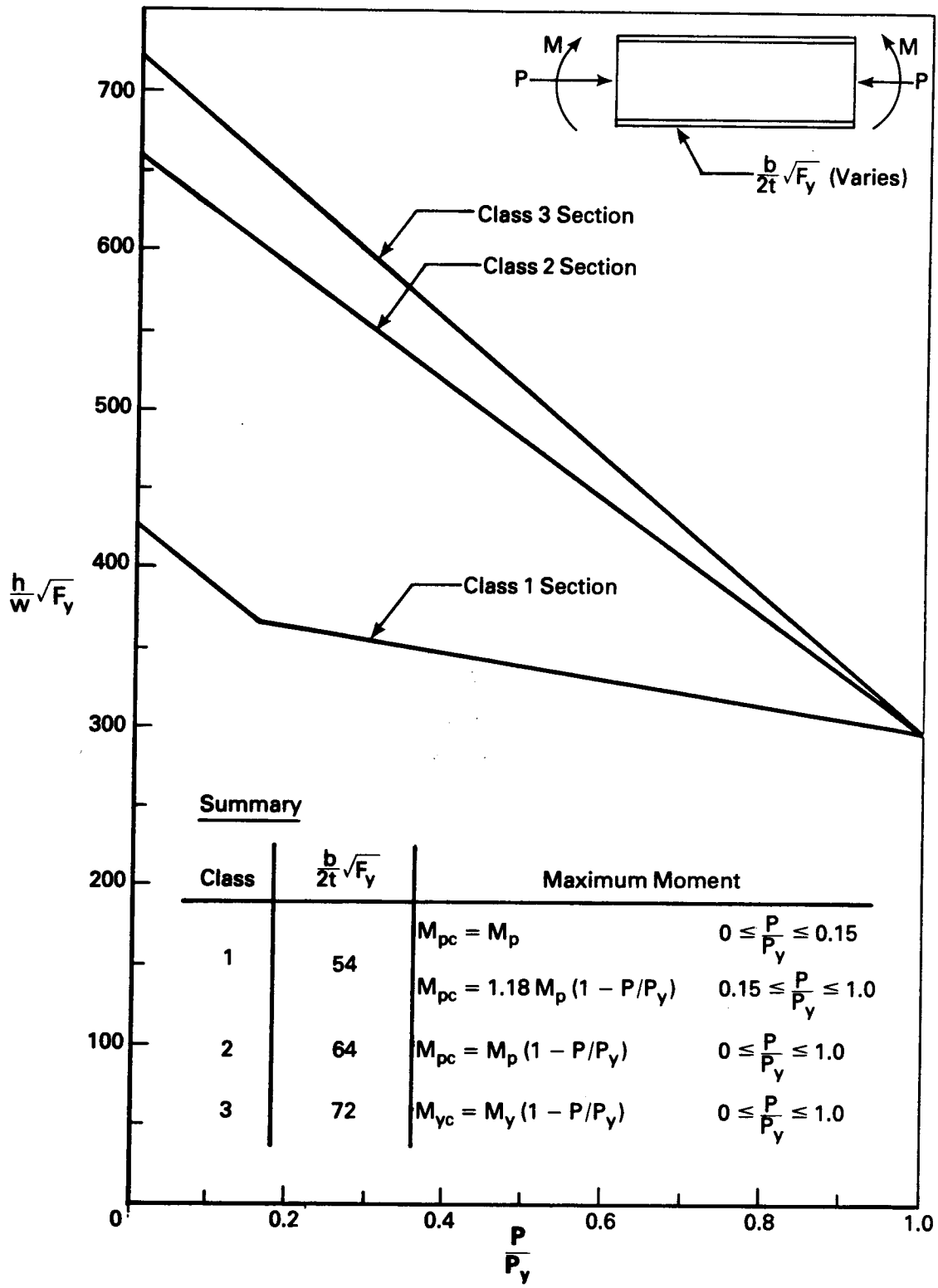

Figure 7.1 Summary of Indicated Modifications

LIST OF REFERENCES

1. Adams, P.F., Krentz, H.A., and Kulak, G.L., "Limit States Design in Structural Steel", Canadian Institute of Steel Construction, Willowdale, Ontario, 1977.

2. Timoshenko, S. and Gere, J., "Theory of Elastic Stability", Second Edition, McGraw-Hill Book Co., Inc., New York, N.Y., 1961.

3. "Guide to Stability Design Criteria for Metal Structures", Third Edition, B.G. Johnston, Editor, John Wiley and Sons, New York, N.Y., 1976.

4. "CSA S 16.1-1974 "Steel Structures for Buildings - Limit States Design", Canadian Standards Association, Rexdale, Ontario, 1975.

5. Galambos, T.V., "Structural Members and Frames", Prentice-Hall, Inc., Englewood Cliffs, N.J., 1968.

6. Bleich, F., "Buckling Strength of Metal Structures", McGraw-Hill Book Co., Inc., New York, N.Y., 1952.

7. Haaijer, G., and Thurlimann, B., "On Inelastic Buckling in Steel", Proceedings, ASCE, Volume 84, No. EM2, April, 1958.

8. Fung, Y.C., "Foundations of Solid Mechanics", Prentice-Hall, Inc., Englewood Cliffs, N.J., 1965.

9. "CSA S16.2-1975 "Steel Structures for Buildings - Working Stress Design", Canadian Standards Association, Rexdale, Ontario, 1975.

10. Holtz, N.M, and Kulak, G.L., "Web Slenderness Limits for Compact Beams", Structural Engineering Report No. 43, Department of Civil Engineering, University of Alberta, March, 1973.

11. Holtz, N.M., and Kulak, G.L., "Web Slenderness Limits of Non-Compact Beams", Structural Engineering Report No. 51, Department of Civil Engineering, University of Alberta, August, 1975.

12. Perlynn, M.J., and Kulak, G.L., "Web Slenderness Limits for Compact Beam-Columns", Structural Engineering Report No. 50, Department of Civil Engineering, University of Alberta, September, 1974.

13. Nash, D.S. and Kulak, G.L., "Web Slenderness Limits for Non-Compact Beam-Columns", Structural Engineering Report No. 53, Department of Civil Engineering, University of Alberta, March 1976.

14. Bryan, G.H., "On the Stability of a Plane Plate under Thrusts in its Own Plane with Applications to the Buckling of the Sides of a Ship", Proceedings of London Mathematical Society, v. 22, pp. 54-67, 1891.

15. Gerard, G., and Becker, H., "Handbook of Structural Stability - Part I: Buckling of Flat Plates", National Advisory Council for Aeronautics, Technical Notes 3781, Washington, D.C., 1957.

16. "Handbook of Structural Stability", Construction Research Council Japan, Corona Publishing Co., Tokyo, Japan, 1971.

17. Ros, M.,and Eichinger, A., Reports, 3rd International Congress, Bridge and Structural Engineer, Paris, 1932.

18. Bijlaard, P.P., "Theory and Tests on the Plastic Stability of Plates and Shells", Journal of Aeronautical Science, v. 16, pp. 529-541, September, 1949.

19. Ilyushin, A.A., "Stability of Plates and Shells Beyond the Proportional Limit", National Advisory Council for Aeronautics, Technical Memorandum No. 116, October, 1947.

20. Stowell, E.Z., "A Unified Theory of Plastic Buckling of Columns and Plates", National Advisory Council for Aeronautics, Technical Notes 1556, 1948.

21. Onat, E.T., and Drucker, D.C., "Inelastic Instability and Incremental Theories of Plasticity", Journal of Aeronautical Sciences, Volume 20, p. 181, March, 1953

22. Handelman, G.H., and Prager, W., "Plastic Buckling of a Rectangular Plate under Edge Thrusts", National Advisory Council for Aeronautics, Technical Note No. 1530, August, 1948.

23. Drucker, D.C., "A Discussion of the Theories of Plasticity", Readers' Forum, Journal of Aeronautical Sciences, Volume 16, No. 9, P. 567, September, 1949.

24. Dubey, R.N., "Bifurcation in Elastic-Plastic Plates", Transactions, CSME, Volume 5, NO. 2, pp. 79-88, 1978-79.

25. Lay, M.G., "Yielding of Uniformly Loaded Steel Members", Journal of the Structural Division, ASCE, Volume 91, No. ST6, Proceedings Paper 4580, December, 1965.

26. Timoshenko, S., "Stability of Webs of Plate Girders", Engineering, Volume 138, p. 207, 1934.

27. Kato, B., "Buckling Strength of Plates in the Plastic Range", Publications, IABSE, Volume 25, pp. 127-141, 1965.

28. Ueda, Y., and Tall, L., "Inelastic Buckling of Plates with Residual Stresses", Publications, IABSE, Volume 27, pp. 211-254, 1967.

29. Paramasivam, P., and Rao, J.K.S., "Buckling of Plates of Abruptly Varying Stiffnesses", Journal of the Structural Division, Proceedings, ASCE, Volume 95, NO. ST6, pp. 1313-1337, June, 1969.

30. Sherbourne, A.N., and Korol, R.M., "Post-Buckling of Axially Compressed Plates", Journal of the Structural Division, Proceedings, ASCE, Volume 98, No. ST10, pp. 2223-2234, October, 1972.

31. Crisfield, M.A., "Full Range Analysis of Steel Plates and Stiffened Plating Under Uniaxial Compression", Institute of Civil Engineers, Proceedings, Part 2, Volume 59, pp. 595-624, December, 1975.

32. Przemieniecki, J.S., "Finite Element Structural Analysis of Local Instability" American Institute of Aeronautics and Astronautics Journal, Volume 11, No. 1, January, 1973.

33. Lay, M.G., "Flange Local Buckling in Wide-Flange Shapes", Journal of the Structural Division, Proceedings, ASCE, Volume 91, No. ST6, pp. 95-116, December, 1965.

34. Culver, C.G., and Nasir, G., "Inelastic Flange Buckling of Curved Plate Girders", Journal of the Structural Division, Proceedings, ASCE, Volume 97, No. ST4, pp. 1239-1256, April, 1971.

35. McDermott, J.F., "Local Plastic Buckling of A514 Steel Members" Journal of the Structural Division, Proceedings, ASCE, Volume 95, No. ST9, pp. 1837-1850, September, 1969.

36. Lukey, A.F., and Adams, P.F., "Rotation Capacity of Beams Under Moment Gradient", Journal of the Structural Division, ASCE, Volume 95, No. ST6, June, 1969.

37. Basler, K., and Thurlimann, B., "Strength of Plate Girders in Bending", Journal of the Structural Division, Proceedings, ASCE, Volume 87, No. ST6, pp. 153-181, August, 1961.

38. Croce, A.D., "The Strength of Continuous Welded Girders with Unstiffened Webs", thesis presented at the University of Texas at Austin, Texas in 1970 in partial fulfillment of the requirements for the degree of Master of Science.

39. Rajasekaran, S., and Murray, D.W., "Coupled local Buckling in Wide-Flange Beam Columns", Journal of the Structural Division, ASCE, Volume 99, No. ST6, Proceedings Paper 9774, pp. 1003-1023, June, 1973.

40. Akay, H.V., Johnson, C.P., and Will, K.M., "Lateral and Local Buckling of Beams and Frames", Journal of the Structural Division, ASCE, Volume 103, No. ST9, Proceedings Paper 13226, pp. 1821-1832, September, 1977.

41. Hancock, G.J., "Local, Distortional and Lateral Buckling of I-Beams", Journal of the Structural Division, Proceedings, ASCE, Volume 104, No. ST11, pp. 1787-1798, November, 1978.

42. Plank, R.J., and Wittrick, W.H., "Buckling Under Combined Loading of Thin, Flat-Walled Structures by a Complex Finite Strip Method", International Journal of Numerical Methods in Engineering, Volume 8, No. 2, pp. 323-339, 1974.

43. Goldberg, J.E., Bogdanoff, J.L., and Glauz, W.D., "Lateral and Torsional Buckling of Thin-Walled Beams", Proceedings, IABSE, Volume 24, pp. 91-100, 1964.

44. MacFarland, D.E., Smith, B.L., and Bernhart, W.D., "Analysis of Plates", First Edition, Spartan Books, N.Y., 1972.

45. Lecture Notes, Civil Engineering 664, University of Alberta, 1977, Instructors: Dr. D.W. Murray and Dr. T.M. Hrudey.

46. Chou, P.C., and Pagano, N.J., "Elasticity: Tensor, Dyadic and Engineering Approaches", D. Van Nostrand Company, Inc., Princeton, New Jersey, 1967.

47. Cook, R.D., "Concepts and Applications of Finite Element Analysis", First Edition, John Wiley and Sons, Inc., N.Y., 1974.

48. Clough, R.W., and Penzien, J., "Dynamics of Structures", McGraw-Hill Book Co., N.Y., 1975.

49. Simitses, G.J., "An Introduction to the Elastic Stability of Structures", Prentice-Hall, Inc., Englewood Cliffs, New Jersey, 1976.

50. Bathe, K.J., and Wilson, E.L., "Numerical Methods in Finite Element Analysis", Prentice-Hall, Inc., Englewood Cliffs, New Jersey, 1976.

51. Trahair, N.S., and Kitipornchai, S., "Buckling of Inelastic I-Beams Under Uniform Moment", Journal of the Structural Division, Proceedings, ASCE, Volume 98, No. ST11, pp. 2551-2566, November, 1972.

52. Carskaddan, P.S., "Shear Buckling of Unstiffened Hybrid Beams", Journal of the Structural Division Proceedings Paper 6077, ASCE, Volume 94, No. ST8, pp. 1965-1990, August 1968.

53. Culver, C.G., and Frampton, R.E., "Local Instability of Horizontally Curved Members", Journal of the Structural Division, Proceedings Paper 7079, ASCE, Volume 96, No. ST2, pp. 245-265, February, 1970.

54. Galambos, T.V., and Ravindra, M.K., "Properties of Steel for Use in LRFD", Journal of the Structural Division, Proceedings, ASCE, Volume 104, No. ST9, pp. 1459-1468, September, 1978.

55. Zienkiewicz, O.C., "The Finite Element Method", Third Edition, McGraw-Hill Book Co., Inc., New York, 1977.

56. Kreyszig, E., "Advanced Engineering Mathematics", Second Edition, John Wiley and Sons, Inc., New York, 1967.

57. Yoshida, H., "Lateral Buckling Strength of Plate Girders", Publications, IABSE, Volume 35-11, pp. 163-182, 1975.

58. Yoshida, H., and Imoto, Y., "Inelastic Lateral Buckling of Restrained Beams", Engineering Mechanics Division, ASCE, Volume 99, No. EM2, April, 1973.

59. Thurlimann, B., "New Aspects Concerning Inelastic Instability of Steel Structures", Journal of the Structural Division, Proceedings, ASCE, Volume 86, No. ST1, pp. 99-120.

60. Nash, D.S., Personal Comm., Montreal, June, 1979.

61. McGuire, W., "Steel Structures", Prentice-Hall, Inc., Englewood Cliffs, N.Y., 1968.

62. "Structural Steel Design", First Edition, Lambert Tall, Editor, The Ronald Press Company, New York, 1964.

63. Beedle, L.S., "Plastic Design of Steel Frames", First Edition, John Wiley and Sons, Inc., New York, 1958.

64. Driscoll, G.C., and Beedle, L.S., "The Plastic Behaviour of Structural Members and Frames", The Welding Journal, vol. 36, No. 6, June, 1957.

65. Ketter, R.L., Kaminsky, E.L., and Beedle, L.S., "Plastic Deformation of Wide-Flange Beam-Columns", Transactions, ASCE, vol. 120, 1955.

66. Lay, M.G., and Gimsing, N., "Experimental Studies of the Moment-Thrust-Curvature Relationship", The Welding Journal, Welding Research Suplement, vol. 30, No. 2, February, 1965.

67. Stanley, F.R., "Mechanics of Materials", First Edition, McGraw-Hill Book Co., Inc., New York, N.Y., 1967.

68. Nadai, A., "Theory of Flow and Fracture of Solids", McGraw-Hill Book Co., Inc., New York, N.Y., 1950.

69. Hrudey, T.M., Personal Comm., Edmonton, 1978.

70. Dubey, R.N., and Pindera, M.J., "Effect of Rotation of Principal Axes on Effective Shear Modulus in Elastic-Plastic Solids", Journal of Structural Mechanics, vol. 5, No. 1. 1977.

71. Drucker, D,C,. "Introduction to Mechanics of Deformable Solids", McGraw-Hill Book Co., Inc., New York, N.Y., 1967.

72. Lekhnitskii, S.G., "Anisotropic Plates", Gordon and Breach Science Publishers, Second Edition, New York, 1968.

73, Haaijer, G., "Plate Buckling in the Strain-Hardening Range", Journal of the Engineering Mechanics Division, Proceedings, ASCE, vol. 83, No. EM2, April, 1957.

APPENDIX A

DERIVATION OF A PLATE BUCKLING CONDITION

A-1 Introduction

In this section a plate buckling condition is established using the principle of virtual work[2,8,55]. For a body in equilibrium, the principle states that the work done by an internal equilibrium stress field, σ_{ij}, is equal to the work done by the surface tractions, T_i, when the body is subjected to a virtual displacement field, δu_i. The principle may be expressed as follows:

$$\int_V \sigma_{ij}\delta e_{ij} dV = \int_S T_i \delta u_i dS \qquad \text{(A-1)}$$

where δe_{ij} is the virtual strain field resulting from a virtual displacement field, δu_i, V refers to the volume, and S refers to the surface area over which surface tractions, T_i, are specified. In this expression, the effects of body forces, F_i, have been neglected.

A-2 Assumptions

In the following derivation it is assumed that:

1. second order strain terms resulting from in-plane displacement components due to buckling are small and may be neglected[8].
2. at the point of bifurcation of a plate, an in-plane or a buckled equilibrium configuration is possible while

the system of external forces remains constant,

3. a state of plane stress[46] exists within the plate,
4. the plate thickness is small relative to the surface dimensions,
5. deflections are small relative to the plate thickness,
6. straight lines perpendicular to the middle surface of an undeformed plate remain straight and perpendicular to the middle surface after buckling,
7. longitudinal strips of a plate may be elastic or inelastic,
8. stresses are constant or vary linearly across the thickness of a plate,
9. stretching of the middle plane of the plate during buckling is small and may be neglected.

A-3 Strain - Displacement Relationships

The strain - displacement relationships in tensor form may be written as follows[8]:

$$e_{ij} = \frac{1}{2} (u_{i,j} + u_{j,i} + u_{k,i}\, u_{k,j}) \qquad \text{(A-2)}$$

where i,j, and k cyclically represent the subscripts x, y, and z corresponding to Cartesian coordinates. In this and subsequent expressions, the comma-notation is used to represent differentiation,

and double subscripts indicate summation[46]. Here also, e and u represent strain and displacement components, respectively.

In the present case of plane stress, Equation A-2 may be expanded to the following components of strain:

$$e_x = u_{,x} + \frac{1}{2}\left(u_{,x}^2 + v_{,x}^2 + w_{,x}^2\right) \tag{A-3}$$

$$e_y = v_{,y} + \frac{1}{2}\left(u_{,y}^2 + v_{,y}^2 + w_{,y}^2\right) \tag{A-4}$$

$$e_{xy} = \frac{1}{2}\left(u_{,y} + v_{,x} + u_{,x}\, v_{,y} + w_{,x} w_{,y}\right) \tag{A-5}$$

where u, v, and w represent displacement components in the x-, y-, and z-coordinate directions, and subscripts x, y, and z indicate differentiation with respect to that particular variable.

According to Assumption No. 1, strain terms depending on the squares and products of $u_{,x}$, $u_{,y}$, $v_{,x}$, and $v_{,y}$ may be neglected. Second order terms based on $w_{,x}$ and $w_{,y}$ result from a buckled configuration and therefore they are retained. Thus, Equations A-3 to A-5 may be rewritten as follows:

$$e_x = u_{,x} + \frac{1}{2} w_{,x}^2 \tag{A-6}$$

$$e_y = v_{,y} + \frac{1}{2} w_{,y}^2 \tag{A-7}$$

$$e_{xy} = \frac{1}{2}\left(u_{,y} + v_{,x} + w_{,x}\, w_{,y}\right) \tag{A-8}$$

A-4 Displacement Components

Figure A-1 shows a plate oriented in a 3-dimensional Cartesian coordinate system. The displacement components of a point in the middle plane of the plate during buckling are given as:

$$u = u' \tag{A-9}$$

$$v = v' \tag{A-10}$$

$$w = w \tag{A-11}$$

Figure A-2 shows a portion of a plate before and after buckling in the x - y plane. During buckling, a point P moves tangentially to P' by a distance u'. Due to out-of-plane deflection, P' moves to P" by a distance equal to w. As a result of rotation of a cross-section of the plate, P" moves to P'''. Making use of Assumption No. 5 concerning small deflections, and recognizing similar observations for buckling in the y - z plane, the following displacement components are obtained:

$$u = u' - zw_{,x} \tag{A-12}$$

$$v = v' - zw_{,y} \tag{A-13}$$

$$w = w \tag{A-14}$$

Using these results in Equations A-6 to A-8, the following strain-displacement relationships are obtained:

$$e_x = u'_{,x} - zw_{,xx} + \frac{1}{2} w^2_{,x} \tag{A-15}$$

$$e_y = v'_y - zw_{,yy} + \frac{1}{2} w^2_{,y} \tag{A-16}$$

$$e_{xy} = \frac{1}{2}(u'_y + v'_x) - zw_{,xy} + \frac{1}{2} w_{,x} w_{,y} \tag{A-17}$$

A-5 Application of the Principle of Virtual Work

Using Equations A-15 to A-17, the left hand side of Equation A-1, for the case of plane stress, (Assumption No. 3), may be written as follows:

$$\int_V \sigma_{ij}\delta e_{ij} dV = \int_x \int_y \left[N_x \delta u'_x + N_{xy}(\delta u'_y + \delta v'_x) + N_y \delta v'_y\right] dxdy$$

$$+ \int_x \int_y \left[N_x w_{,x} \delta w_{,x} + N_{xy}(w_{,x}\delta w_{,y} + w_{,y}\delta w_{,x})\right.$$

$$\left. + N_y w_{,y} \delta w_{,y}\right] dxdy + \int_x \int_y \left[M_x \delta w_{,xx}\right.$$

$$\left. + 2M_{xy}\delta w_{,xy} + M_y \delta w_{,yy}\right] dxdy \tag{A-18}$$

In developing this expression, the following relationships were used:

$$\sigma_{ij}\delta e_{ij} = \sigma_x \delta e_x + 2\sigma_{xy}\delta e_{xy} + \sigma_y \delta e_y \tag{A-19}$$

$$\delta e_x = \delta u',_x - z\delta w,_{xx} + w,_x \delta w,_x \tag{A-20}$$

$$\delta e_y = \delta v',_y - z\delta w,_{yy} + w,_y \delta w,_y \tag{A-21}$$

$$\delta e_{xy} = \frac{1}{2}(\delta u',_y + \delta v',_x) - z\delta w,_{xy} + \frac{1}{2}(w,_x \delta w,_y + w,_y \delta w,_x) \tag{A-22}$$

from Equation A-15 to A-17, and,

$$N_x = \int_{-t/2}^{t/2} \sigma_x d_y \tag{A-23a}$$

$$N_{xy} = \int_{-t/2}^{t/2} \sigma_{xy} dz \tag{A-23b}$$

$$N_y = \int_{-t/2}^{t/2} \sigma_y dz \tag{A-23c}$$

$$M_x = -\int_{-t/2}^{t/2} \sigma_x z d\check{z} \tag{A-24a}$$

$$M_{xy} = -\int_{-t/2}^{t/2} \sigma_{xy} z dz \tag{A-24b}$$

$$M_y = -\int_{-t/2}^{t/2} \sigma_y z dz \tag{A-24c}$$

where N_x, N_{xy}, and, N_y are forces and M_x, M_{xy}, and M_y are moments per unit length of a plate having a thickness, t.

The first integral on the right hand side of expression A-18, may be integrated by parts as follows:

$$\int_y \left[N_x \delta u' \Big|_0^a + N_{xy} \delta v' \Big|_0^a \right] dy + \int_x \left[N_y \delta v' \Big|_0^b + N_{xy} \delta u' \Big|_0^b \right] dx$$

$$- \int_x \int_y \delta u' (N_{x,x} + N_{xy,y}) dxdy - \int_x \int_y \delta v' (N_{y,y} + N_{xy,x}) dxdy \qquad \text{(A-25)}$$

where a and b refer to the length and width of a rectangular plate as shown in Figure A-1. The first two integrals of this expression represent the virtual work done by the applied forces per unit length evaluated at the boundaries of the plate. If body forces are negligible, the conditions of equilibrium[2,8,46] require that the last two integrals of this expression equal zero. Therefore the first integral on the right hand side of expression A-18 represents the virtual work done by the applied external forces acting through mid-plane displacements.

It is assumed that the strain in the middle plane of a plate at buckling is negligible. Therefore, from Equations A-15 to A-17,

$$u'_{,x} = - \frac{1}{2} w_{,x}^2 \qquad \text{(A-26)}$$

$$u'_{,y} = - \frac{1}{2} w_{,y}^2 \qquad \text{(A-27)}$$

$$\frac{1}{2}(u'_{,y} + v'_{,x}) = - \frac{1}{2} w_{,x} w_{,y} \qquad \text{(A-28)}$$

Substituting these values into the first two integrals of

expression A-25 gives:

$$\int_x\int_y\left[N_x\delta u',_x + N_{xy}(\delta u',_y + \delta v',_x) + N_y\delta v',_y\right]dxdy =$$

$$-\int_x\int_y\left[N_x w,_x\delta w,_x + N_{xy}(w,_x\delta w,_y + w,_y\delta w,_x) + N_y w,_y\delta w,_y\right]dxdy$$

(A-29)

Using this relationship in Equation A-18, the left hand side of Equation A-1 finally reduces to:

$$\int_V \sigma_{ij}\delta e_{ij}dV = \int_x\int_y\left[M_x\delta w,_{xx} + M_{xy}\delta w,_{xy} + M_y\delta w,_{yy}\right]dxdy$$

(A-30)

The right hand side of Equation A-1 represents the work done by the surface tractions when the body is subjected to a virtual displacement field. This quantity has already been evaluated in expression A-29 above. Using expressions A-29 and A-30, Equation A-1 finally reduces to:

$$\int_x\int_y\left[M_x\delta w,_{xx} + 2M_{xy}\delta w,_{xy} + M_y\delta w,_{yy}\right]dxdy$$

$$=-\int_x\int_y\left[N_x w,_x\delta w,_x + N_{xy}(w,_x\delta w,_y + w,_y\delta w,_x) + N_y w,_y\delta w,_y\right]dxdy$$

(A-31)

In this equation, the integral on the left hand side represents the strain energy of bending of an equilibrium stress field when a virtual displacement field is superimposed on a buckled configuration. The integral on the right hand side represents the virtual work done by the in-plane stresses acting at the boundaries. In this form, Equation A-31 defines the buckling condition of a plate subjected to in-plane stresses.

In the present analysis, the equilibrium stress field is derived from the general stress-strain relationships for an orthotropic plate. The moments per unit length can be expressed in terms of the plate deflections as follows[7]:

$$M_x = - D_x w,_{xx} - D_{xy} w,_{yy} \qquad \text{(A-32)}$$

$$M_y = - D_y w,_{yy} - D_{yx} w,_{xx} \qquad \text{(A-33}$$

$$M_{xy} = - 2G_t I w,_{xy} \qquad \text{(A-34)}$$

where D_x, D_y, D_{xy}, and D_{yx} are plate bending rigidities, G_t is the tangent shear modulus, and I is the moment of inertia per unit length of the plate. These properties are further discussed in Appendix B.

Substituting Equations A-32 to A-34 into Equation A-31, the buckling condition for a uniaxially stressed plate may be expressed as:

$$\int_x\int_y (D_x w,_{xx}\delta w,_{xx} + D_y w,_{yy}\delta w,_{yy} + D_{xy} w,_{yy}\delta w,_{xx} + D_{yx} w,_{xx}\delta w,_{yy}$$

$$+ 4G_t Iw,_{xy}\delta w,_{xy})dxdy - \int_x\int_y N_x w,_x\delta w,_x dxdy = 0 \qquad (A\text{-}35)$$

A-6 Development of a Matrix Buckling Condition

The first integral of Equation A-35 leads to the bending stiffness matrix of a plate and the second integral results in a geometric stiffness matrix. The subscript, x, refers to integration along the length of a plate, and the subscript, y, refers to integration along its width. In the present analysis, the integration along x is continuous since material properties along the length of a strip of plate under uniaxial stress will be constant. In the transverse direction of a plate however, the uniaxial stress may vary in intensity and therefore certain longitudinal strips may be yielded while others are still elastic or strain-hardened. To account for this, integration in the y direction is done in a piecewise manner and the appropriate material properties for a given strip are incorporated into the integration in a piecewise fashion.

As explained in Chapter 3, a Rayleigh-Ritz technique is applied using a displacement function of the form:

$$w = f<\phi>\{\theta\} \qquad (A\text{-}36)$$

In this expression, f is a function of x only and it describes the buckled shape in the longitudinal direction, $<\phi>$ is a row vector of

interpolating functions of y only and $\{\theta\}$ is a column vector of nodal coordinate displacements. Together, $\langle\phi\rangle$ and $\{\theta\}$ define the transverse buckled shape of a plate.

The derivatives and corresponding variations for w are defined as follows:

$$w,_{xx} = f,_{xx}\langle\phi\rangle\{\theta\} \qquad \delta w,_{xx} = f,_{xx}\langle\phi\rangle\{\delta\theta\} \tag{A-37}$$

$$w,_{yy} = f\langle\phi,_{yy}\rangle\{\theta\} \qquad \delta w,_{yy} = f\langle\phi,_{yy}\rangle\{\delta\theta\} \tag{A-38}$$

$$w,_{xy} = f,_{x}\langle\phi,_{y}\rangle\{\theta\} \qquad \delta w,_{xy} = f,_{x}\langle\phi,_{y}\rangle\{\delta\theta\} \tag{A-39}$$

$$w,_{x} = f,_{x}\langle\phi\rangle\{\theta\} \qquad \delta w,_{x} = f,_{x}\langle\phi\rangle\{\delta\theta\} \tag{A-40}$$

Substituting these expressions into Equation A-35 gives:

$$\langle\delta\theta\rangle\left[F_1[\Phi_1] + F_2[\Phi_2] + F_3[\Phi_3] + F_4[\Phi_4]\right]\{\theta\}$$

$$-\langle\delta\theta\rangle\left[F_5[\Phi_5]\right]\{\theta\} = 0 \tag{A-41}$$

where the following relationships have been used:

$$F_1 = D_x \int_x f^2,_{xx} dx, \tag{A-42}$$

$$F_2 = D_y \int_x f^2 dx, \tag{A-43}$$

$$F_3 = 2D_{xy} \int_x f \cdot f_{,xx} dx, \tag{A-44}$$

$$F_4 = 4G_t I \int_x f_{,x}^2 dx, \tag{A-45}$$

$$F_5 = t \int_x f_{,x}^2 dx, \tag{A-46}$$

and,

$$[\Phi_1] = \int_y \{\phi\}\langle\phi\rangle dy \tag{A-47}$$

$$[\Phi_2] = \int_y \{\phi_{,yy}\}\langle\phi_{,yy}\rangle dy \tag{A-48}$$

$$[\Phi_3] = \int_y \left[\{\phi_{,yy}\}\langle\phi\rangle + \{\phi\}\langle\phi_{,yy}\rangle\right] dy \tag{A-49}$$

$$[\Phi_4] = \int_y \{\phi_{,y}\}\langle\phi_{,y}\rangle dy \tag{A-50}$$

$$[\Phi_5] = \int_y \sigma_x \{\phi\}\langle\phi\rangle dy \tag{A-51}$$

where, for a plate of constant thickness, t, $N_x = \sigma_x t$ is used.

In Equation A-41, the virtual displacement coordinates are completely arbitrary and therefore the relationship must hold for all values $\langle\delta\theta\rangle$. Therefore the buckling condition defined by Equation A-41 may be written as follows:

$$[K]\{\theta\} - [K_G]\{\theta\} = \{0\} \tag{A-52}$$

where the bending stiffness matrix, [K] is given by:

$$[K] = F_1[\Phi_1] + F_2[\Phi_2] + F_3[\Phi_3] + F_4[\Phi_4] = F_i[\Phi_i] \tag{A-53}$$

where, $i = 1, 2, 3, 4$, and repeated subscripts indicate summation, and the geometric stiffness matrix, $[K_G]$ is given by:

$$[K_G] = F_5[\Phi_5] \tag{A-54}$$

In Equations A-53 and A-54, the Φ matrices are evaluated by piecewise integration across the width of a plate. The integration is performed for each strip of plate which may be in the elastic, the yielded, or the strain-hardening region. For each such strip, the appropriate bending rigidities, as defined in Appendix B, are used in Equation A-53.

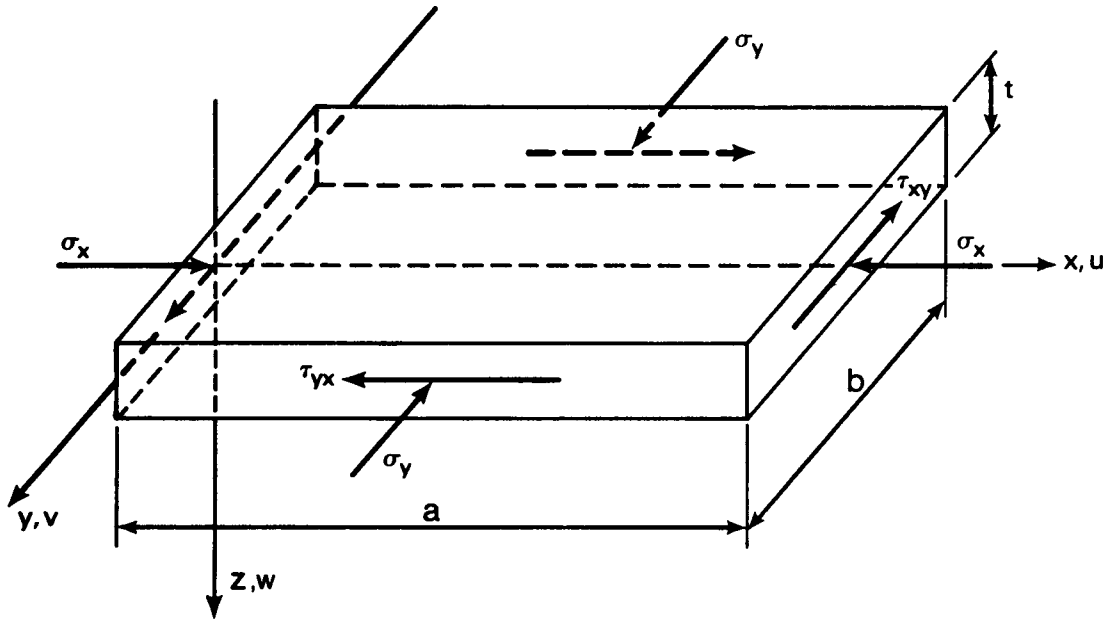

Figure A-1 Rectangular Plate Subjected to Plane Stress

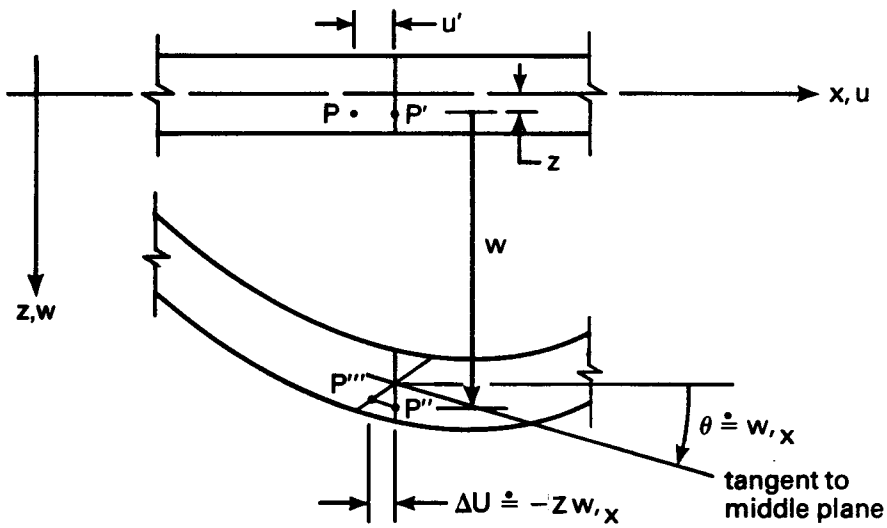

Figure A-2 Plate Buckling in the x-y Plane

APPENDIX B

MATERIAL PROPERTIES

B-1 Introduction

The determination of material properties used in the present study is based on a tangent modulus concept[5], and therefore, the material properties that determine a critical buckling strain, are those that exist in a plate at the instant before buckling. This concept is considered to give very good correlation between predicted and test results in inelastic buckling of columns[3,5,6], and the correlation is further improved with the inclusion of residual stress effects[5], as in the present study.

B-2 Incremental Stress-Strain Relationships

Figure B-1(a) shows a stress - strain relationship for a strain-hardening material. An increment of total strain, $\Delta\bar{e}$, is assumed to be sufficiently small so that it may be separated into an elastic strain increment and a plastic strain increment[71]. Thus,

$$de_{ij} = de_{ij}^{(e)} + de_{ij}^{(p)} \tag{B-1}$$

Elastic strain increments are related to elastic stress increments as follows[71]:

$$de_{ij}^{(e)} = \left(\frac{1+\nu}{E}\right)d\sigma_{ij} - \frac{\nu}{E}\, d\sigma_{kk}\delta_{ij} \tag{B-2}$$

In these relationships, Cartesian tensor notation is used[46], and

$$\delta_{ij} = 1 \text{ for } i = j, \text{ and}$$

$$\delta_{ij} = 0 \text{ for } i \neq j,$$

and ν and E are Poisson's ratio and Young's modulus respectively[46].

The relationship between plastic strain increments and corresponding stress increments may be defined for an assumed yield criterion, an associated flow rule, and a work hardening rule[45,71]. For a material which yields according to von Mises yield criterion[8,71], the plastic strain increment tensor coincides with the plastic stress deviator tensor and the following relationship may be used[45,71]:

$$de_{ij}^{(p)} = S_{ij} d\lambda \tag{B-3}$$

where $d\lambda$ is a positive constant of proportionality and the stress deviator tensor is defined as:

$$S_{ij} = \sigma_{ij} - \frac{\sigma_{kk}}{3} \delta_{ij} \tag{B-4}$$

According to von Mises yield criterion, yielding occurs when the second invariant of the stress deviator tensor reaches a critical value[71]. This may be expressed as:

$$J_2 - k^2 = 0 \tag{B-5}$$

where,

$$J_2 = \frac{1}{2} S_{ij} S_{ij} \tag{B-6}$$

and k is a critical constant.

When a work-hardening material is subjected to a uniaxial stress state, σ, Equation B-6 gives:

$$J_2 = \frac{1}{3}\sigma^2 \tag{B-7}$$

or,

$$\bar{\sigma} = \sqrt{3J_2} = \sqrt{\frac{3}{2} S_{ij}S_{ij}} \tag{B-8}$$

where $\bar{\sigma}$ is an effective stress invariant corresponding to an effective plastic strain, $\bar{e}^{(p)}$. In a similar manner, an effective plastic strain increment, $d\bar{e}^{(p)}$ may be obtained. For a uniaxial stress state, Equation B-3 gives:

$$d\bar{e}^{(p)} = \frac{2}{3}\sigma d\lambda \tag{B-9}$$

Equation B-3 may be written as:

$$de_{ij}^{(p)}\, de_{ij}^{(p)} = S_{ij}S_{ij}d\lambda^2 = \frac{2}{3}\sigma^2 d\lambda^2 \tag{B-10}$$

Combining Equations B-9 and B-10 results in the following effective plastic strain increment:

$$d\bar{e}^{(p)} = \sqrt{\frac{2}{3} de_{ij}^{(p)} de_{ij}^{(p)}} \tag{B-11}$$

Figure B-1(b) shows a plot of the effective stress $\bar{\sigma}$, plotted against effective plastic strain, $\bar{e}^{(p)}$. The slope of this curve is defined as:

$$H' = \frac{d\bar{\sigma}}{d\bar{e}^{(p)}} \cdot \tag{B-12}$$

It is assumed that for all monotonic loading paths the same $\bar{\sigma} - \bar{e}^{(p)}$ relationship is obtained.

Combining Equations B-8 and B-11 with Equation B-10 gives:

$$d\lambda = \frac{3}{2} \left(\frac{d\bar{e}^{(p)}}{d\bar{\sigma}}\right) \frac{d\bar{\sigma}}{\bar{\sigma}} = \frac{3}{2} \frac{d\bar{\sigma}}{H'\bar{\sigma}} \tag{B-13}$$

where the value H' is defined in Equation B-12. Substituting this value of $d\lambda$ into Equation B-3 gives the following relationship between plastic strain and corresponding stress increments:

$$de_{ij}^{(p)} = \frac{3}{2} \frac{d\bar{\sigma}}{H'\bar{\sigma}} S_{ij} \tag{B-14}$$

Referring to Figure B-1(b), the slope of the effective stress vs. plastic strain curve is given by:

$$H' = \frac{d\bar{\sigma}}{d\bar{e}^{(p)}} = \lim_{\Delta\bar{e} \to 0} \frac{\Delta\bar{\sigma}}{\Delta\bar{e} - \Delta\bar{\sigma}/E} \tag{B-15}$$

where $\Delta\bar{e}$ is the total effective strain increment, $\Delta\bar{\sigma}$ is the effective stress increment, and E is Young's modulus. In this relationship, $\Delta\bar{\sigma}/E$ is the elastic portion of the total strain increment. Multiplying the numerator and the denominator of Equation B-15 by $E/\Delta e$ and taking the limit gives:

$$H' = \lim_{\Delta\bar{e} \to 0} \frac{E\Delta\bar{\sigma}/\Delta\bar{e}}{E - \Delta\bar{\sigma}/\Delta\bar{e}} = \frac{E \cdot E_t}{E - E_t} \tag{B-16}$$

where the tangent modulus is defined as:

$$E_t = \frac{d\bar{\sigma}}{d\bar{e}} \tag{B-17}$$

B-4 Stress-Strain Relationships for Plane Stress

In the case of plane stress[46],

$$\sigma_z = \tau_{zx} = \tau_{yz} = 0 \tag{B-18}$$

and the effective stress for this case may be obtained from Equation B-8 as follows:

$$\bar{\sigma} = \sqrt{\sigma_x^2 + \sigma_y^2 - \sigma_x\sigma_y + 3\tau_{xy}^2}\,. \tag{B-19}$$

The effective stress increment is obtained from Equation B-19 as:

$$d\bar{\sigma} = \frac{1}{2\bar{\sigma}}\left[(2\sigma_x - \sigma_y)d\sigma_x + (2\sigma_y - \sigma_x)d\sigma_y + 6\tau_{xy}d\tau_{xy}\right] \tag{B-20}$$

In the present analysis a plate element before buckling is in a uniaxial stress state defined by $\sigma_x \neq 0$, $\sigma_y = \tau_{xy} = 0$, and therefore:

$$\bar{\sigma} = \sigma_x \tag{B-21}$$

Immediately after buckling the same element is subjected to a state of plane stress. In applying a tangent modulus theory, only the resulting increment of effective stress is of interest, and it is given by Equation B-20 as:

$$d\bar{\sigma} = d\sigma_x - \frac{1}{2}\,d\sigma_y \tag{B-22}$$

The corresponding increments in plastic strain are obtained by using these values of $\bar{\sigma}$ and $d\bar{\sigma}$ in Equation B-14 where S_{ij} is the stress deviator tensor for a state of uniaxial stress prior to buckling. The resulting plastic strain increments are:

$$de_x^{(p)} = \frac{d\sigma_x}{H'} - \frac{d\sigma_y}{2H'} \tag{B-23}$$

$$de_y^{(p)} = -\frac{d\sigma_x}{2H'} + \frac{d\sigma_y}{4H'} \tag{B-24}$$

$$de_{xy}^{(p)} = 0 \tag{B-25}$$

Combining Equations B-2, B-23, B-24, and B-25 with Equation B-1, the increments of total strain may be obtained for the strain-hardening region as:

$$de_x = (\frac{1}{E} + \frac{1}{H'})d\sigma_x - (\frac{\nu}{E} + \frac{1}{2H'})d\sigma_y \tag{B-26}$$

$$de_y = -(\frac{\nu}{E} + \frac{1}{2H'})d\sigma_x + (\frac{1}{E} + \frac{1}{4H'})d\sigma_y \tag{B-27}$$

$$de_{xy} = \frac{1+\nu}{E} d\tau_{xy} \tag{B-28}$$

B-5 Stress - Strain Relationships for an Orthotropic Plate

For the general case of a homogeneous elastic body, the generalized stress - strain relationship is given by[46]:

$$\sigma_{ij} = C_{ijkl} e_{kl} \tag{B-29}$$

where C_{ijkl} is a fourth-order tensor representing a total of 81 constants. This number is reduced to 21 independent constants when the symmetry of the stress and strain tensors, and the existence of a potential energy function are considered[8,46,72].

If a material is orthotropic and the x, y, and z axes coincide with the principle directions of the material, the following stress-strain relationships apply[47,72]:

$$e_x = \frac{\sigma_x}{E_x} - \frac{\nu_{yx}\sigma_y}{E_y} - \frac{\nu_{zx}\sigma_z}{E_z} \tag{B-30}$$

$$e_y = -\frac{\nu_{xy}\sigma_x}{E_x} + \frac{\sigma_y}{E_y} - \frac{\nu_{zy}\sigma_z}{E_z} \tag{B-31}$$

$$e_z = -\frac{\nu_{xz}\sigma_x}{E_x} - \frac{\nu_{yz}\sigma_y}{E_y} + \frac{\sigma_z}{E_z} \tag{B-32}$$

$$\gamma_{xy} = \frac{\tau_{xy}}{G_{xy}} \tag{B-33}$$

$$\gamma_{yz} = \frac{\tau_{yz}}{G_{yz}} \tag{B-34}$$

$$\gamma_{zx} = \frac{\tau_{zx}}{G_{zx}} \tag{B-35}$$

where each Poisson ratio, ν_{ij} represents the strain in the j direction

per unit strain in the i direction for i, j = x, y, z. The above relationships contain 9 independent material constants and:

$$\frac{\nu_{yx}}{E_y} = \frac{\nu_{xy}}{E_x}, \quad \frac{\nu_{zx}}{E_z} = \frac{\nu_{xz}}{E_x}, \quad \frac{\nu_{zy}}{E_z} = \frac{\nu_{yz}}{E_y} \tag{B-36}$$

Referring to Equations B-30 to B-35, the incremental stress - strain relationships for an orthotropic plate element subjected to a state of plane stress may be written as follows:

$$de_x = \frac{1}{E_x} d\sigma_x - \frac{\nu_y}{E_y} d\sigma_y \tag{B-37}$$

$$de_y = -\frac{\nu_x}{E_x} d\sigma_x + \frac{1}{E_y} d\sigma_y \tag{B-38}$$

$$de_{xy} = \frac{1}{2G} d\tau_{xy} \tag{B-39}$$

B-6 Effective Moduli in the Strain Hardening Range

A steel plate subjected to a uniaxial stress yields by the formation of slip bands along preferential shear planes characterised by a dissipation of minimum plastic distortional energy[67,68]. For a thin steel plate these shear planes will be normal to the stress axis and inclined with respect to the middle plane of the plate. As a result, in the strain-hardening range, the steel plate will be orthotropic at the instant before buckling.

Based on a tangent modulus theory, the effective moduli in the strain-hardening range may be obtained by comparing Equations B-37

to B-39 with Equations B-26 to B-28[69]. Using the results of this comparison and the value of H' as given by Equation B-16 gives the following effective tangent moduli:

$$E_x = E_t \tag{B-40}$$

$$E_y = \frac{4E \cdot E_t}{3E_t + E} \tag{B-41}$$

$$G_t = G = \frac{E}{2(1+\nu)} \tag{B-42}$$

and the corresponding Poisson's ratios:

$$\nu_x = \frac{(2\nu-1)E_t + E}{2E} \tag{B-43}$$

$$\nu_y = \frac{4\nu_x E}{3E_t + E} \tag{B-44}$$

B-7 Material Properties Used in the Present Analysis

In the elastic range, the tangent modulus is equal to Young's modulus, E, and Equations B-40 to B-44 reduce to:

$$E_x = E_y = E \tag{B-45}$$

$$G_t = G \tag{B-46}$$

$$\nu_x = \nu_y = \nu \tag{B-47}$$

In the yielding range, the tangent modulus $E_t = 0$ and Equations B-40 to B-44 give:

$$E_x = E_y = 0 \tag{B-48}$$

$$G_t = G \tag{B-49}$$

$$\nu_x = 0.5 \tag{B-50}$$

$$\nu_y = 2.0 \tag{B-51}$$

The results given by Equations B-40 to B-44 were originally presented by Handelmann and Prager[22]. However, since that time it has been well recognized that these values may result in significant error in the prediction of inelastic critical plate buckling stresses. It has further been observed that these discrepancies are mainly due to an over-estimation of the effective shear modulus, G_t, at stresses above the yield[7,28,33,70].

For E = 29,600 ksi. and $\nu = 0.3$, Equation B-42 gives a value of G_t = 11,385 ksi. Using experimental results, Haaijer and Thurlimänn determined that the value of G_t for steel above the yield should be between 2000 and 3000 ksi.[7], with an actual value selected at 2400 ksi. This 79 per cent reduction in the theoretical value of G_t, which resulted in better correlation with test results, was attributed to the effects of initial imperfections. Independently, Lay[33] disregarded the effects of initial imperfections and, using slip field theory, predicted a value of G of about 3000 ksi. As a result of this work, Lay

presented the following expression for the tangent shear modulus for strain-hardening:

$$G_t = \frac{2G}{1 + \frac{E}{4E_t(1+\nu)}} \tag{B-52}$$

where G is the elastic shear modulus, E is Young's modulus, E_t is the tangent modulus, and ν is Poisson's ratio. For E = 29,600 ksi., G = 11,385 ksi., ν = 0.3, and E_t = 800 ksi., Equation B-52 gives a value of G_t = 2806 ksi. In the present study, Equations B-40, B-41, B-43, B-44, and B-52 are used to determine material properties in the inelastic range.

B-8 Plate Bending Rigidities

The plate bending rigidities D_x, D_y, D_{xy}, and D_{yx} were introduced in Appendix A. In terms of the material properties discussed previously the plate bending rigidities may be expressed as follows[73].

$$D_x = \frac{E_x I}{1-\nu_x \nu_y} \tag{B-53}$$

$$D_y = \frac{E_y I}{1-\nu_x \nu_y} \tag{B-54}$$

$$D_{xy} = \nu_y D_x \tag{B-55}$$

$$D_{yx} = \nu_x D_y \tag{B-56}$$

where I is the moment of inertia per unit length of a plate.

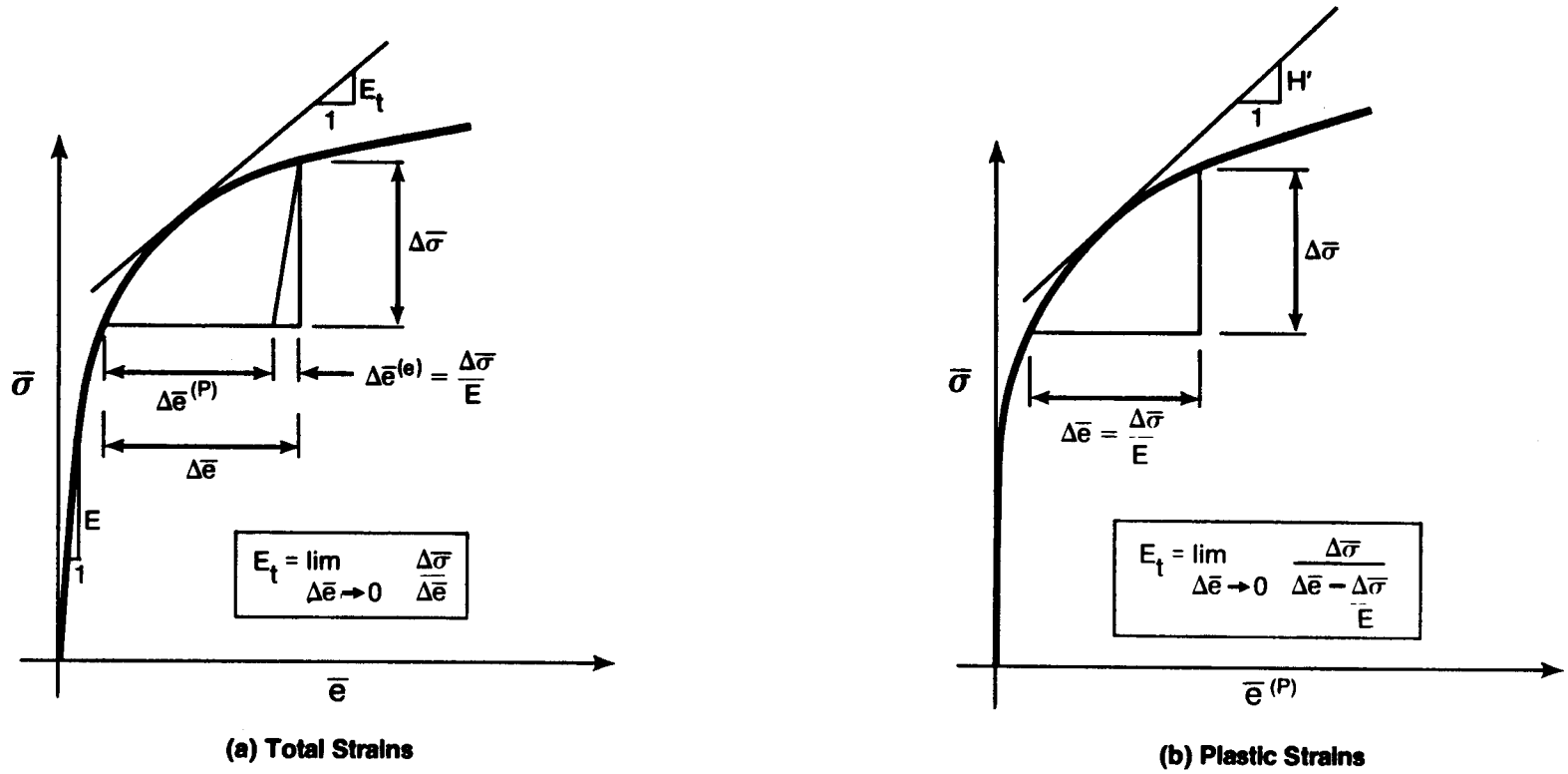

Figure B-1 Effective Stress - Effective Strain Relationships

RECENT STRUCTURAL ENGINEERING REPORTS

Department of Civil Engineering

University of Alberta

64. *Substructure Analysis of Plane Frames* by A.A. Elwi and D.W. Murray, June 1977.

65. *Strength and Behavior of Cold-Formed HSS Columns* by Reidar Bjorhovde, December 1977.

66. *Some Elementary Mechanics of Explosive and Brittle Failure Modes in Prestressed Containments* by D.W. Murray, June 1978.

67. *Inelastic Analysis of Prestressed Concrete Secondary Containments* by D.W. Murray, L. Chitnuyanondh, C. Wong and K.Y. Rijub-Agha, July 1978.

68. *Strength of Variability of Bonded Prestressed Concrete Beams* by D.K. Kikuchi, S.A. Mirza and J.G. MacGregor, August 1978.

69. *Numerical Analysis of General Shells of Revolution Subjected to Arbitrary Loading* by A.M. Shazly, S.H. Simmonds and D.W. Murray, September 1978.

70. *Concrete Masonry Walls* by M. Hatzinikolas, J. Longworth and J. Warwaruk, September 1978.

71. *Experimental Data for Concrete Masonry Walls* by M. Hatzinikolas, J. Longworth and J. Warwaruk, September 1978.

72. *Fatigue Behaviour of Steel Beams with Welded Details* by G.R. Bardell and G.L. Kulak, September 1978.

73. *Double Angle Beam-Column Connections* by R.M. Lasby and Reidar Bjorhovde, April 1979.

74. *An Effective Uniaxial Tensile Stress-Strain Relationship for Prestressed Concrete* by L. Chitnuyanondh, S. Rizkalla, D.W. Murray and J.G. MacGregor, February 1979.

75. *Interaction Diagrams for Reinforced Masonry* by C. Feeg and J. Warwaruk, April 1979.

76. *Effects of Reinforcement Detailing for Concrete Masonry Columns* by C. Feeg, J. Longworth, and J. Warwaruk, May 1979.

77. *Interaction of Concrete Masonry Bearing Walls and Concrete Floor Slabs* by N. Ferguson, J. Longworth and J. Warwaruk, May 1979.

78. *Analysis of Prestressed Concrete Wall Segments* by B.D.P. Koziak and D.W. Murray, June 1979.

79. *Fatigue Strength of Welded Steel Elements* by M.P. Comeau and G.L. Kulak, October 1979.

80. *Leakage Tests of Wall Segments of Reactor Containments* by S.K. Rizkalla, S.H. Simmonds and J.G. MacGregor, October 1979.

81. *Tests of Wall Segments from Reactor Containments* by S.H. Simmonds, S.H. Rizkalla and J.G. MacGregor, October 1979.

82. *Cracking of Reinforced and Prestressed Concrete Wall Segments* by J.G. MacGregor, S.H. Rizkalla and S.H. Simmonds, October 1979.

83. *Inelastic Behavior of Multistory Steel Frames* by M. El Zanaty, D.W. Murray and R. Bjorhovde, April 1980.

84. *Finite Element Programs for Frame Analysis* by M. El Zanaty and D.W. Murray, April 1980.

85. *Test of a Prestressed Concrete Secondary Containment Structure* by J.G. MacGregor, S.H. Simmonds and S.H. Rizkalla, April 1980.

86. *An Inelastic Analysis of the Gentilly-2 Secondary Containment Structure* by D.W. Murray, C. Wong, S.H. Simmonds and J.G. MacGregor, April 1980.

87. *Nonlinear Analysis of Axisymmetric Reinforced Concrete Structures* by A.A. Elwi and D.W. Murray, May 1980.

88. *Behavior of Prestressed Concrete Containment Structures - A Summary of Findings* by J.G. MacGregor, D.W. Murray, S.H. Simmonds, April 1980.

89. *Deflection of Composite Beams at Service Load* by L. Samantaraya and J. Longworth, June 1980.

90. *Analysis and Design of Stub-Girders* by T.J.E. Zimmerman and R. Bjorhovde, August 1980.

91. *An Investigation of Reinforced Concrete Block Masonry Columns* by G.R. Sturgeon, J. Longworth and J. Warwaruk, September 1980.

92. *An Investigation of Concrete Masonry Wall and Concrete Slab Interaction* by R.M. Pacholok, J. Warwaruk, and J. Longworth, October 1980.

93. FEPARCS5 - *A Finite Element Program for the Analysis of Axisymmetric Reinforced Concrete Structures - Users Manual* by A. Elwi and D.W. Murray, November 1980.

94. *Plastic Design of Reinforced Concrete Slabs* by D.M. Rogowsky and S.H. Simmonds, November 1980.

95. *Local Buckling of W Shapes Used as Columns, Beams, and Beam-Columns* by J.L. Dawe and G.L. Kulak, March 1981.